KfK 3026
September 1980

Velocity Distribution and Pressure Loss at Three-Dimensional Roughnesses

L. Meyer
Institut für Neutronenphysik und Reaktortechnik
Projekt Schneller Brüter

Kernforschungszentrum Karlsruhe

KERNFORSCHUNGSZENTRUM KARLSRUHE

Institut für Neutronenphysik und Reaktortechnik

Projekt Schneller Brüter

KfK 3026

Velocity Distribution and Pressure Loss at Three-Dimensional Roughnesses

L. Meyer

Kernforschungszentrum Karlsruhe GmbH, Karlsruhe

Kernforschungszentrum Karlsruhe GmbH
ISSN 0303-4003

Abstract

Measurements of the pressure drop and the velocity distribution at three-dimensional roughnesses in a rectangular channel of variable channel width were performed with air. The friction factors of the extreme roughness (p/h=2.5, g/e=1) were found to be the highest which were measured up to now. The velocity distribution showed great differences to that observed at other roughnesses. The 'law of the wall' is not adequate to decribe the velocity profile over these roughnesses, the velocity profiles are much flatter.

Geschwindigkeitsverteilung und Druckverlust an dreidimensionalen Rauhigkeiten

Zusammenfassung

In einem rechteckförmigen Kanal mit variablem Plattenabstand wurden Messungen des Druckverlustes und der Geschwindigkeitsverteilung an dreidimensionalen Rauhigkeiten mit Luft durchgeführt.

Die mit der extremen Rauhigkeit (p/h=2.5,g/e=1) gefundenen Reibungskoeffizienten sind die höchsten bisher gemessenen. Die Geschwindigkeitsverteilung unterscheidet sich sehr von der an anderen Rauhigkeiten beobachteten. So kann das Wandgesetz das Geschwindigkeitsprofil an dieser Rauhigkeit nicht mehr richtig beschreiben, die Profile sind sehr viel flacher.

1. Introduction

Artificial roughness at the surface of fuel element rods is used in gas cooled reactors to improve the heat transfer capacity at a limited mass flow rate. The roughness which is presently used consists of repeated ribs or threads on the rod surface. With parts of the ribs cut away in an alternating pattern, we get a three-dimensional roughness, which was found to have an even higher heat transfer capacity /1,2/. The R-functions, which describe the friction characteristics of the roughness could, however, not be correlated in the same manner as it was done for two dimensional roughnesses /2/. In order to eliminate those inconsistencies measurements of the flow distribution at artificial three-dimensional roughnesses were undertaken. This report is the third in a series about measurements in a rectangular channel. The other two were on two-dimensional rectangular roughnesses and on round edged ribs /3,4/ (see also /5,6,7/).

2. Experimental Setup

Since the test rig and measuring methods were described in great detail in reference /3,5/ and /7/ only the main features and modifications shall be described here.

The measurements were performed with air near the open outlet of a vertical rectangular channel (Fig.1). The internal dimensions of the channel are 700 mm in the wide direction (z) and 60 mm minimum and 210 mm maximum in the y-direction with tolerances of $\pm$ 0.5 mm. The roughness elements which were made of aluminium were fixed to one of the wide walls, respectively to both wide walls. The axial pressure drop was measured by 13 pressure taps (0.2 mm i.d.) in the smooth wide wall over a length of 6500 mm.

The velocities were measured by means of a circular Pitot tube with an outer diameter of 0.6 mm. The corresponding static pressures were measured with a second tube, axially aligned to the flow direction, which has four holes at its circumference and an ellipsoid shaped head. The lateral distance between static tube and Pitot tube was set to 8 mm. The wall shear stress at the smooth wall was determined by the Preston method, using the same Pitot tube and a static pressure tap in the smooth wall.

The cross slide, which was used to position the probes with an accuracy of 0.01 mm at any position of the flow cross section, was installed 150 mm downstream of the channel outlet in order not to block the flow.The probe support with a diameter of 4 mm at its end extended approximately 300 mm into the channel, where the velocity measurements were taken. Velocity traverses parallel to the wide walls at the position of maximum velocity at the center, show a small zone in the center which seems to be unaffected by the short side walls (Fig.2). Here the velocity measurements were taken. There is, however, a strong variation of the velocity close to the short side walls, especially for the narrow channel widths. This overshooting of the velocity was not observed at two dimensional roughnesses. Because of difficulties in fixing the last row of elements closest to the side walls, this row was left out for this particular roughness (No.5), thus creating a narrow strip of smooth wall near the corners. This might be one reason for the peculiar velocity distribution.

3. Test parameters

Five different three-dimensional roughnesses were tested. The geometry is shown in figure 3 and the parameters are listed in table 1. The parameters were chosen in such a way, that the friction factors to be expected were high. In a simple experiment where the spacing p and g was systematically varied and the force upon a roughness rib was measured a relationship between friction factor and roughness geometry had been found /3,6/.

Figure 4 shows those results in terms of a friction factor based on the maximum velocity in the flow cross section for e/h=4. The parameters which were chosen for this investigation are marked (No.1,2 and 3) in figure 4. Roughness No.1 had, however, a ratio e/h=6, which had been found to yield higher friction factors than a ratio of e/h=4.

The roughness with the highest friction factor (No.2) was tested again with a smaller roughness height (No.5) and a somewhat different e/h-ratio of e/h=5. This roughness was also used to test a symmetrical rough channel, by placing roughnesses on both wide walls. Different from the rectangular roughness geometry is roughness No.4 with a rhombic geometry (see figure 3b). This shape was chosen because it was used in single pin tests in our laboratory /2/.

The relative roughness height was varied by changing the channel width L. Thus, the aspect ratio of the channel varied between 3.3:1 and 11.7:1.

The mean velocities were in the range between 8 and 30 m/s which resulted in a Reynolds number range of $0.8 \cdot 10^5 < Re < 5 \cdot 10^5$. The values of h^+ ranged between 500 and 3300. Most roughness-channel width combinations were tested at four different mass flow rates.

4. Evaluation

The time mean velocity u was calculated with the differential pressure between Pitot tube and static tube and the density of the humid air. The position of the Pitot tube close to the smooth wall was corrected according to Mac Millan /8/. A correction of the velocities for the effect of turbulence was not applied.

The shear stress at the smooth wall was determined by Preston tubes using the Patel /15/ calibration. The shear stress at the rough wall was determined by the knowledge of the axial pressure drop dp/dx and the shear stress at the smooth wall τ_s. Since there is a region in the center of the channel in which the influence of the short side walls on the flow is negligible, a force balance of steady flow yields

$$(\tau_s+\tau_r)dzdx = L\ dzdp. \tag{1}$$

Because of the discrete roughnesses the average over one pitch must be taken at least, thus the mean shear stress is

$$\tau_r = L\ \frac{\Delta p}{\Delta x} - \tau_s \tag{2}$$

The reference surface of this shear stress is the smooth wall between the ribs (ε=0,see Fig.5). For another reference surface ($\varepsilon\neq 0$) τ_r changes to

$$\tau_r = (L-\varepsilon)\ \frac{\Delta p}{\Delta x} - \tau_s \tag{3}$$

The extension of the zones influenced by the smooth ($\hat{y}_s$) and rough ($\hat{y}_r$) wall respectively is given by the ratio of the wall shear stresses

$$\frac{\hat{y}_s}{\hat{y}_r} = \frac{\tau_s}{\tau_r} \tag{4}$$

With $\hat{y}_s = L-\hat{y}_r-\varepsilon$, the length of the rough velocity profile is given by

$$\hat{y}_r = \frac{L-\varepsilon}{1+\tau_s/\tau_r} \tag{5}$$

It can be seen that the position of zero shear, however, is not dependent on ε if it is defined by $\hat{y}_s$. From equation (2) and (5) we get

$$\hat{y}_s = \frac{\tau_s}{\Delta p/\Delta x} \cdot \tag{6}$$

The average velocities in the two zones were determined by numerical integration of the measured values between the respective walls and the zero shear stress line. At the rough wall the integration started at the rib tip or at the root depending on the measuring position.

The friction factors are calculated by

$$f_{r,s} = 2/\bar{u}^{+2}_{r,s} \tag{7}$$

with

$$\bar{u}^{+}_{r,s} = \frac{\bar{u}_{r,s}}{(\tau_{r,s}/\rho)^{1/2}} \tag{8}$$

The Reynolds numbers are given by

$$Re_{r,s} = \frac{\bar{u}_{r,s}\ 4\ \hat{y}_{r,s}}{\nu} \tag{9}$$

The experiments with single pins in annuli and with rod bundles are usually evaluated by the assumption of logarithmic velocity profiles near the smooth and rough wall with

$$u^+_s = A_s \ln y^+_s + B \tag{10}$$

and

$$u^+_r = A_r \ln (y_r/h) + R. \tag{11}$$

If the results of the present experiment are to be used in this way the profile parameters A_s,A_r,B and R must be determined from integral quantities. As described before /3-7/, the following conditions must be met:

$$\bar{u}_s = \frac{u_{\tau s}}{\hat{y}_s} \int_0^{\hat{y}_s} (A_s \ln y^+ + B)\,dy \tag{12}$$

$$\bar{u}_r = \frac{u_{\tau r}}{\hat{y}_r} \int_0^{\hat{y}_r} (A_r \ln \frac{y}{h} + R)\,dy \tag{13}$$

$$u_{s_{max}} = u_{r_{max}} \tag{14}$$

Integration of equation (12) and (13) for the flow in a plane channel yields

$$\bar{u}_s = u_{\tau s} \left[A_s \ln \left(\frac{\hat{y}_s u_{\tau s}}{\nu}\right) + B - A_s \right] \tag{15}$$

$$\bar{u}_r = u_{\tau r} \left[A_r \ln \left(\frac{\hat{y}_r}{h}\right) + R - A_r \right] \tag{16}$$

and equation (14) reads

$$\left[A_s \ln \left(\frac{\hat{y}_s u_{\tau s}}{\nu}\right) + B \right] u_{\tau s} = \left[A_r \ln \left(\frac{\hat{y}_r}{h}\right) + R \right] u_{\tau r} \tag{17}$$

with $\hat{y}_r = L - \varepsilon - \hat{y}_s$

Of the five variables A_s, B, A_r, R and ε, two must be preset the other three are determined by equations (15), (16) and (17). A presetting of the parameters ε and B has turned out to be most suitable.

5. Results

5.1 Velocity profiles

Figures 6.1 - 6.27 show all measured velocity profiles reduced with the respective maximum velocity. The position of the Pitot tube relative to the roughness ribs was varied and is given by the x/h-value. Values of x/h>0.5 represent measurements starting at the smooth wall between the ribs. The other measurements were taken above a rib. Most measurements were taken at the exact center of the channel and of a rib (z-position). The influence of the measuring position of the velocity distribution was especially large for narrow channel widths and the roughness with the highest friction factors (No.2). Here we get also different velocity distributions at the same x/h-position but different z-positions. This was verified by measuring the velocity at a fixed distance from the wall in z-direction (not shown). The level of turbulence at these measurements was extremely high, which made the measurements difficult because of the large fluctuations of the Pitot-readings. In figures 6.24-6.27 the velocity profiles of the channel with two rough walls are shown. The velocity distribution turned out to be exactly symmetrical, therefore only one half of the velocity profile was measured and is shown here twice. The velocity distribution at different relative roughness heights does not show a systematic variation. For some roughnesses it shows a tendency to become flatter with higher h/L-ratios, but this trend is reversed for other roughnesses. In order to check, whether there was an effect of the channel outlet, some measurements were performed 840 mm upstream instead of only 300 mm, but no difference was found.

5.2 Friction factors

The bulk friction factors were determined by

$$f_B = \frac{\Delta p}{\Delta x} \frac{(L-\varepsilon)}{\rho \bar{u}^2} \qquad (18)$$

with the bulk velocity $\bar{u}$ from integration of the velocity profiles and the axial pressure drop $\Delta p/\Delta x$. From the 12 differential pressures measured along the channel an average value was formed without the first four measurements at the entrance and the last one at the exit because of deviations from a linear pressure gradient.

Figure 7 shows the friction factors determined with $\varepsilon=0$, i.e. neglecting the volume of the roughness, as function of the relative roughness height. Plotted are the average values of all measurements at a certain channel width with the range of scatter. The large scatter stems mainly from the different bulk velocities due to different axial measuring positions. Since there is a lateral velocity variation due to the limited length of the roughness ribs, the integrated velocity at a certain traverse is different at different axial positions. This was not the case at two-dimensional roughnesses. As for other roughnesses the friction factor grows with increasing relative roughness height. But there is one distinctive difference to former measurements. The function $f=f(h/L)$ is not linear but has a maximum at a certain value of h/L for three roughnesses which were tested up to the highest h/L-ratio. This does not change if the friction factor of the rough zone f_r is plotted over the $h/\hat{y}_r$-ratio (Fig.8). Neither does another definition of the hydraulic diameter change this tendency. For the other extreme of $\varepsilon,\varepsilon=h$, the friction factors are lower but the maximum is even more pronounced (Fig.9). The maximum is reached at different $h/\hat{y}_r$-ratios for the different roughnesses; for the roughness with the highest friction factor it is reached at the lowest $h/\hat{y}_r$-ratio. At the highest $h/\hat{y}_r$-ratio all three

roughnesses have the same friction factor.

Because of this strange characteristics the roughness No.5 was tested with similar parameters as No.2 but with a smaller height. The agreement in the friction factors for the lower $h/\hat{y}_r$-ratios is very good, but this roughness does not show a maximum friction factor at a high $h/\hat{y}_r$-ratio. It could, however, not be tested up to the same $h/\hat{y}_r$-ratio.

Errors in measurements of pressures and velocities or in the integration of the velocity cannot account for this characteristics. It is also very unlikely that secondary flows can cause a difference in the friction factor by a factor of two, between the measured and the expected ones. Besides, secondary flows tend to increase the friction factors, rather than decrease them. The possible explanation, that the flow at the mid-plane is not uneffected by the short side walls, is not convincing since the aspect ratio at high h/L-ratios is also the highest. So, it can only be speculated about the reason for these results. It might be possible that due to the restricted flow cross section the dead water regions behind the ribs are changed in length, and a roughness which had a high friction factor at low relative roughness heights is no longer in the optimum range of the parameter field, but a different pitch would result in higher friction factors. No measurements at roughnesses, however, are known to the author, which yielded friction factors as high as the present ones. Measurements at single pins with three-dimensional roughness contained in different smooth tubes yielded friction factors which were increasing less than linear with increasing relative roughness height, but no maximum was found /9/. These friction factors were similar to those of roughness No.4.

The Reynolds number range of those measurements was large and the flow was in the fully rough regime at Reynolds numbers and h^+-values which were reached in the present experiment. The

highest friction factors obtained by Nikuradse /10/ with sand grain roughness are well below the present ones and are even lower than the highest friction factors obtained with two dimensional roughnesses /3,6,7,11/.

The results at high h/L-ratios cannot be generalized, more measurement would be necessary. So, the further discussion should be restricted mainly to the results for low h/L-ratios, up to h/L=0.08, especially for roughness No.5, where agreement with No.2 is good.

This roughness was tested with one wall rough and with both walls rough, i.e. a symmetrical rough channel. The friction factors of the rough zone should be the same for both cases at the same relative roughness height $h/\hat{y}_r$. However, this friction factor depends on the definition of the hydraulic diameter. The shear stress at the rough wall in the channel with one rough wall is given by equation (3),

$$\tau_r = (L-\varepsilon)\ \frac{\Delta p}{\Delta x} - \tau_s \ , \tag{3}$$

and for the channel with two rough walls it is

$$\tau_r = (\frac{L}{2}-\varepsilon)\ \frac{\Delta p}{\Delta x} \ . \tag{19}$$

Since the friction factor is

$$f_r = \frac{2(\tau_r/\rho)^{1/2}}{\bar{u}_r} \ , \tag{20}$$

and $\bar{u}_r$ is changed by the same amount in both cases if ε is changed, there must be one ε-value which produces the same friction factors for the asymmetrical and the symmetrical case.

Figure 10 shows the friction factor over the $h/\hat{y}_r$-ratio for different definitions of the hydraulic diameter.

Besides $\varepsilon=h$ and $\varepsilon=0$, there is a volumetric definition $\varepsilon=hb(1+g/e)/p$ and the definition $\varepsilon=-h$, which is physically absurd but which yields the same friction factors for both cases, the symmetrical and the asymmetrical flow. Experiments at two-dimensional roughnesses (p/h=7.7) had shown that the same friction factors are obtained with a volumetric definition ($\varepsilon=hb/p$).

From other experiments it is known that the friction factor of the smooth zone, f_s, increases due to the opposite roughness. Therefore the friction factor f_s reduced by the theoretical friction factor f_o of a smooth pipe at the same Reynolds number

$$1/f_o^{1/2} = 4 \log(Re_s \, f_o^{1/2}) - 0.4 \qquad (21)$$

was plotted over various parameters in figure 11-14.
In figure 11 the parameter is the ratio of the friction factors of the rough and the smooth zone. The relation from Warburton /12/ gives too low friction factor multipliers, which was already found for two-dimensional roughnesses /3,6,7/. A better relation would be

$$\frac{f_s}{f_{os}} = 1.025 + 0.008 \, \frac{f_r}{f_s} \qquad (22)$$

The relation from Warburton and Pirie /13/, which uses the parameter f_r/f_{or}, with f_{or} being the friction factor of a smooth tube at the Reynolds number of the rough zone, gives too high friction factor multipliers. Here the data are better correlated by

$$\frac{f_s}{f_{os}} = 1.036 + 0.004 \, \frac{f_r}{f_{or}} \, . \qquad (23)$$

The correlation

$$\frac{f_s}{f_{os}} = 1.056 + 0.062 \frac{h}{\hat{y}_s} \qquad (24)$$

which was found for two-dimensional roughnesses /3,6,7/ correlates the present data as well with a tolerable amount of scatter. Plotting f_s/f_{os} over $\log(h/\hat{y}_s)$ reduces the amount of scatter somewhat (Fig.14).

Since the correlation (24) using the roughness height and length of the smooth profile as parameter is the only one which is independent of the parameter ε and fits for both two-dimensional and three-dimensional roughnesses, it is regarded superior to the other two.

5.3 Logarithmic velocity profiles at the smooth wall

The mean velocity profiles near the smooth wall are plotted in figures 15.1-15.22 in non-dimensional form, together with a straight line representing the 'law of the smooth wall'

$$u^+ = A_s \ln y^+ + B \qquad (10)$$

with $A_s = 2.5$ and $B = 5.5$

Especially for the roughness No.2 the measured velocity profiles depart from this line already far from the maximum velocity, which is due to the large turbulent energy transfer from the rough zone. The line of zero shear stress and the position of maximum velocity lie extremely far apart. For this roughness the distance from the smooth surface to the position of maximum velocity was approximately 2 $\hat{y}_s$ for all channel widths.

The slope A_s of almost all measured profiles is lower than 2.5 while the parameter B is higher, both tendencies getting stronger for higher relative roughness heights.

The slope A_s calculated from integral quantities by equation (15) with B=5.5 is plotted in figure 16.

The correlation

$$A_s = 2.55 + 0.4 \; / \; \ln \; (0.1 \; \frac{h}{\hat{y}_s}) \qquad (25)$$

which was found for two-dimensional square roughnesses, fits quite well.

For a fixed slope of A_s=2.5, the resulting B-values would be in the range of $3.8 < B < 5.8$, decreasing with increasing $h/\hat{y}_s$ but with a relatively large amount of scatter (see B_{SA} in table 2).

5.4 The breakdown of the 'law of the rough wall'

Figures 17.1-17.27 show the non-dimensional profiles at the rough wall together with a line representing the 'law of the rough wall' with the slope A_r=2.5. The origin of the velocity profile was put at the root of the ribs (ε=0). No effect of the Reynolds number could be detected, but there is a strong effect of the measuring position for most roughnesses.

The big discrepancy between the measured velocity profiles and the 'law of the wall' is evident. Exept for some profiles for low relative roughness heights, it does not seem to be sensible to force a straight line through the points in order to define a slope A_r and the parameter R. All slopes would be less than 2.5 and some would be as low as 0.5. A displacement of the origin ε by several rib heights would be necessary in order to get a value of 2.5. There is no big difference between symmetric and asymmetric flow (Fig.17.21-17.27). Since the position of zero shear stress is far beyond the position of

maximum velocity a large region of the velocity field cannot lie on any straight line, and a discription of the flow by a law of the wall would be inadequate. Nevertheless, for the calculation of the flow in an asymmetrical channel some description of the velocity field is necessary. For lack of a better one, the logarithmic discription was used. The values of A_r and R were calculated by equation (16) and (17). Most values of A_r are between 0.5 and 1.5, but there is no systematic variation (see table 2). For roughness No.5 the average value is A_r=0.52.

From a plot $(2/f_r)^{1/2}$ versus $(\ln \frac{\hat{y}}{h} - 1)$ the parameters A_r and R can be obtained /14/. Figure 18 shows the result for roughness No.5. For symmetrical flow we get A_r=1.8 and for asymmetrical flow A_r=2.9.

6. Transformation of bulk data with different profile parameters

For the transformation of results from pressure drop measurements at rough rods in annular channels and the application of these transformed data on a bundle geometry it is important to know the errors which arise from using different velocity profile parameters.

Therefore the transformation was applied on the measurements with roughness No.5 (For a derivation of the transformation equations for parallel plates see /3/). Input data are the bulk friction factor and the bulk Reynolds number (table 2), a constant B=5.5 and the different values of A_s and A_r. For A_s, only A_s=2.5 and the correlation (25) was used. For A_r, the values 0.52,1.8,2.9 and 2.5 were used.

The calculated friction factors of the smooth and rough zone and the position of zero shear stress were compared to the experimentally determined results (1.line) and the difference in per cent is given in table 3. Also the calculated R-value is given. While the differences in the smooth friction factor are rather large, the error in the friction factor of the rough

zone is relatively small.

Even for the simple assumption of a constant A_s and A_r=2.5 the maximum error is only 4.75%. It is of interest, that a modification of A_s alone does not change the friction factor considerably. Exept for the extreme value of A_r=2.9 , where the errors in f_s and f_r are greatest, no constant R value is obtained.

7. Eddy viscosity

Calculations of turbulent flow are often based on semi-empirical turbulence models /16/, using the distribution of the eddy viscosity as an input parameter.

In analogy with the fluid viscosity ν an eddy viscosity ε in turbulent flow can be defined by

$$- \rho \overline{u'v'} = \rho \varepsilon \frac{\partial u}{\partial y}, \tag{26}$$

with $\overline{u'v'}$ as the time-mean correlation of the velocity fluctuations in the main direction of the flow (u') and in the direction normal to the wall (v'), u is the time-mean fluid velocity and y is coordinate normal to the wall.
In contrast to the viscosity ν the eddy viscosity ε is not a constant in the flow field. One of the models for the distribution of the eddy viscosity in smooth tubes which can be expressed explicitly was given by Reichardt /17/:

$$\frac{\varepsilon}{u_\tau R} = \frac{\kappa}{3} \left[1 - \left(\frac{R-y}{R}\right)^2\right] \left[\frac{1}{2} + \left(\frac{R-y}{R}\right)^2\right] \tag{27}$$

with κ = 0.4, R being the radius of the tube and u_τ the friction velocity.

If the turbulent shear stress is defined by equation (26) than the total shear stress is given by

$$\tau = \rho \, (\varepsilon + \nu) \, \frac{\partial u}{\partial y} \tag{28}$$

The assumption of a linear variation of the shear stress in a plane channel

$$\frac{\tau}{\tau_w} = 1 - \frac{y}{\hat{y}} \tag{29}$$

together with (28) leads to the relation

$$\varepsilon^+ = \frac{\varepsilon}{u_\tau \hat{y}} = \left[\frac{1-y/\hat{y}}{\partial u^+ / \partial (y/\hat{y})} - \frac{\nu}{\hat{y} u_\tau} \right] \tag{30}$$

where ε^+ is the nondimensional eddy viscosity. In asymmetrical flow the friction velocities $u_{\tau s}$ and $u_{\tau r}$ and the lengths of the smooth ($\hat{y}_s$) and rough ($\hat{y}_r$) velocity profiles in the respective zones are used to evaluate ε_s^+ and ε_r^+. The eddy viscosity was determined at discrete positions where velocity measurements were taken.

For roughness No.5 the non-dimensional eddy viscosity ε^+ is shown in figure 19 for the smooth zones and in figure 20 for the respective rough zones versus the non-dimensional distance $(y/\hat{y})_{s,r}$ from the wall. For comparison with the smooth tube data the line according to equation (27) is added in the figures.

The eddy viscosity distributions of the smooth zones look similar. Compared to the smooth tube values they are higher in the center of the smooth zone by approximately 50% and decrease towards zero close to the zero shear stress line. In this region the scatter is large due to the low velocity gradient which approaches zero.

There are however differences close to the wall depending on the channel width. At large channel widths the data measured close to the smooth wall are coincident with the smooth tube results. At narrow channel widths which corresponds to a large relative roughness height the data very close to the wall are below the smooth tube results and show a steep increase. Looking for possible errors in measurement or evaluation there are two facts which might cause errors. The outer diameter of the Pitot tube which was used was 0.6 mm. This is 1/6 of the length of the smooth zone in figure 20.4. The measuring position was defined by $y = y_c + 0.15\ d_{Pitot}$ according to Mac Millan, with y_c being the position of the Pitot tube center. The measurements close to the wall were taken in steps of 0.1 mm and were evaluated at the position half-way between two points taking their difference of u^+ and y for equation (30). Taking a close look at the data, it does not seem possible that these facts can account for the deviation of the eddy viscosity from the smooth tube results. The measurements in a rectangular water channel with one rough wall /11/ showed similar results. Higher values far from the wall were also reported by Rehme /18/, which were obtained in a subchannel of a rod bundle.

The distribution of the eddy viscosity in the rough zone shows a large deviation of that in the smooth zone. Although the scatter of the points is large, it is obvious that the eddy diffusivity is much higher for these three-dimensional roughnesses than for two-dimensional roughnesses as reported in /11/ and /19/. There are no points near $y/\hat{y}=1.0$ because the maximum velocity is reached already at lower $y/\hat{y}$ values.

8. Conclusion

The investigation on three-dimensional roughnesses gave the following results:

1. Three-dimensional roughnesses produce very high friction factors, higher ones than ever measured before.

2. The friction factor does not raise linearly with increasing relative roughness height, but shows a maximum value.

3. There is no agreement between the friction factors in symmetrical and asymmetrical flow at the same relative roughness height, unless the hydraulic diameter is defined with a negative ε.

4. The non-coincidence of the position of zero shear stress and that of maximum velocity is more pronounced than for two-dimensional roughness.

5. The slope of the non-dimensional velocity profile at the smooth wall is lowered by the roughness opposite, which means higher friction factors. The correlation, which was found for two-dimensional roughnesses describes also the present results.

6. The 'law of the rough wall' does not hold for the description of the rough velocity profiles.

7. The transformation of bulk data with profile parameters as they were used up to now, result in friction factors up to 20% too low for the smooth zone and up to 5% too high for the rough zone for roughness heights smaller than 10% of the channel width.

Acknowledgement

The author wishes to thank Mr. K. Ghezel-Ahmadi and Mr. K. Schorb for their help with the performance of the experiments and the preparation of diagramms.

Nomenclature

A	slope of the logarithmic velocity profile
B	constant of the logarithmic velocity profile at smooth walls;
b	width of the roughness rib (m)
d_h	hydraulic diameter (m)
e	length (z-direction) of a rib (m)
f	friction factor = $2\tau/\rho u^2$
f_o	friction factor of a smooth tube
g	gap (z-direction) between two ribs (m)
h	height of roughness rib (m)
h^+	dimensionless height of roughness rib = $h\ u_\tau/\nu$
L	width of channel (m)
p	axial pitch of the repeated roughness rib (m)
p	pressure (Nm^{-2})
u	mean velocity (ms^{-1})
u_τ	friction velocity = $(\tau/\rho)^{1/2}$ (ms^{-1})
u^+	dimensionless velocity = u/u_τ
$\bar{u}$	average velocity in a section (ms^{-1})
R	parameter of the logarithmic velocity profile at rough walls

Re	Reynolds number = $\bar{u}d_h/\nu$
x	axial distance
y	distance normal to the wall
y^+	dimensionless distance from the wall = yu_τ/ν
$\hat{y}$	position of the zero shear stress line, length of respective zones
z	distance parallel to the wall normal to the flow

Greek symbols

ε	displacement of the origin of the velocity profile at rough walls (m)
ν	kinematic viscosity (m^2s^{-1})
ρ	density (kgm^{-3})
τ	shear stress (Nm^{-2})

Subscripts

max	maximum
r	at the rough wall or pertaining to the rough zone
s	at the smooth wall or pertaining to the smooth zone
vol	volumetric definition of origin of velocity profile

References

/1/ M. Dalle Donne and E. Meerwald:
Alternate Studs: A new type of artificial roughness to improve the performance of a Gas-Cooled Reactor, ANS Trans. 15 (2), 846-847 (1972)

/2/ M. Dalle Donne and L. Meyer:
Experimental heat transfer and pressure drop at rods with three-dimensional roughnesses in annuli OECD-NEA Coordinating Group on GCFR Development, Heat Transfer Specialist Meeting, Petten, Holland (1975)

/3/ L. Meyer:
Turbulente Strömung an Einzel- und Mehrfachrauhigkeiten im Plattenkanal, KfK-Bericht Nr. 2764 (1979)

/4/ L. Meyer and L. Vogel:
The velocity distribution and pressure loss at artificial roughnesses with sharp and rounded edges, Kernforschungszentrum Karlsruhe, KfK-Report 2885 (1979)

/5/ L. Meyer:
Flow resistance of rectangular roughnesses with varying density, OECD-NEA Coordinating Group on Gas-Cooled Fast Reactor Development, 5th Heat Transfer Specialists Meeting, Würenlingen, (1979)

/6/ L. Meyer:
Pressure and velocity distribution in a plane channel having one or two rough walls. OECD-NEA, 5th Specialists Meeting on GCFR heat transfer, Würenlingen, Schweiz (1979)

/7/ L. Meyer:
Turbulent flow in a plane channel having one or two rough walls. Int. J. Heat Mass Transfer, 23 (5), 591-608 (1980)

/8/ F.A. Mac Millan:
Experiments on Pitot-tubes in shear flow, ARC RM No.3028, London (1956)

/9/ L. Meyer:
Pressure drop and heat transfer experiments at single rods roughened with three-dimensional roughness, (to be published)

/10/ J. Nikuradse:
Strömungsgesetze in rauhen Rohren, Forschungshefte VDI, 361, (1933), also NACA TM 1292 (1950)

/11/ W. Baumann:
Geschwindigkeitsverteilung bei turbulenter Strömung an rauhen Wänden, KfK-Bericht Nr. 2618 (1978) und Nr. 2680 (1978)

/12/ C. Warburton:
The interpretation of tests on roughened pins in rough channels and the prediction of cluster pressure drop from single-pin data, CEGB RD/B/N 2930, Berkeley Nucl. Labs. (1974)

/13/ C. Warburton, M.A.M. Pirie:
An improved method for analysing heat transfer and pressure drop tests on roughened rods in smooth channels CEGB RD/B/N 2621, Berkeley Nucl. Labs. (1973)

/14/ S.A. Hodge, J.P. Sanders and D.E. Klein:
Slope and intercept of the dimensionless velocity profile for artificially roughened surfaces, Int. J. Heat Mass Transfer, 23, 135-140 (1980)

/15/ V.C. Patel:
Calibration of the Preston tube and limitation on its use in pressure gradients, J. Fluid Mechanics, 23 (1), 185-208 (1965)

/16/ R.J. Firth:
A method for analysing heat transfer and pressure drop data obtained from partially roughened annular channels, OECD-NEA 5th Heat Transfer Specialists Meeting, Würenlingen, Schweiz (1979)

/17/ M. Reichardt:
Vollständige Darstellung der turbulenten Geschwindigkeitsverteilung in glatten Leitungen ZAMM 31,7,208-219 (1951)

/18/ K. Rehme:
The structure of turbulent flow through a wall subchannel of a rod bundle with roughened rods. KfK-Report 2716 (1978)

/19/ L. Meyer:
Eddy viscosity in a plane channel with two-dimensional roughness. (unpublished)

No	p	h	e	p/h	g/e	h/L
1	35	10.4	60	3.37	0.5	0.050/0.077/0.122
2	25	10.4	40	2.40	1.0	0.050/0.065/0.077/0.095/0.122/0.173
3	35	10.4	40	3.37	1.25	0.049/0.065/0.095/0.122/0.172
4	32	10.2	60	3.14	0.783	0.049/0.076/0.120/0.170
5	15	6.1	30	2.46	1.0	0.029/0.045/0.072/0.100
5	same parameters, but both walls rough					

Table 1: Geometrical parameters of the roughnesses and channel

No.	p/h	h/b	g/e	h/L	$\hat{y}_s/L$	$\hat{y}_r/L$	$h/\hat{y}_r$	$h/\hat{y}_s$	$\bar{u}$	$\bar{u}_r$	$\frac{u_s}{u_r}$	$\frac{u_{max}}{\bar{u}}$	h^+	$Re_{10^{-3}}$	f	f_s	$Re_{s\ 10^{-3}}$	f_r	$Re_{r\ 10^{-3}}$	f_r/f_s	f_r/f_{or}	f_s/f_{os}	B=5.5 eq.(15-17) A_s	A_r	B	A_{s_B}=2.5
1A	3.37	1.0	0.50	.050	.114	.886	.056	0.440	17.39	17.27	1.059	1.23	1630	458	.02144	.00468	109	.0409	807	8.74	13.55	1.061	2.45	1.29	4.57	5.19
2A	3.37	1.0	0.50	.050	.110	.890	.056	0.453	24.11	23.96	1.054	1.22	2193	623	.02103	.00448	144	.04011102		8.95	14.01	1.074	2.43	1.24	4.73	5.02
3Z	3.37	1.0	0.50	.050	.111	.889	.056	0.450	21.07	20.98	1.038	1.20	1902	546	.02092	.00454	125	.0392	967	8.62	13.37	1.058	2.45	1.14	5.01	5.21
4Z	3.37	1.0	0.50	.050	.121	.879	.057	0.413	12.85	12.73	1.078	1.24	1206	335	.02171	.00501	86	.0422	584	8.43	13.18	1.080	2.42	1.43	4.21	5.01
5A	3.37	1.0	0.50	.077	.089	.911	.086	0.874	22.31	22.13	1.092	1.24	2634	374	.03321	.00542	72	.0658	676	12.14	21.10	1.125	2.34	1.24	3.71	4.58
6Z	3.37	1.0	0.50	.077	.091	.909	.086	0.859	24.53	24.43	1.042	1.20	2689	405	.03032	.00534	76	.0579	734	10.85	18.85	1.122	2.35	0.99	4.44	4.61
7Z	3.37	1.0	0.50	.077	.091	.909	.086	0.863	27.36	27.26	1.038	1.21	2977	454	.02818	.00520	85	.0562	826	10.81	18.66	1.118	2.36	0.97	4.56	4.63
8Z	3.37	1.0	0.50	.077	.093	.907	.086	0.839	19.98	19.94	1.026	1.18	2194	333	.03015	.00556	63	.0569	603	10.23	17.89	1.122	2.35	0.91	4.61	4.63
9Z	3.37	1.0	0.50	.077	.088	.912	.086	0.885	31.79	31.70	1.033	1.18	3431	520	.03005	.00520	94	.0572	946	11.01	19.45	1.142	2.32	0.92	4.58	4.38
10Z	3.37	1.0	0.50	.122	.065	.935	.134	1.920	24.44	24.59	0.905	1.12	3262	258	.04259	.00685	30	.0804	485	11.75	24.31	1.172	2.27	0.13	4.86	4.32
11Z	3.37	1.0	0.50	.122	.069	.931	.135	1.818	20.35	20.37	0.985	1.22	2937	216	.04320	.00715	29	.0937	403	13.10	27.37	1.211	2.21	0.53	4.09	4.01
12A	3.37	1.0	0.50	.122	.065	.935	.134	1.927	19.88	19.97	0.928	1.16	2748	208	.04421	.00712	25	.0881	391	12.37	25.58	1.163	2.28	0.26	4.51	4.44
13A	3.37	1.0	0.50	.122	.068	.932	.134	1.842	21.03	21.20	0.887	1.13	2737	224	.03846	.00693	27	.0747	421	10.77	21.99	1.153	2.30	0.03	5.14	4.50
14Z	2.40	1.0	1.00	.050	.082	.918	.054	0.612	16.88	16.93	0.962	1.13	1823	431	.02933	.00546	68	.0568	795	10.39	18.73	1.118	2.36	0.47	5.03	4.66
15Z	2.40	1.0	1.00	.050	.082	.918	.055	0.607	9.18	9.22	0.947	1.12	1072	247	.03110	.00595	38	.0595	456	10.00	17.78	1.075	2.43	0.42	4.90	5.15
16Z	2.40	1.0	1.00	.050	.080	.920	.054	0.627	18.52	18.69	0.886	1.08	1916	475	.02761	.00563	67	.0509	883	9.05	17.12	1.151	2.30	-0.04	6.34	4.35
17A	2.40	1.0	1.00	.050	.079	.921	.054	0.629	14.26	14.39	0.888	1.09	1533	373	.02844	.00581	53	.0531	692	9.14	17.11	1.127	2.34	0.00	6.13	4.62
18A	2.40	1.0	1.00	.065	.079	.921	.071	0.838	9.98	9.93	1.058	1.20	1360	202	.04238	.00638	33	.0838	372	13.13	24.12	1.116	2.36	0.97	3.29	4.79
19A	2.40	1.0	1.00	.065	.079	.921	.072	0.832	9.91	9.87	1.050	1.19	1338	203	.04086	.00628	33	.0806	372	12.83	23.20	1.098	2.39	0.95	3.43	4.96
20A	2.40	1.0	1.00	.065	.082	.918	.072	0.807	18.53	18.48	1.027	1.17	2260	378	.03394	.00557	63	.0661	693	11.87	21.29	1.122	2.35	0.85	4.11	4.63
21A	2.40	1.0	1.00	.065	.081	.919	.072	0.817	18.83	18.82	1.006	1.16	2229	376	.03346	.00560	61	.0647	692	11.55	20.83	1.120	2.35	0.73	4.36	4.66
22Z	2.40	1.0	1.00	.077	.068	.932	.084	1.143	9.75	9.67	1.120	1.25	1624	171	.05853	.00700	26	.1195	316	17.08	33.35	1.152	2.30	1.12	2.44	4.52
23Z	2.40	1.0	1.00	.077	.067	.933	.084	1.169	15.58	15.47	1.105	1.24	2459	271	.05366	.00641	39	.1091	502	17.04	33.18	1.164	2.28	1.06	2.71	4.33
24A	2.40	1.0	1.00	.077	.069	.931	.084	1.126	9.08	8.96	1.202	1.32	1613	157	.06657	.00725	26	.1401	289	19.34	38.48	1.193	2.24	1.37	1.75	4.19
25A	2.40	1.0	1.00	.077	.068	.932	.084	1.147	14.61	14.44	1.173	1.29	2467	256	.05973	.00659	40	.1239	472	18.80	37.25	1.203	2.22	1.30	2.10	4.01
26Z	2.40	1.0	1.00	.095	.062	.938	.103	1.564	8.80	8.73	1.124	1.27	1647	125	.07339	.00782	17	.1507	233	19.26	39.71	1.165	2.28	1.04	2.32	4.49
27Z	2.40	1.0	1.00	.095	.059	.941	.102	1.643	14.35	14.23	1.136	1.28	2627	200	.07302	.00724	26	.1500	374	20.72	43.23	1.197	2.23	1.05	2.30	4.15
28Z	2.40	1.0	1.00	.095	.060	.940	.102	1.616	12.00	11.90	1.135	1.27	2188	167	.07285	.00736	22	.1494	312	20.30	41.62	1.170	2.27	1.07	2.30	4.40
29A	2.40	1.0	1.00	.095	.044	.936	.103	1.512	8.12	8.00	1.239	1.36	1618	112	.08525	.00814	17	.1834	207	22.54	47.24	1.216	2.20	1.36	1.57	4.10
30A	2.40	1.0	1.00	.095	.059	.941	.102	1.624	12.89	12.69	1.270	1.40	2596	176	.08826	.00757	26	.1935	325	25.58	54.33	1.246	2.15	1.41	1.41	3.77
31A	2.40	1.0	1.00	.095	.060	.940	.103	1.602	10.60	10.43	1.276	1.41	2180	145	.09110	.00784	22	.1993	269	25.42	53.98	1.239	2.16	1.42	1.35	3.87
32Z	2.40	1.0	1.00	.122	.056	.944	.133	2.233	10.78	10.76	1.025	1.21	2041	119	.07487	.00844	13	.1490	225	17.67	38.99	1.186	2.25	0.64	3.01	4.38
33Z	2.40	1.0	1.00	.122	.055	.945	.133	2.276	13.92	13.91	1.018	1.20	2545	151	.07242	.00811	16	.1441	285	17.77	39.47	1.202	2.22	0.60	3.11	4.21
34Z	2.40	1.0	1.00	.173	.067	.933	.192	2.674	16.82	16.93	0.903	1.18	2423	124	.04809	.00818	15	.0927	233	11.33	24.44	1.180	2.26	0.16	4.54	4.40
35Z	2.40	1.0	1.00	.173	.066	.934	.192	2.718	20.46	20.58	0.916	1.18	2881	148	.04736	.00775	18	.0919	279	11.86	25.07	1.168	2.28	0.21	4.53	4.46
36Z	3.37	1.0	1.25	.049	.136	.864	.058	0.366	11.64	11.68	0.978	1.17	967	318	.01554	.00489	84	.0297	551	6.08	9.20	1.050	2.47	0.80	6.71	5.33
37Z	3.37	1.0	1.25	.049	.133	.867	.057	0.373	14.94	14.97	0.982	1.17	1221	403	.01634	.00471	106	.0295	701	6.26	9.51	1.060	2.45	0.81	6.73	5.21
38Z	3.37	1.0	1.25	.049	.136	.864	.058	0.366	18.07	18.06	1.002	1.17	1452	484	.01606	.00455	131	.0291	837	6.39	9.69	1.070	2.43	0.98	6.47	5.06
39A	3.37	1.0	1.25	.049	.138	.862	.058	0.361	14.92	14.94	0.990	1.18	1202	402	.01573	.00468	109	.0287	695	6.14	9.26	1.061	2.45	0.89	6.69	5.19
40Z	3.37	1.0	1.25	.065	.130	.870	.075	0.504	17.75	17.71	1.017	1.19	1566	366	.01857	.00494	96	.0342	636	6.91	10.84	1.091	2.40	1.05	5.98	4.89
41Z	3.37	1.0	1.25	.065	.136	.864	.076	0.483	13.84	13.78	1.033	1.20	1213	284	.01862	.00504	79	.0343	488	6.80	10.38	1.067	2.44	1.22	5.71	5.16
42Z	3.37	1.0	1.25	.065	.126	.874	.075	0.522	21.86	21.84	1.006	1.18	1878	441	.01833	.00479	111	.0338	771	7.05	11.08	1.088	2.40	0.96	6.17	4.90
43A	3.37	1.0	1.25	.065	.127	.873	.075	0.515	17.76	17.72	1.019	1.19	1549	356	.01884	.00497	92	.0354	620	7.12	11.18	1.086	2.41	1.06	5.83	4.94
44Z	3.37	1.0	1.25	.095	.101	.899	.106	0.945	13.82	13.77	1.037	1.18	1583	194	.03105	.00614	40	.0586	347	9.54	16.65	1.122	2.35	1.00	4.60	4.71
45Z	3.37	1.0	1.25	.095	.098	.902	.106	0.974	17.63	17.57	1.034	1.18	1984	244	.03074	.00592	49	.0582	438	9.82	17.25	1.130	2.34	0.97	4.65	4.60
46Z	3.37	1.0	1.25	.095	.096	.904	.106	1.000	21.95	21.87	1.037	1.18	2462	305	.03008	.00562	60	.0571	550	10.17	17.66	1.121	2.35	0.99	4.69	4.66
47A	3.37	1.0	1.25	.095	.100	.900	.106	0.959	17.06	16.92	1.085	1.23	2002	239	.03105	.00584	51	.0620	427	10.61	18.30	1.125	2.35	1.26	4.11	4.64
48Z	3.37	1.0	1.25	.122	.083	.917	.135	1.497	11.48	11.35	1.145	1.29	1696	122	.05230	.00712	22	.1037	221	14.57	27.03	1.135	2.33	1.34	3.05	4.69
49Z	3.37	1.0	1.25	.122	.082	.918	.135	1.498	14.54	14.37	1.143	1.28	2092	153	.04992	.00683	28	.0991	279	14.53	27.03	1.150	2.31	1.33	3.15	4.52
50A	3.37	1.0	1.25	.122	.082	.918	.135	1.514	13.65	13.45	1.182	1.33	2120	149	.05140	.00692	28	.1088	270	15.72	29.47	1.162	2.28	1.46	2.82	4.42

Table 2: Results evaluated with volumetric definition of the hydraulic diameter.

No.	p/h	h/b	g/e	h/L	$\bar{y}_s/L$	$\bar{y}_r/L$	$h/\bar{y}_r$	$h/\bar{y}_s$	$\bar{u}$	$\bar{u}_r$	$\frac{u_s}{u_r}$	$\frac{u_{max}}{\bar{u}}$	h^+	$Re\ 10^{-3}$	f	f_s	$Re_s\ 10^{-3}$	f_r	$Re_r\ 10^{-3}$	f_r/f_s	f_r/f_{or}	f_s/f_{os}	B=5.5 eq.(15-17) A_s	A_r	R	A_s=2.5 B
51Z	3.37	1.0	1.25	.172	.085	.915	.192	2.075	10.57	10.50	1.085	1.29	1603	81	.05012	.00791	14	.1004	148	12.70	24.21	1.136	2.33	1.09	3.76	4.75
52Z	3.37	1.0	1.25	.172	.085	.915	.192	2.076	16.38	16.20	1.131	1.32	2423	124	.04923	.00727	23	.1003	225	13.80	26.24	1.168	2.28	1.28	3.64	4.40
53Z	3.37	1.0	1.25	.172	.084	.916	.192	2.091	21.94	21.83	1.060	1.26	3016	166	.04403	.00699	29	.0854	303	12.21	23.67	1.187	2.25	0.97	4.21	4.21
54A	3.37	1.0	1.25	.172	.085	.915	.192	2.065	16.03	15.82	1.155	1.34	2435	123	.04733	.00721	23	.1032	222	14.31	26.94	1.164	2.28	1.38	3.51	4.44
55Z	3.14	0.6	0.78	.049	.130	.870	.057	0.378	19.42	19.41	1.006	1.18	1526	497	.01714	.00459	130	.0310	865	6.75	10.38	1.078	2.42	0.99	6.19	4.98
56Z	3.14	0.6	0.78	.049	.134	.866	.057	0.369	13.33	13.33	0.998	1.17	1069	350	.01694	.00475	93	.0306	607	6.45	9.64	1.040	2.49	0.96	6.28	5.43
57Z	3.14	0.6	0.78	.049	.132	.868	.057	0.375	16.54	16.55	0.996	1.17	1311	430	.01693	.00465	112	.0305	748	6.54	9.95	1.061	2.45	0.92	6.39	5.19
58A	3.14	0.6	0.78	.049	.132	.868	.057	0.374	16.75	16.74	1.005	1.18	1346	438	.01704	.00467	116	.0310	761	6.65	10.17	1.070	2.43	0.98	6.19	5.08
59Z	3.14	0.6	0.78	.076	.117	.883	.088	0.664	15.34	15.27	1.042	1.18	1472	256	.02397	.00538	62	.0443	451	8.24	13.22	1.080	2.42	1.16	5.05	5.05
60Z	3.14	0.6	0.78	.076	.114	.886	.087	0.677	18.96	18.88	1.037	1.17	1824	318	.02405	.00530	75	.0443	561	8.35	13.73	1.109	2.37	1.10	5.14	4.74
61Z	3.14	0.6	0.78	.076	.110	.890	.087	0.704	22.90	22.83	1.031	1.17	2181	383	.02363	.00507	86	.0436	680	8.60	13.99	1.092	2.40	1.05	5.26	4.89
62A	3.14	0.6	0.78	.076	.112	.888	.087	0.693	19.34	19.26	1.036	1.18	1835	320	.02368	.00519	73	.0443	566	8.55	13.77	1.080	2.42	1.10	5.13	5.03
63Z	3.14	0.6	0.78	.120	.083	.917	.136	1.498	16.47	16.50	0.975	1.13	1991	168	.03895	.00682	27	.0715	309	10.48	19.89	1.137	2.33	0.57	4.72	4.64
64Z	3.14	0.6	0.78	.120	.086	.914	.136	1.447	21.04	21.09	0.973	1.12	2470	216	.03677	.00668	36	.0671	395	10.04	19.52	1.188	2.24	0.54	4.93	4.15
65A	3.14	0.6	0.78	.120	.082	.918	.136	1.512	18.28	18.30	0.981	1.15	2254	190	.03766	.00672	30	.0721	349	10.73	20.52	1.152	2.30	0.59	4.68	4.49
66Z	3.14	0.6	0.78	.170	.077	.923	.194	2.320	11.81	11.83	0.985	1.24	1619	84	.04122	.00787	12	.0912	156	11.58	22.19	1.088	2.42	0.63	4.28	5.17
67Z	3.14	0.6	0.78	.170	.074	.926	.194	2.428	23.04	23.07	0.978	1.24	3012	162	.03891	.00714	23	.0857	300	12.00	23.68	1.145	2.31	0.55	4.48	4.59
68A	3.14	0.6	0.78	.170	.078	.922	.195	2.299	20.14	20.32	0.887	1.11	2393	141	.03656	.00751	19	.0699	263	9.30	18.84	1.157	2.29	0.06	5.31	4.53
69Z	2.46	1.0	1.00	.100	.052	.948	.108	1.958	14.12	14.20	0.887	1.20	1395	107	.06048	.00893	10	.1272	204	14.25	32.67	1.156	2.30	0.09	3.85	4.67
70Z	2.46	1.0	1.00	.100	.061	.939	.109	1.686	17.41	17.45	0.965	1.20	1650	133	.05546	.00810	15	.1166	250	14.40	31.15	1.176	2.26	0.43	3.62	4.42
71Z	2.46	1.0	1.00	.100	.064	.936	.109	1.603	21.25	21.30	0.962	1.18	1874	159	.05073	.00775	19	.1051	298	13.57	29.04	1.191	2.24	0.42	3.85	4.26
72A	2.46	1.0	1.00	.100	.060	.940	.109	1.702	18.26	18.35	0.918	1.14	1648	138	.05437	.00810	15	.1067	262	13.18	28.75	1.172	2.27	0.22	4.06	4.46
73Z	2.46	1.0	1.00	.072	.068	.932	.078	1.065	17.20	17.30	0.913	1.13	1357	185	.04037	.00706	23	.0802	346	11.35	22.78	1.131	2.34	0.20	4.69	4.72
74Z	2.46	1.0	1.00	.072	.065	.935	.078	1.127	21.03	21.15	0.913	1.13	1671	228	.04007	.00664	27	.0801	429	12.05	23.66	1.104	2.39	0.19	4.70	4.94
75Z	2.46	1.0	1.00	.072	.070	.930	.078	1.043	24.75	24.86	0.937	1.13	1884	262	.03919	.00659	34	.0771	490	11.70	23.35	1.159	2.29	0.31	4.62	4.41
76A	2.46	1.0	1.00	.072	.066	.934	.078	1.110	21.72	21.87	0.893	1.11	1662	234	.03895	.00658	27	.0747	441	11.35	22.20	1.100	2.39	0.08	5.05	4.97
77Z	2.46	1.0	1.00	.045	.101	.899	.051	0.453	12.14	12.18	0.971	1.13	764	213	.02608	.00581	41	.0489	385	8.42	14.17	1.068	2.45	0.63	5.14	5.21
78Z	2.46	1.0	1.00	.045	.099	.901	.051	0.461	17.69	17.73	0.978	1.13	1134	318	.02596	.00558	61	.0487	574	8.73	15.18	1.118	2.36	0.64	5.13	4.68
79Z	2.46	1.0	1.00	.045	.095	.905	.050	0.482	23.25	23.28	0.984	1.14	1445	405	.02570	.00526	75	.0487	735	9.27	15.87	1.102	2.38	0.67	5.08	4.80
80A	2.46	1.0	1.00	.045	.100	.900	.051	0.458	17.92	17.97	0.970	1.12	1120	317	.02584	.00561	61	.0478	572	8.52	14.88	1.123	2.35	0.59	5.30	4.63
81Z	2.46	1.0	1.00	.029	.114	.886	.033	0.256	14.12	14.20	0.948	1.17	723	374	.01882	.00496	81	.0347	667	6.99	11.10	1.056	2.46	0.49	6.41	5.27
82Z	2.46	1.0	1.00	.029	.115	.885	.033	0.253	19.57	19.68	0.954	1.16	998	520	.01857	.00490	115	.0342	926	6.98	11.59	1.123	2.35	0.50	6.45	4.53
83Z	2.46	1.0	1.00	.029	.117	.883	.033	0.249	9.84	9.90	0.948	1.17	515	268	.01875	.00508	60	.0344	476	6.77	10.36	1.012	2.55	0.53	6.34	5.78
84A	2.46	1.0	1.00	.029	.117	.883	.033	0.249	14.37	14.47	0.942	1.15	724	382	.01853	.00500	84	.0334	679	6.69	10.74	1.073	2.43	0.44	6.68	5.09
1Z	2.46	1.0	1.00	.101					11.11			1.36	1225													
2Z	2.46	1.0	1.00	.101					13.93			1.35	1511													
3Z	2.46	1.0	1.00	.101					17.02			1.36	1759													
4A	2.46	1.0	1.00	.101					15.50			1.21	1495													
					roughness No.5																					
5Z	2.46	1.0	1.00	.071					11.79			1.28	1144													
6Z	2.46	1.0	1.00	.071					13.53			1.29	1310													
7Z	2.46	1.0	1.00	.071					16.89			1.28	1613													
8A	2.46	1.0	1.00	.071	on both wide walls				14.32			1.22	1310													
9Z	2.46	1.0	1.00	.045					12.37			1.15	963													
10Z	2.46	1.0	1.00	.045					18.67			1.14	1402													
11Z	2.46	1.0	1.00	.045					23.18			1.14	1745													
12A	2.46	1.0	1.00	.045					18.92			1.12	1402													
13Z	2.46	1.0	1.00	.029					9.03			1.17	624													
14Z	2.46	1.0	1.00	.029					12.84			1.17	890													
15Z	2.46	1.0	1.00	.029					15.40			1.16	1069													
16A	2.46	1.0	1.00	.029					13.02			1.16	888													

Table 2 cont.

h/L	A_s	A_R	R	Δf_s (%)	Δf_r (%)	$\Delta h/\hat{Y}_r$ (%)
	2.43	0.55	6.26	—	—	—
	2.43	0.52	6.33	0.18	-0.01	-0.09
	2.43	1.8	2.80	-7.29	1.61	3.20
0.029	2.43	2.9	0.50	-11.05	3.77	5.43
	2.43	2.5	1.55	-9.41	2.66	4.39
	2.5	2.5	1.53	-12.21	3.02	3.81
	2.38	0.74	4.83	—	—	—
	2.38	0.52	5.27	1.63	-0.13	-0.44
	2.38	1.8	2.35	-7.49	1.67	2.59
0.045	2.38	2.9	0.44	-11.90	4.14	4.67
	2.38	2.5	1.31	-10.01	2.87	3.71
	2.5	2.5	1.28	-14.69	3.25	2.93
	2.31	0.33	4.40	—	—	—
	2.31	0.52	4.11	-1.92	0.09	0.36
	2.31	1.8	1.83	-13.39	2.39	3.36
0.072	2.31	2.9	0.35	-18.63	5.60	5.45
	2.31	2.5	1.02	-16.40	3.95	4.48
	2.5	2.5	0.99	-22.83	4.22	3.51
	2.26	0.52	3.36	—	—	—
	2.26	0.52	3.36	0.0	0.0	0.0
	2.26	1.8	1.55	-14.41	2.82	2.96
0.100	2.26	2.9	0.38	-20.61	6.83	5.07
	2.26	2.5	0.92	-17.99	4.75	4.09
	2.5	2.5	0.89	-25.71	4.82	3.04

Table 3: Comparison of friction factors evaluated with different parameters for roughness No.5

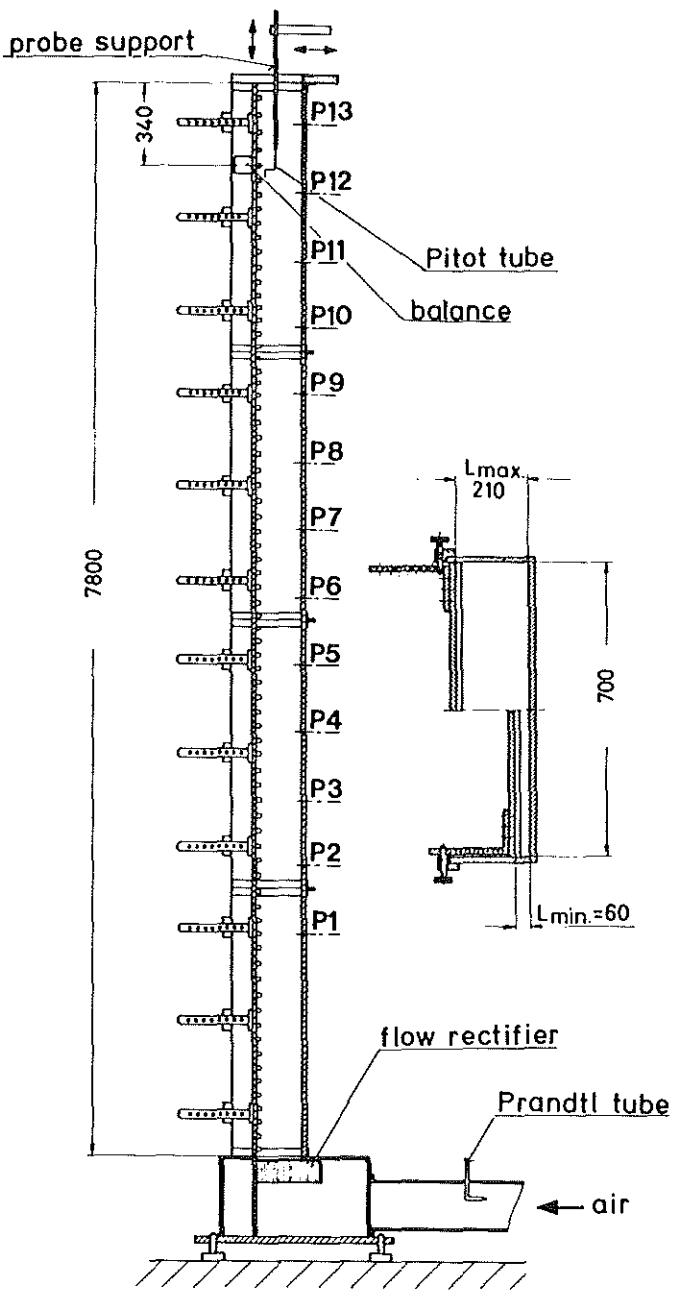

Fig. 1. The test section.

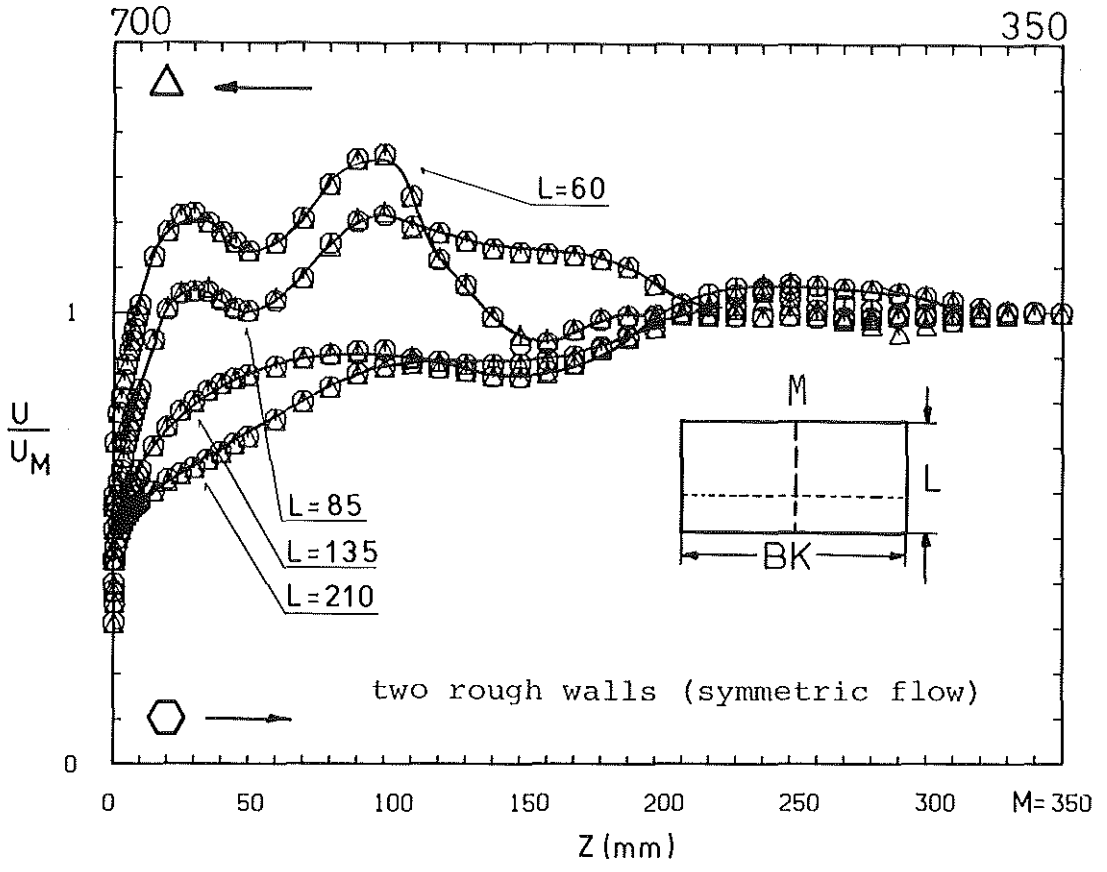

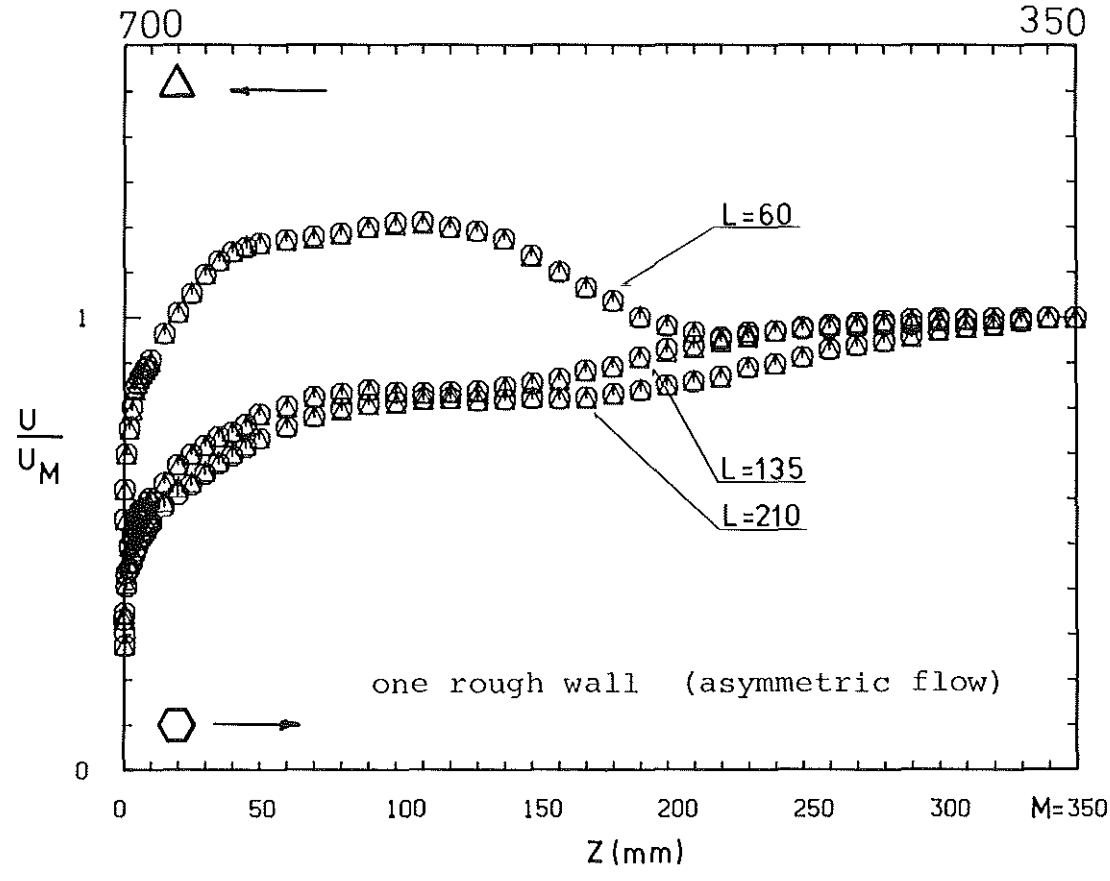

Fig.2: Velocity profiles parallel to the rough wall

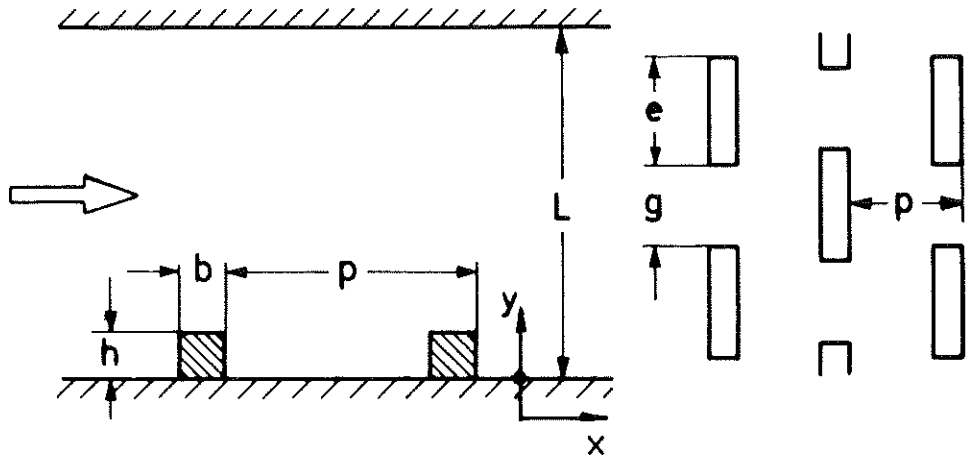

Fig. 3.a: Roughness geometry of No.1,2,3 and 5

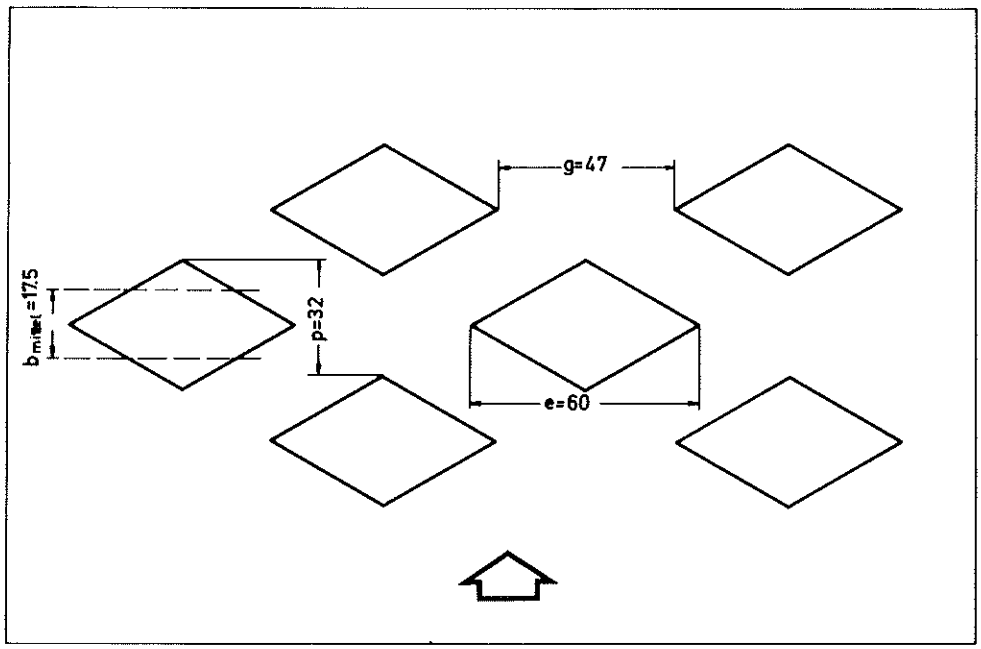

Fig.3.b: Roughness geometry of No.4

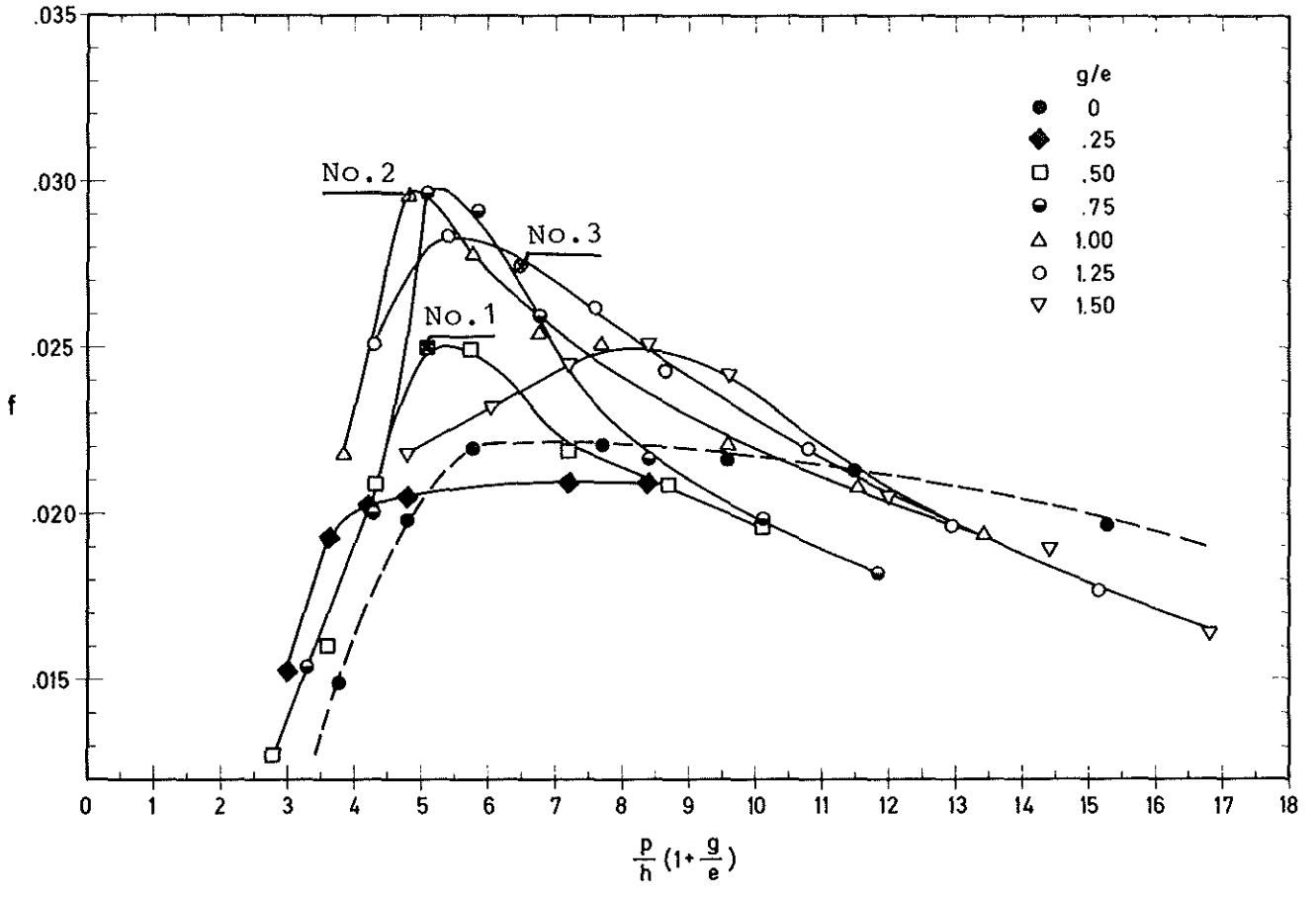

Fig.4: Friction factors as function of the roughness geometry (e/h=4)

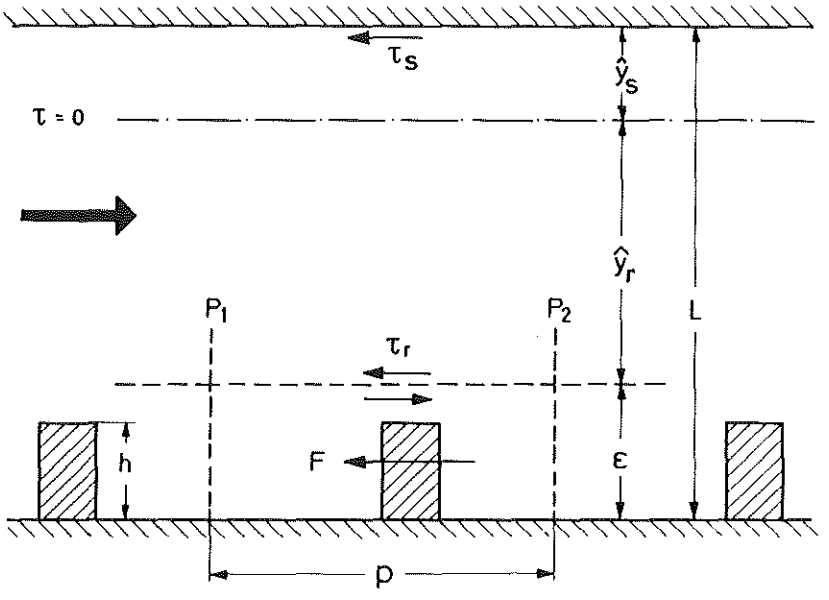

Fig.5: Scheme of flow cross section

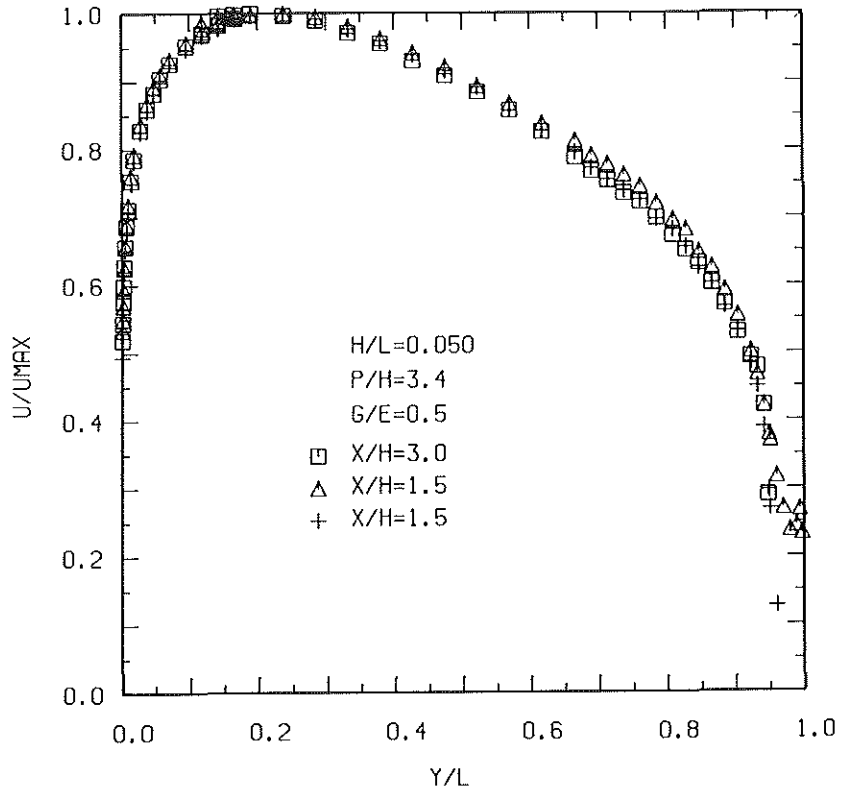

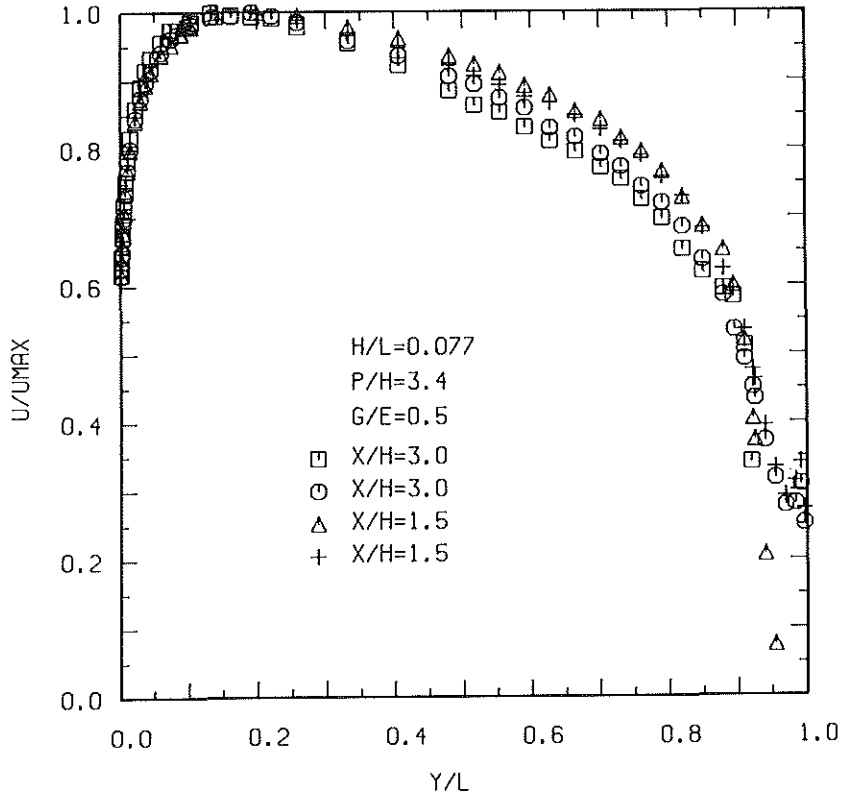

Fig.6.1-6.2: Velocity profiles (No.1)

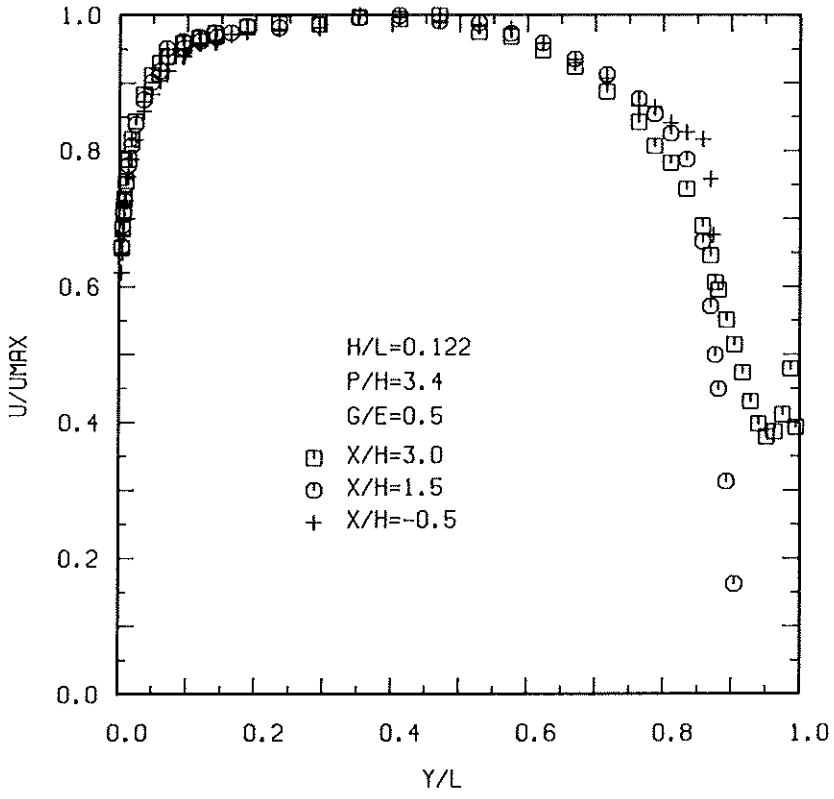

Fig.6.3: Velocity profiles (No.1)

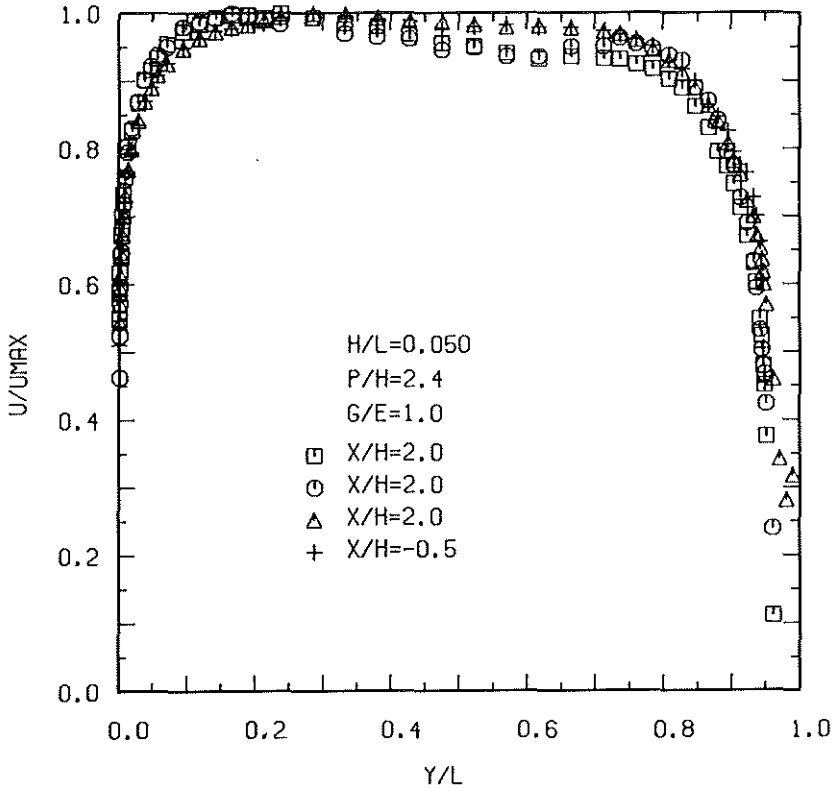

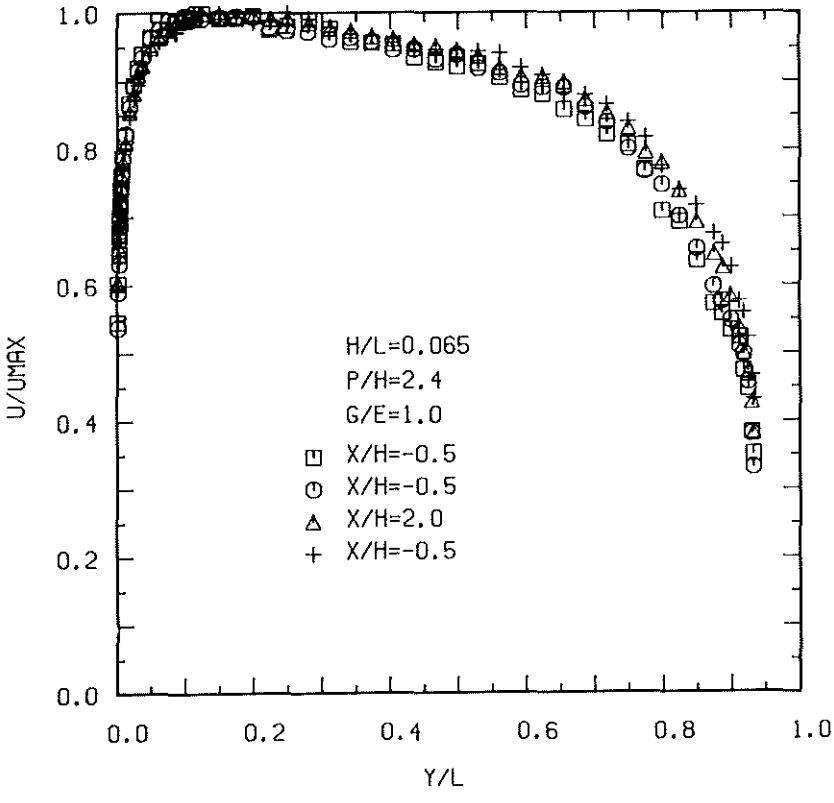

Fig.6.4-6.5: Velocity profiles (No.2)

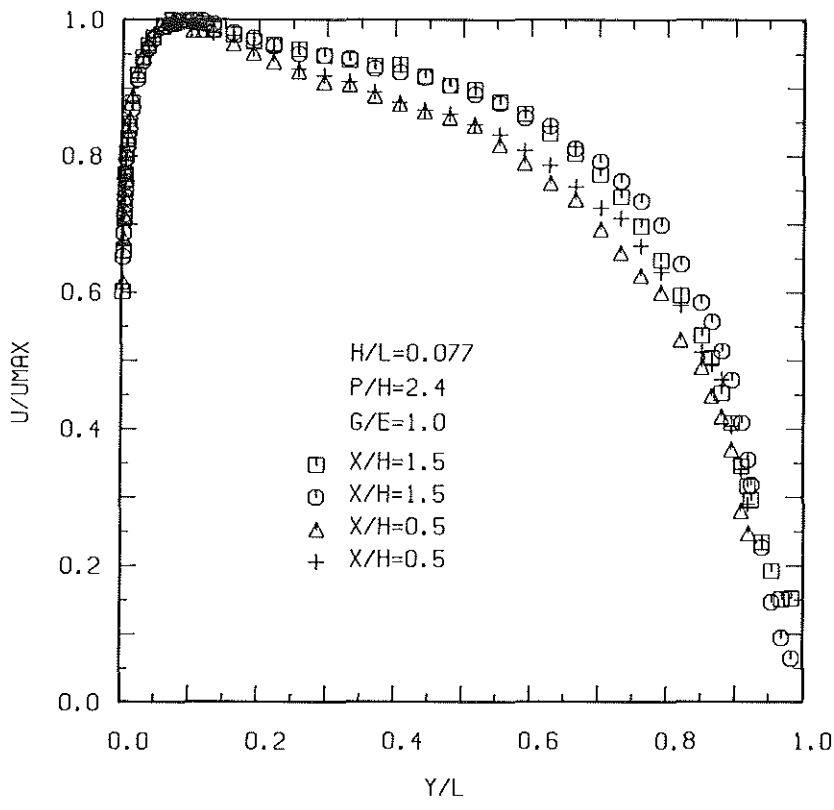

Fig.6.6: Velocity profiles (No.2)

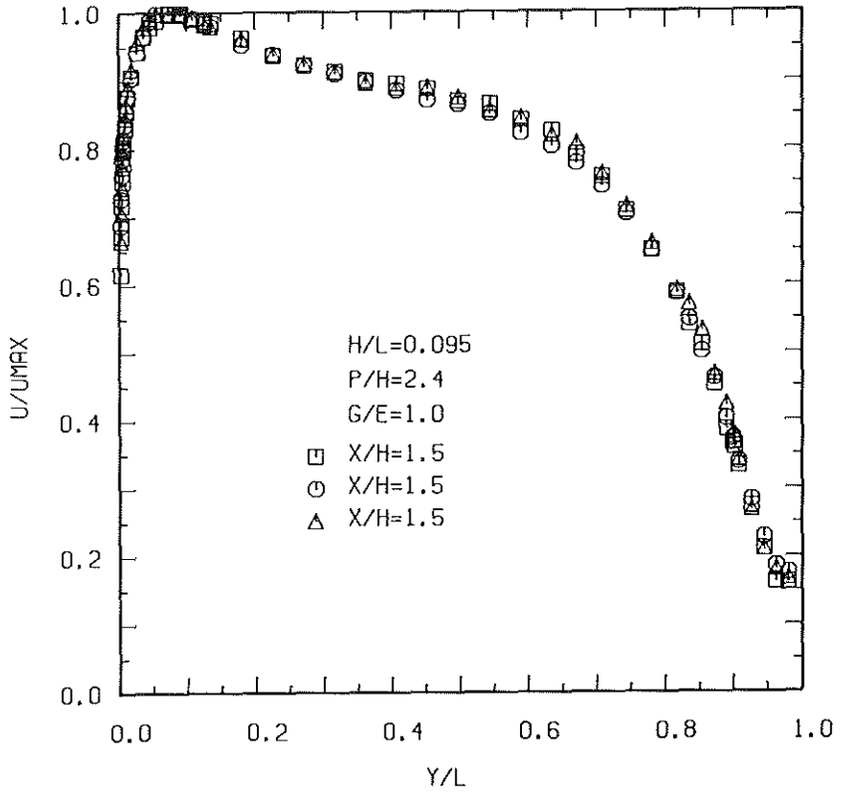

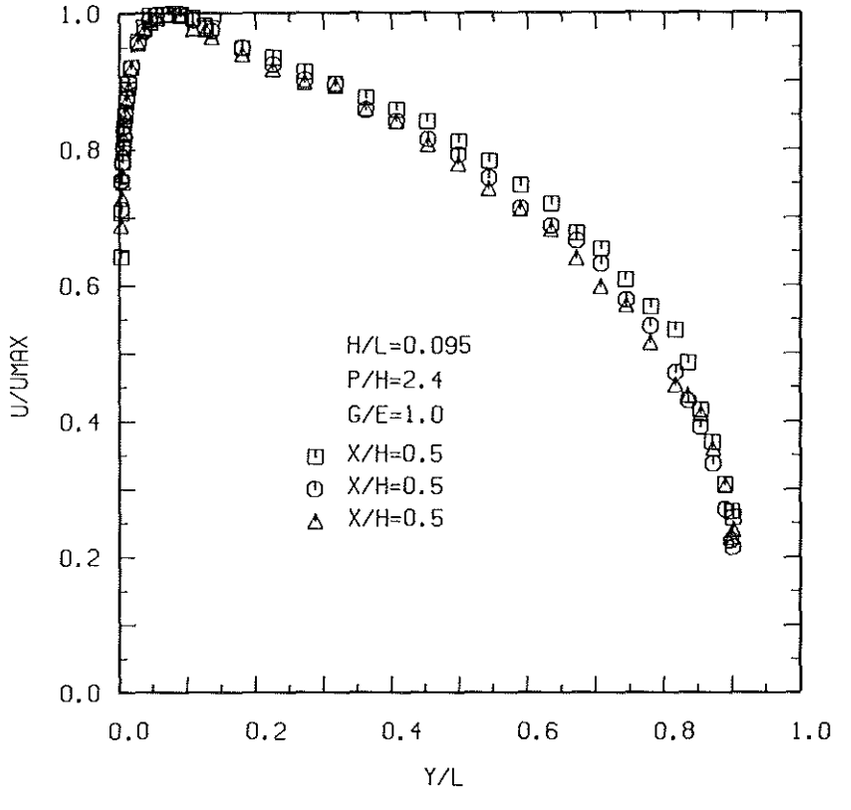

Fig.6.7-6.8: Velocity profiles (No.2)

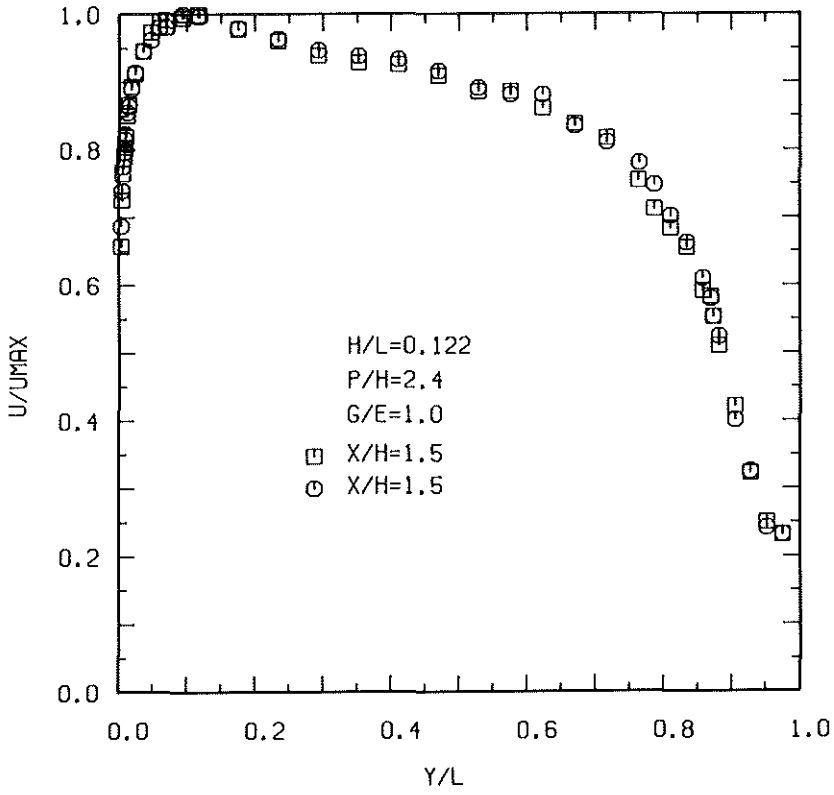

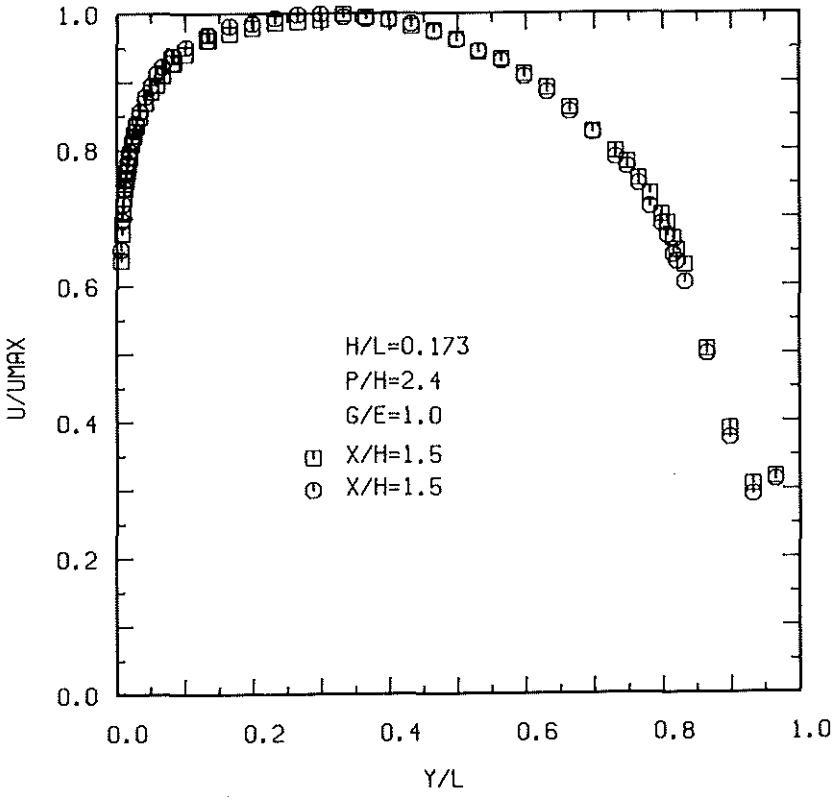

Fig.6.9-6.10: Velocity profiles (No.2)

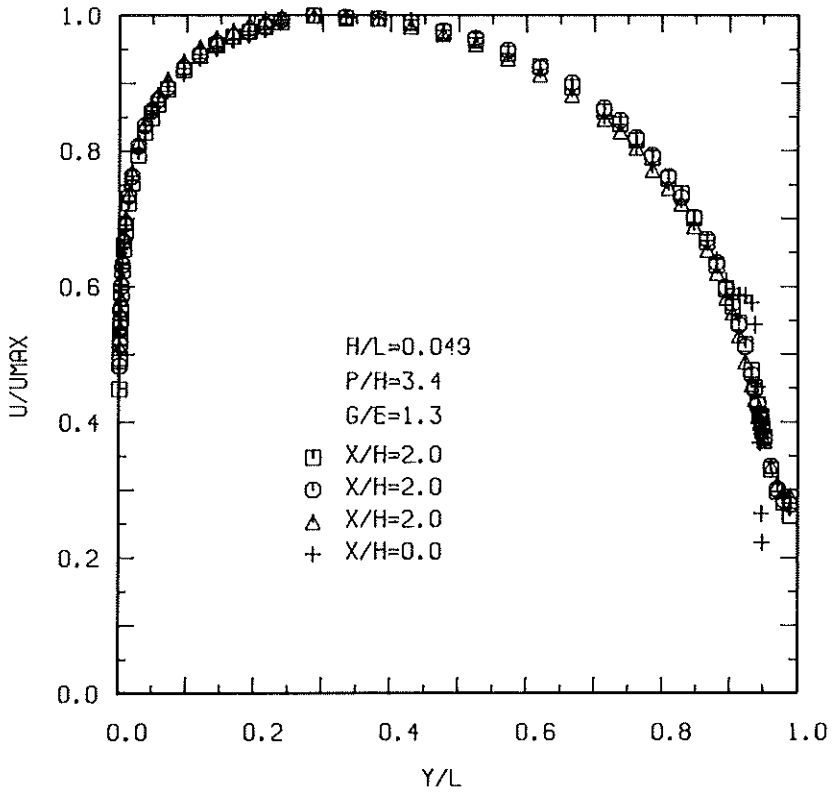

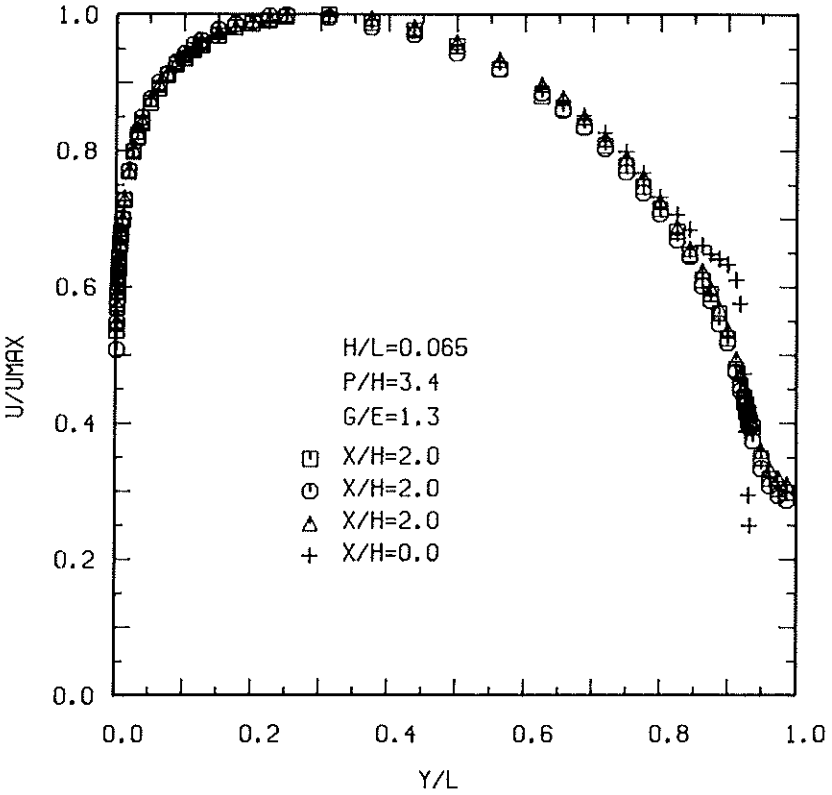

Fig.6.11-6.12: Velocity profiles (No.3)

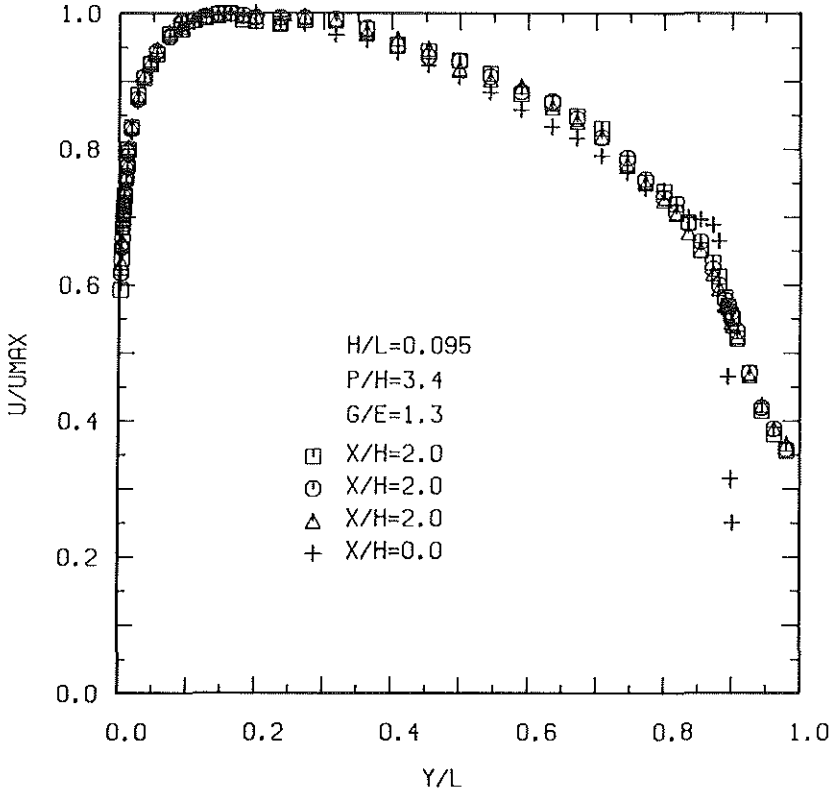

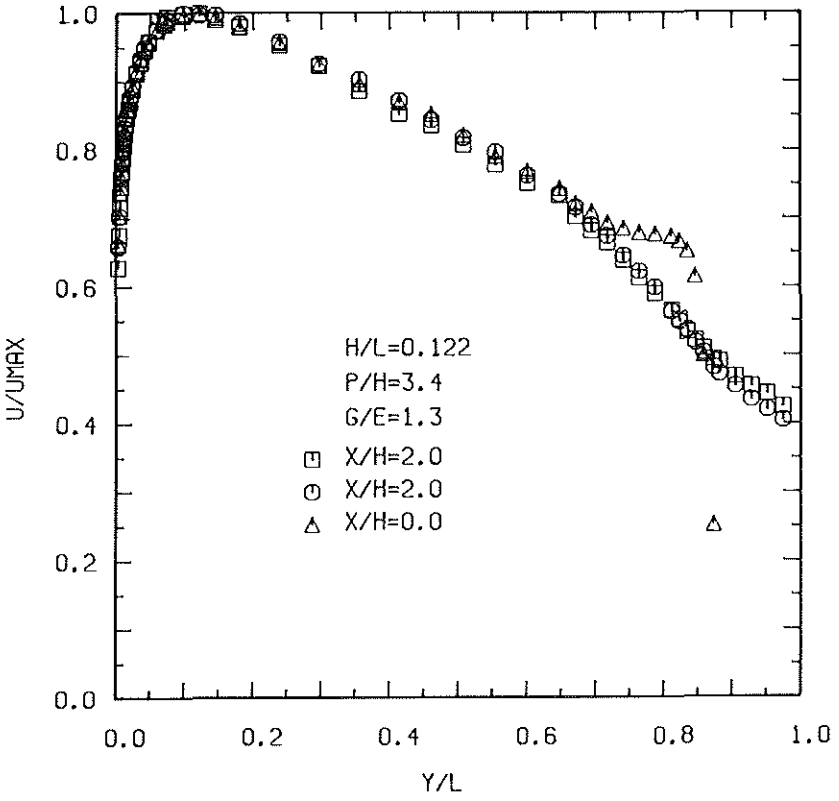

Fig.6.13-6.14: Velocity profiles (No.3)

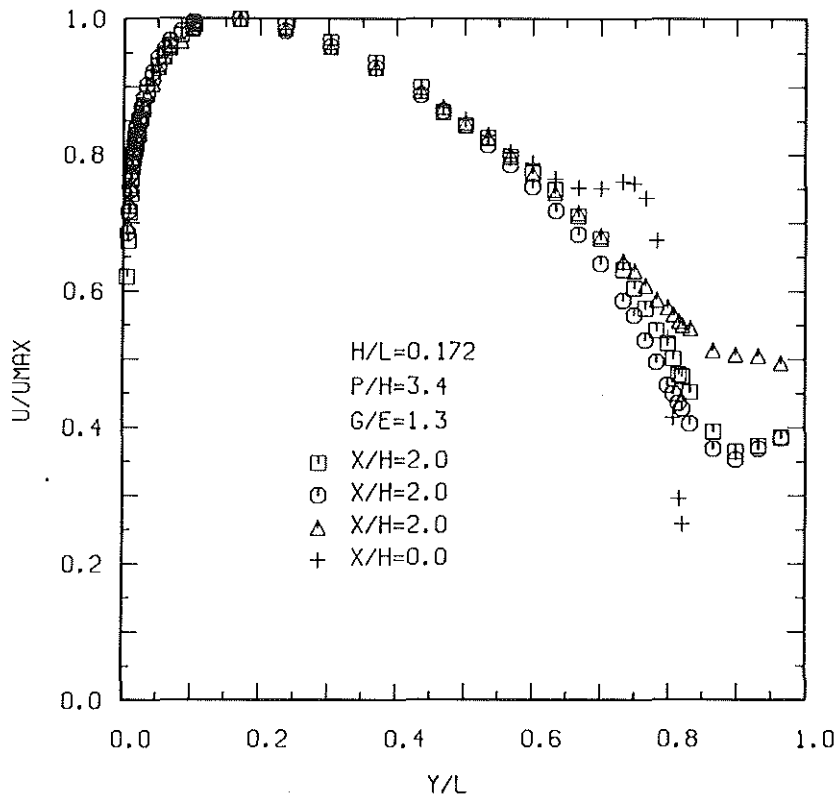

Fig.6.15: Velocity profiles (No.3)

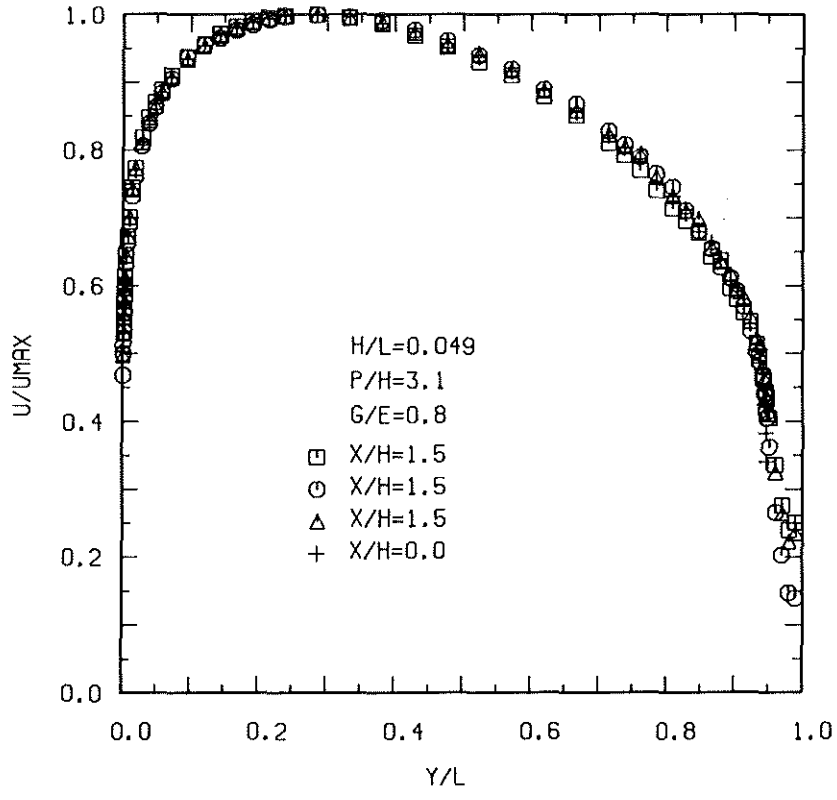

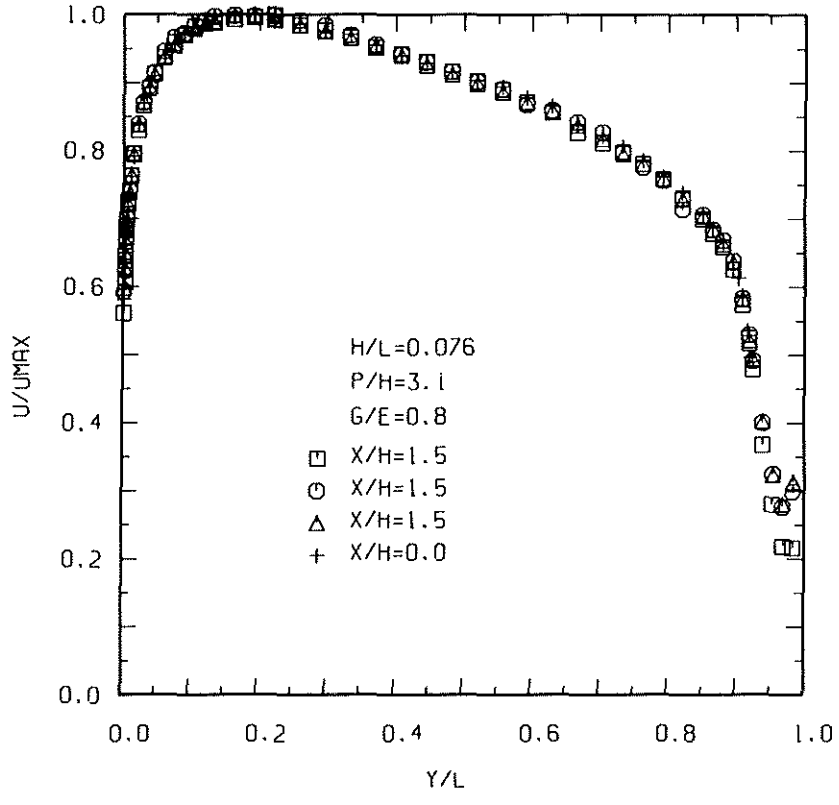

Fig.6.16-6.17: Velocity profiles (No.4)

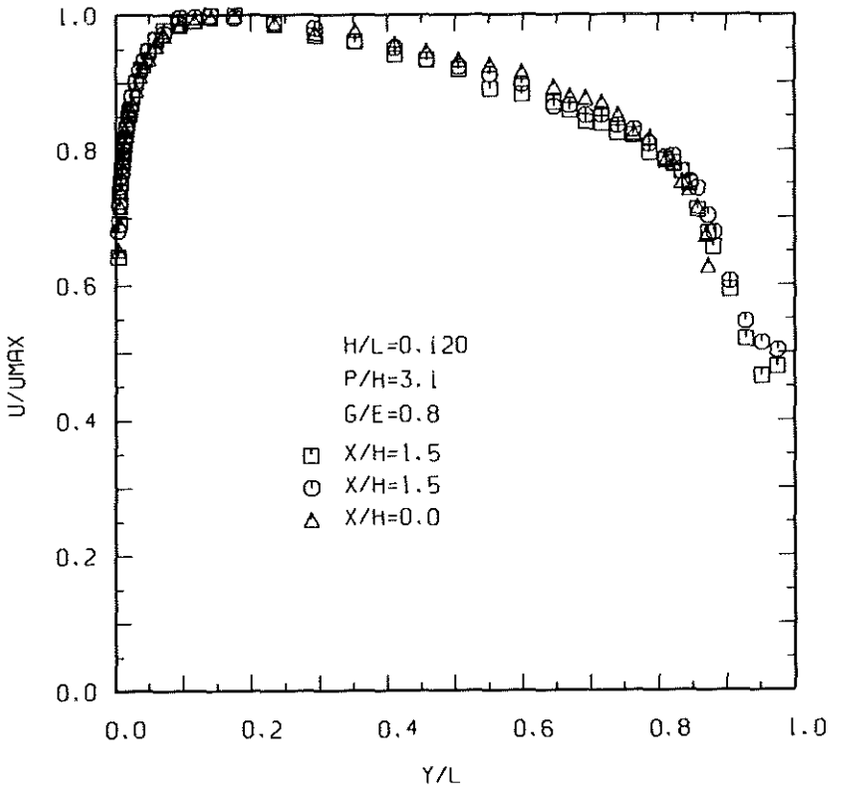

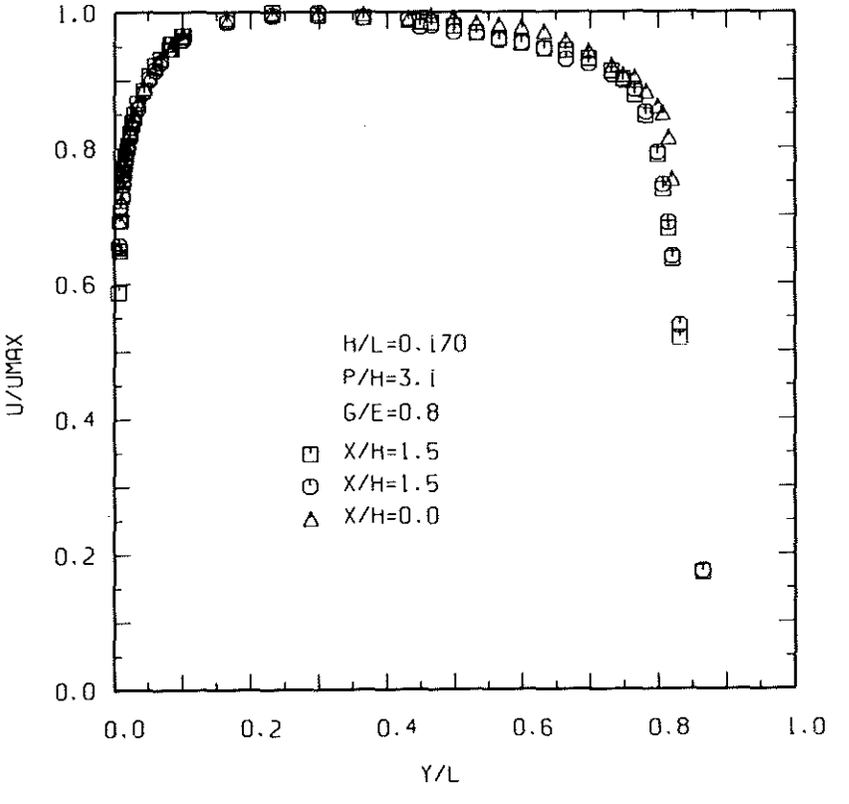

Fig.6.18-6.19: Velocity profiles (No.4)

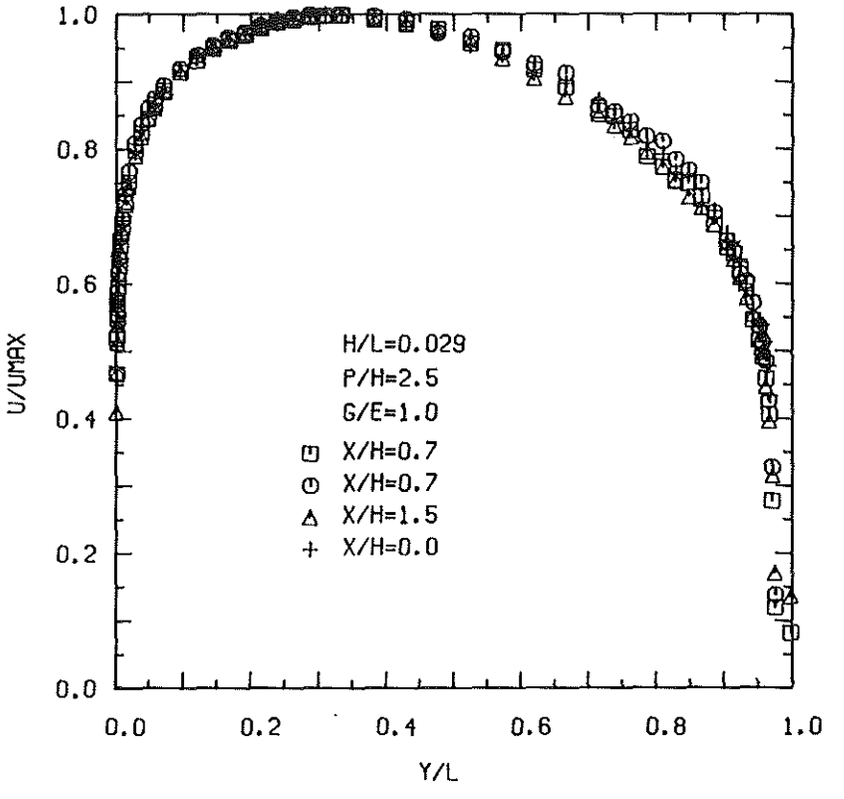

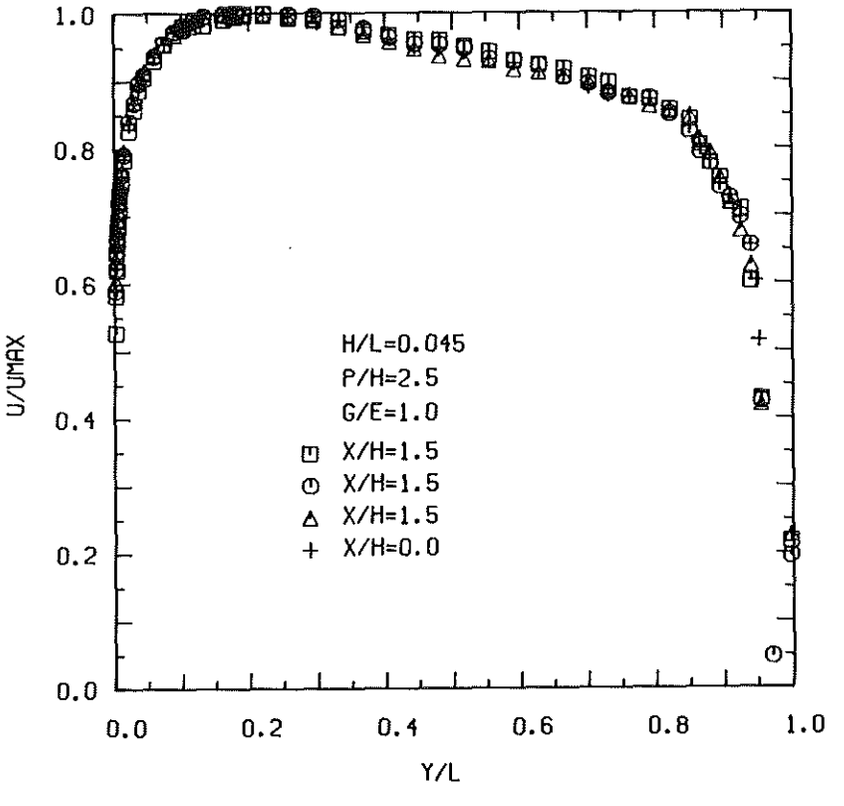

Fig.6.20-6.21: Velocity profiles (No.5)

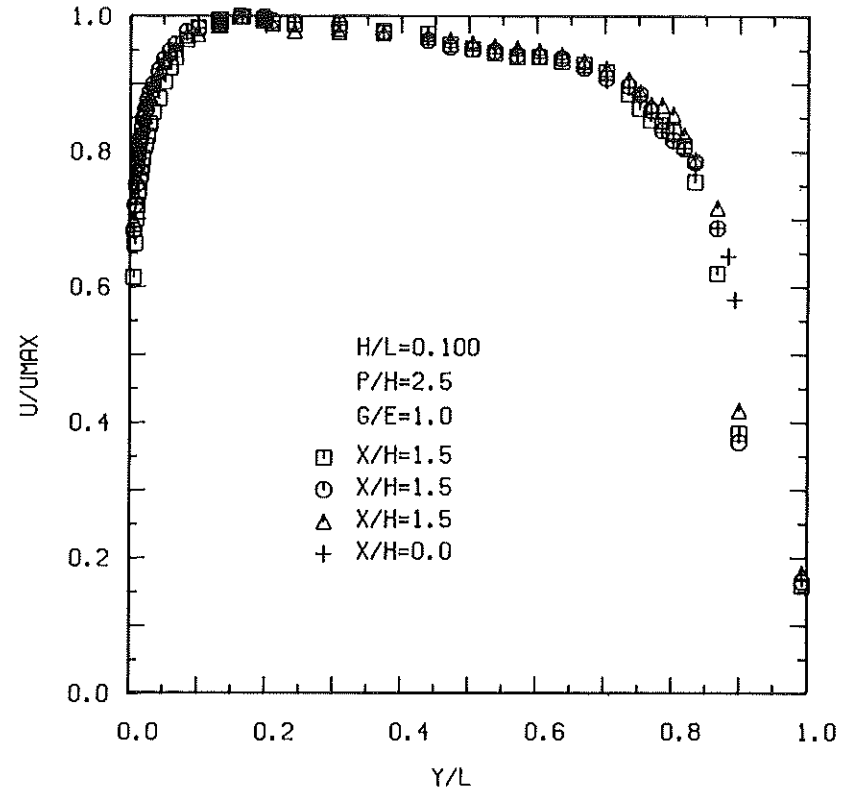

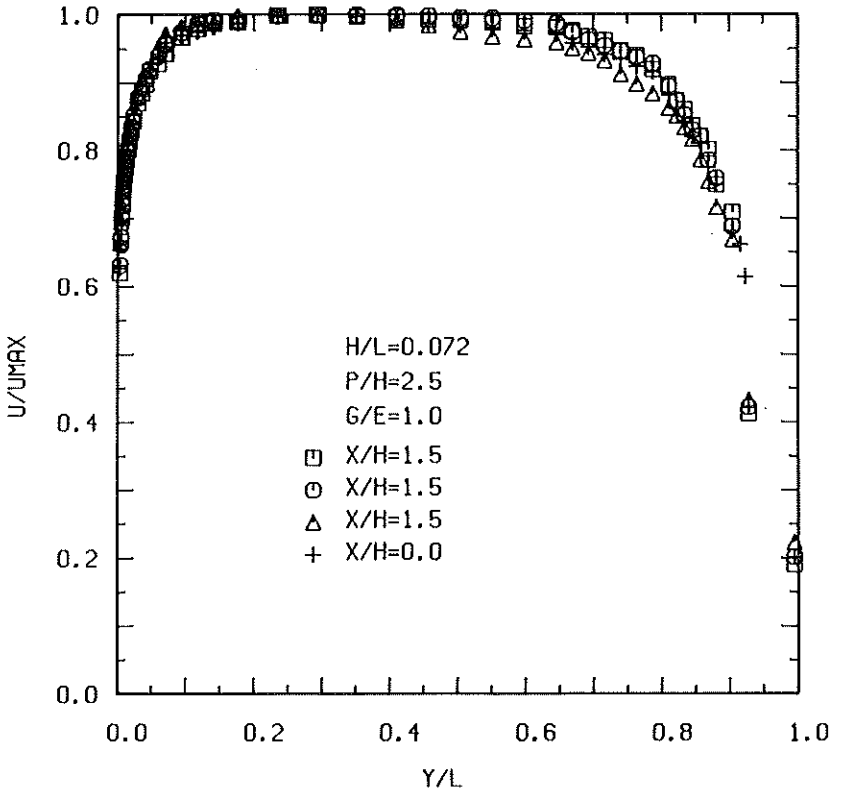

Fig.6.22-6.23: Velocity profiles (No.5)

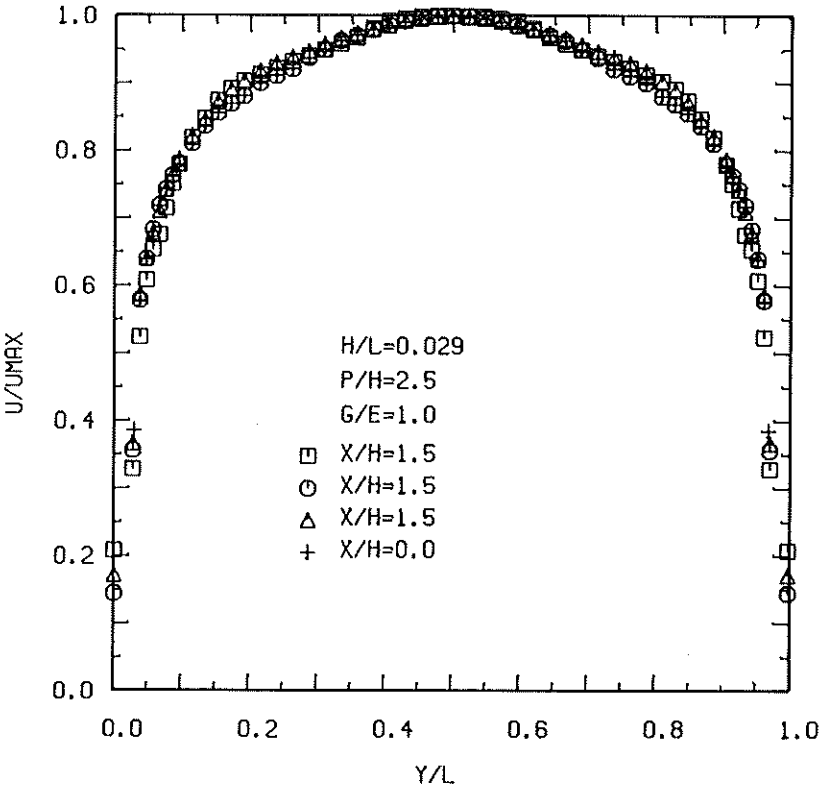

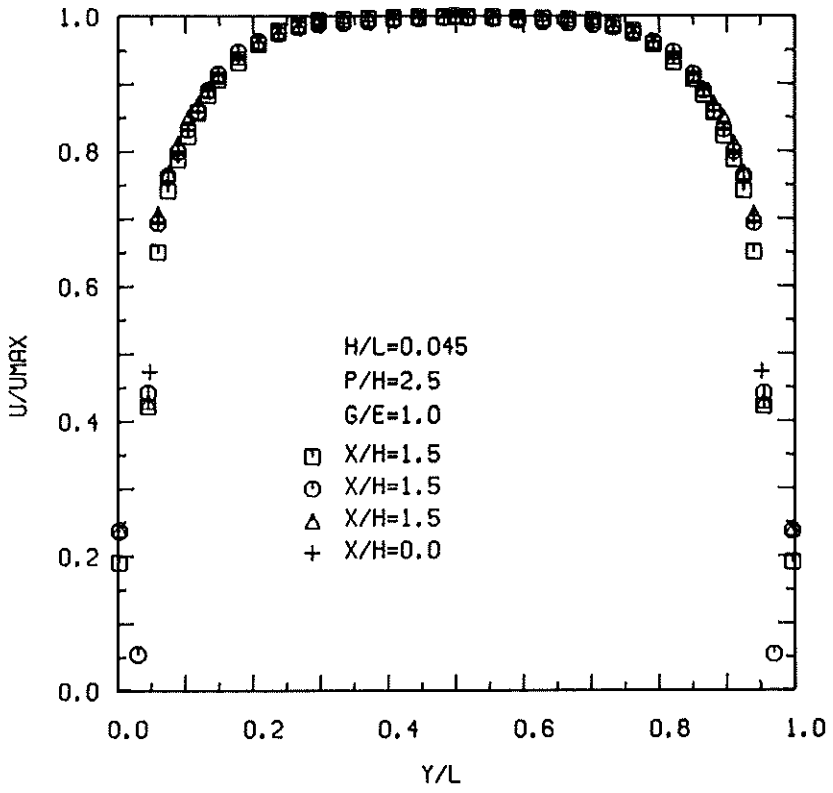

Fig.6.24-6.25: Velocity profiles (No.5 both walls rough)

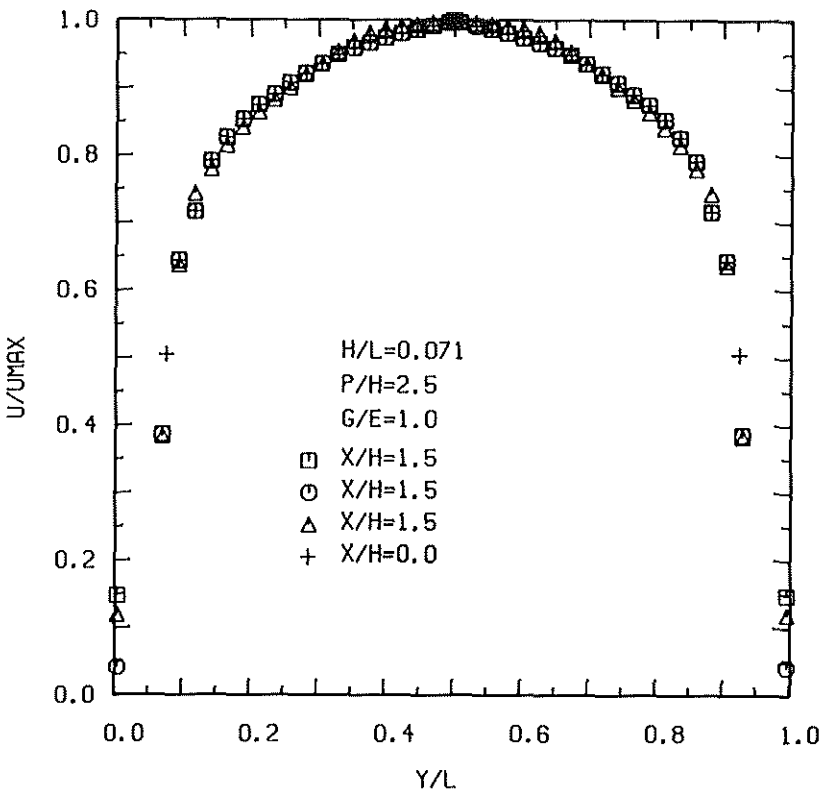

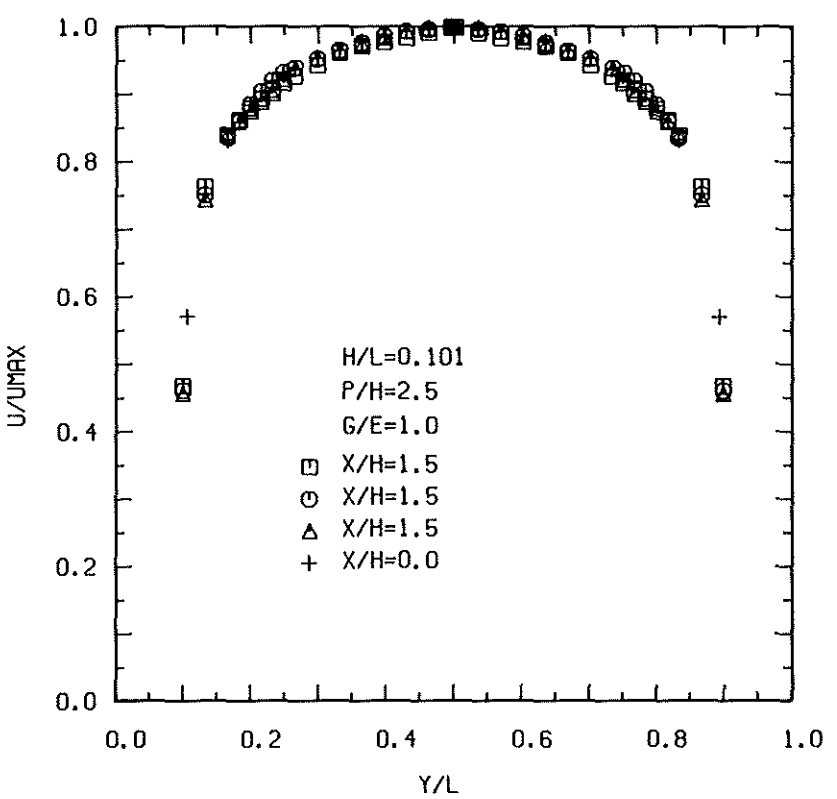

Fig.6.26-6.27: Velocity profiles (No.5 both walls rough)

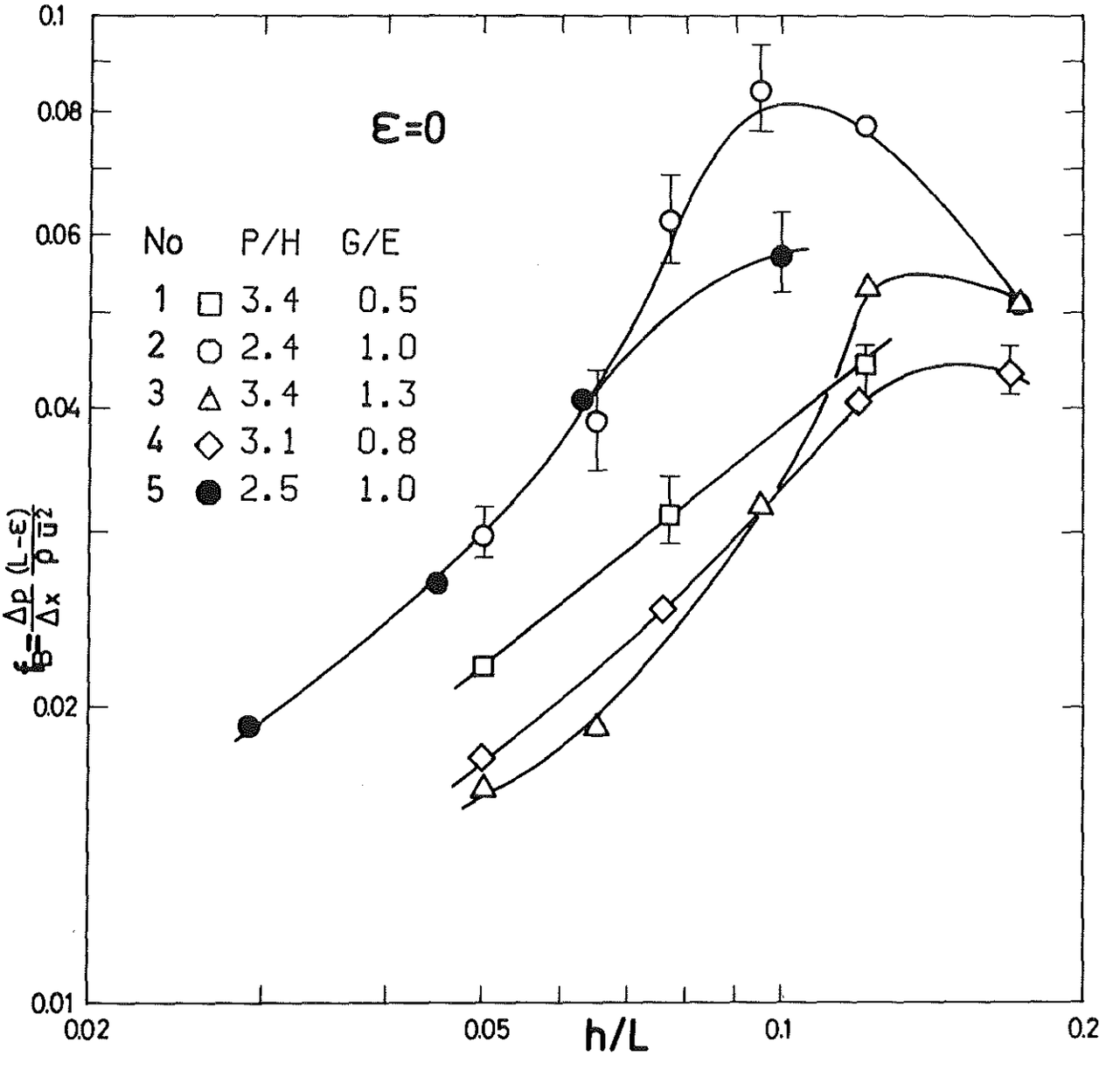

Fig.7: The total friction factor versus the relative roughness height (ε=0)

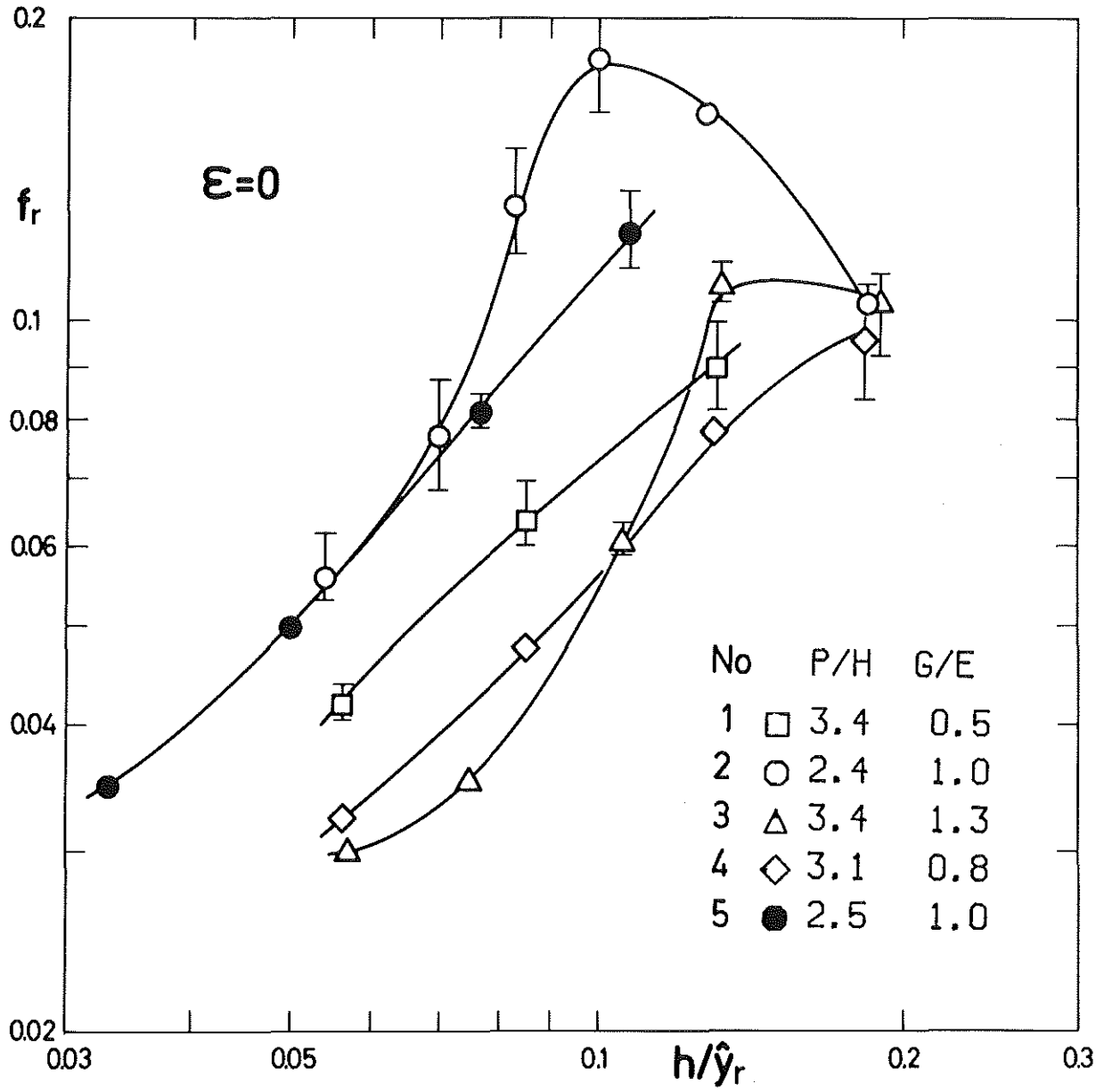

Fig.8: The friction factor of the rough zone versus the relative roughness height (ε=0)

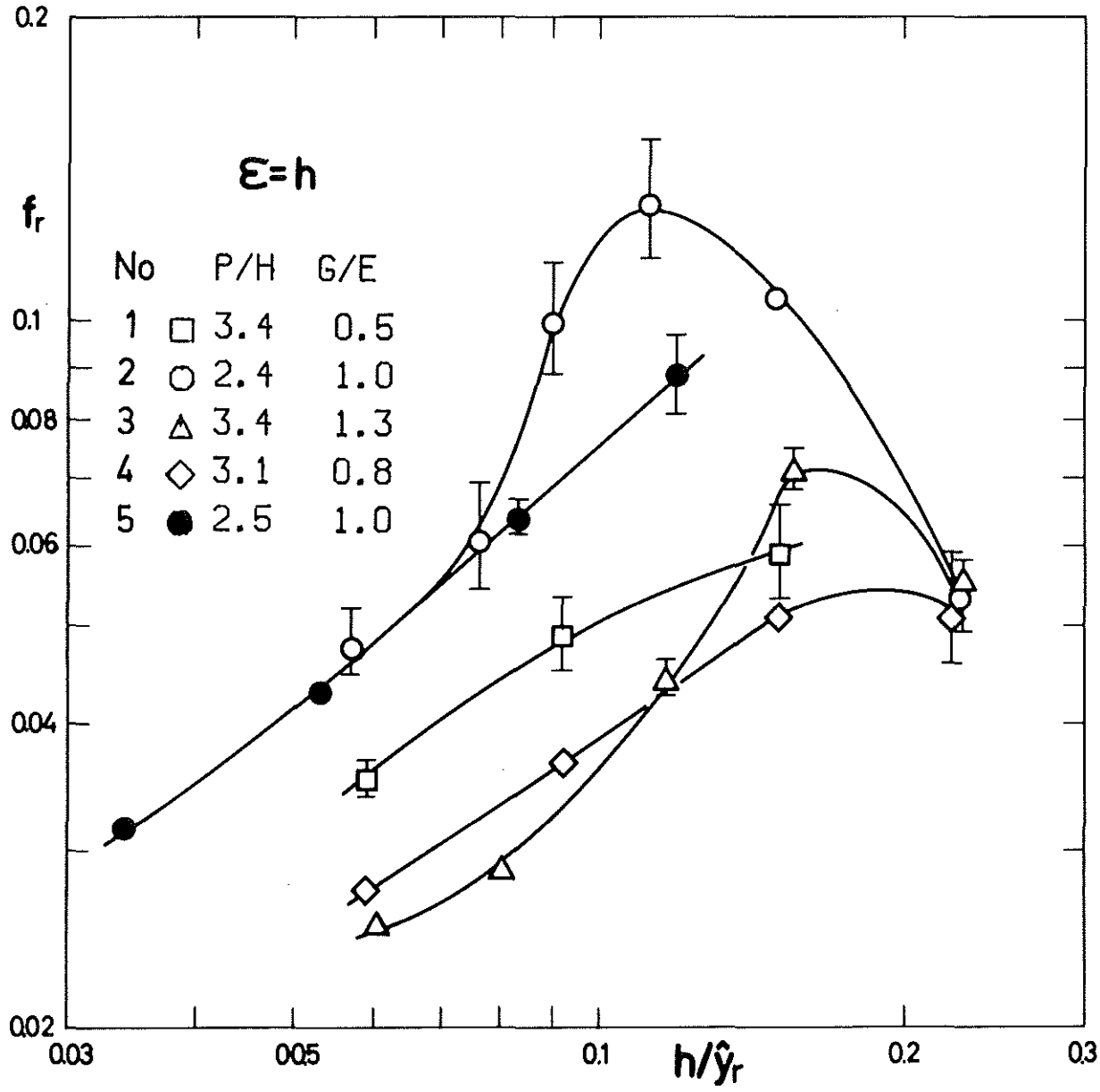

Fig.9: The friction factor of the rough zone versus the relative roughness height (ε=0)

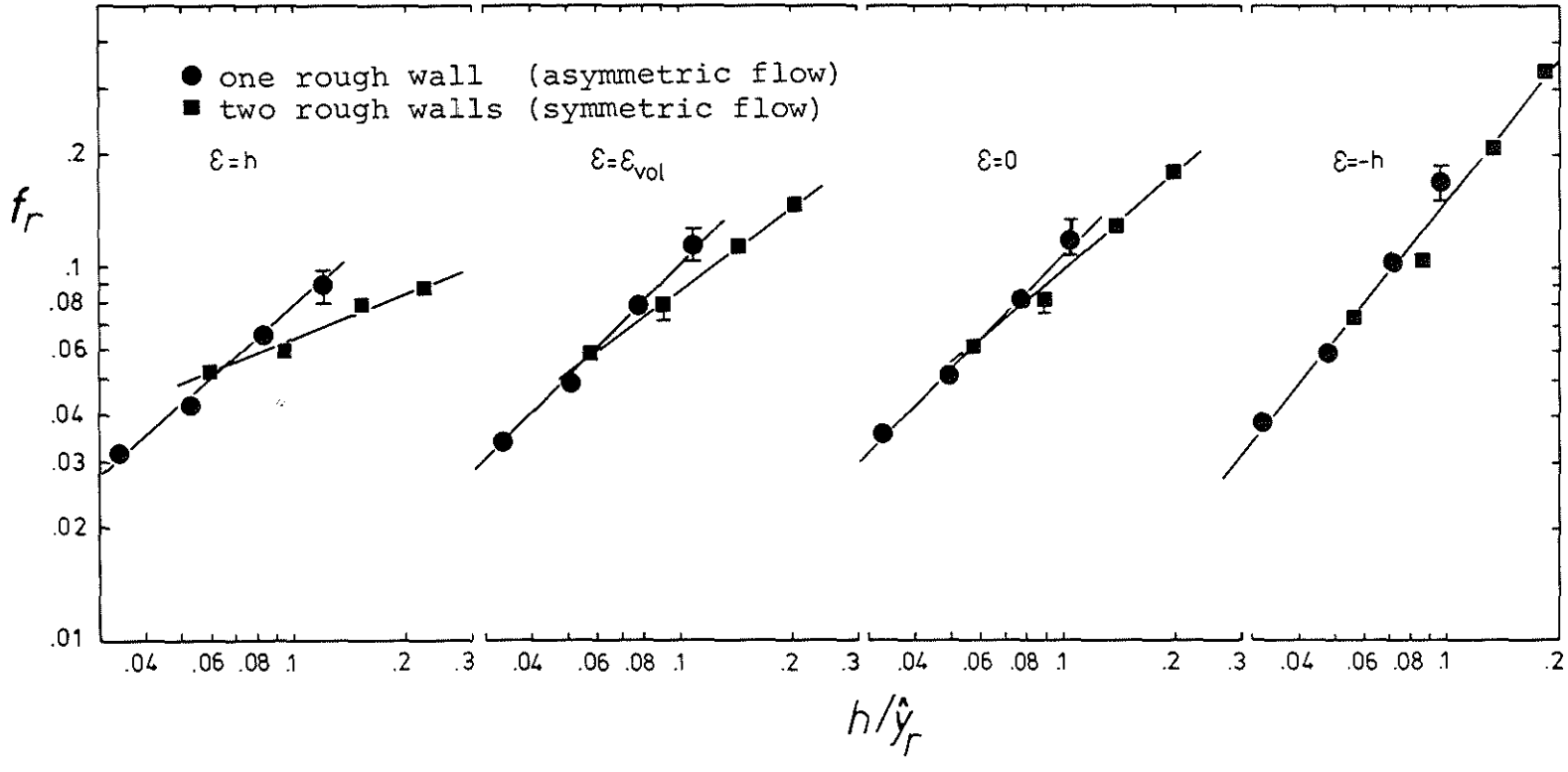

Fig.10: The friction factor of the rough zone in symmetrical and asymmetrical flow for different definitions of the hydraulic diameter.

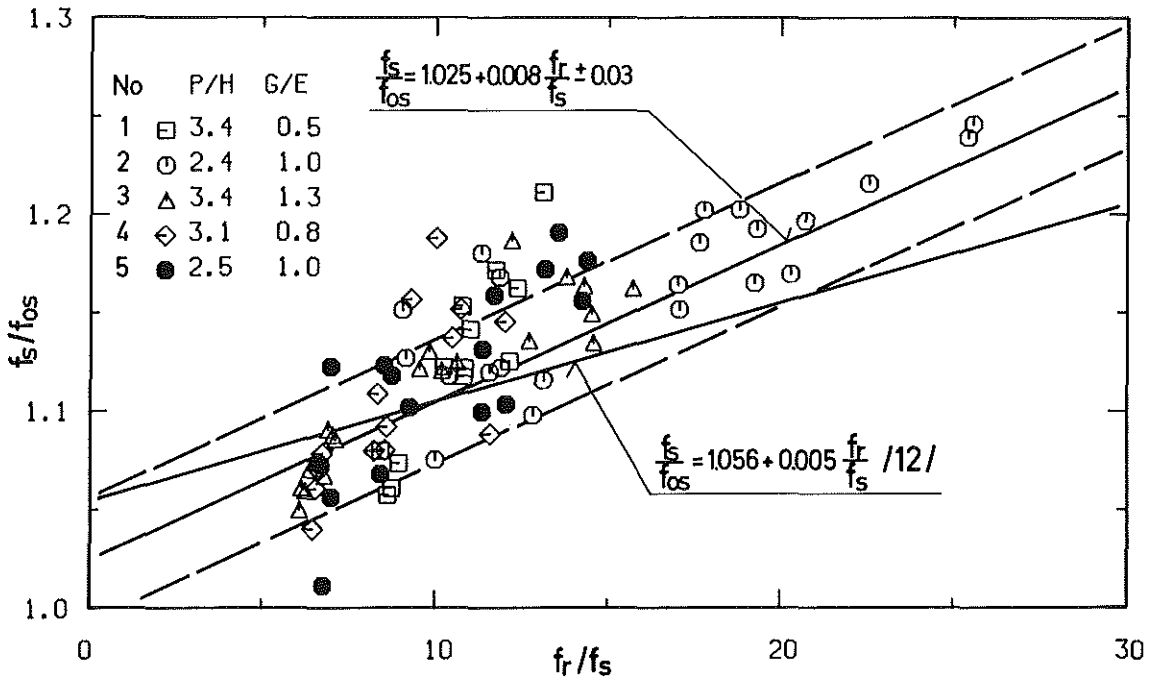

Fig.11: Variation of the friction factor of the smooth zone f_s with the friction factor of the rough zone f_r ($\varepsilon=\varepsilon_{vol}$)

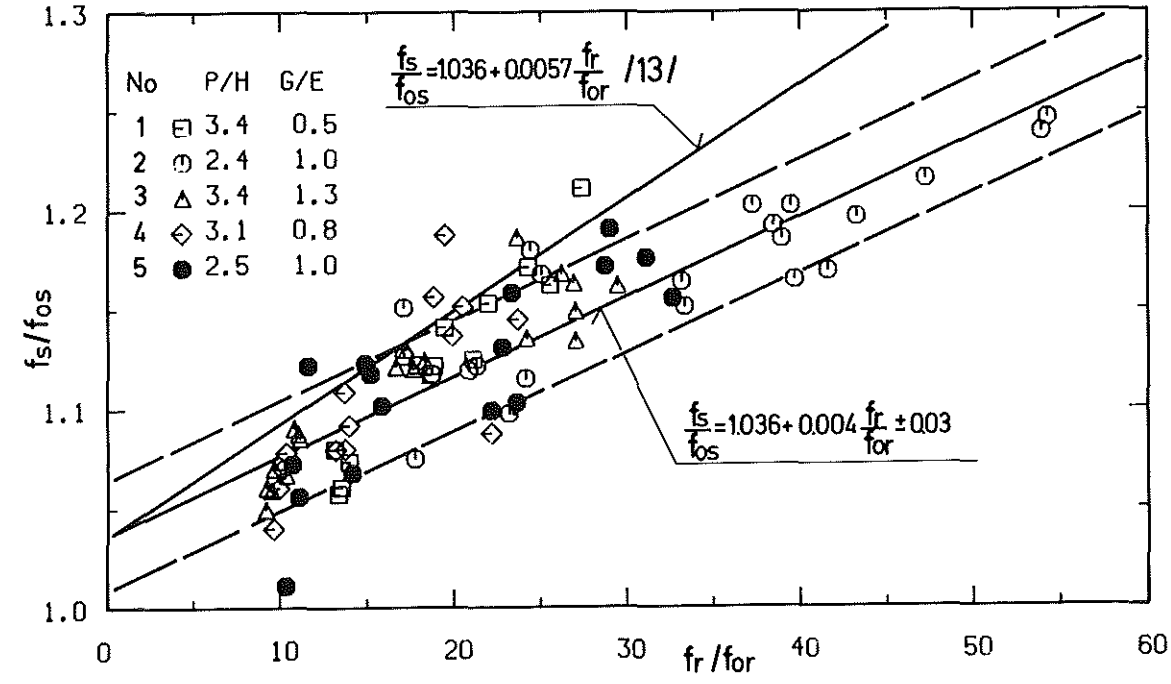

Fig.12: Variation of the friction factor of the smooth zone f_s with the friction factor of the rough zone f_r ($\varepsilon=\varepsilon_{vol}$)

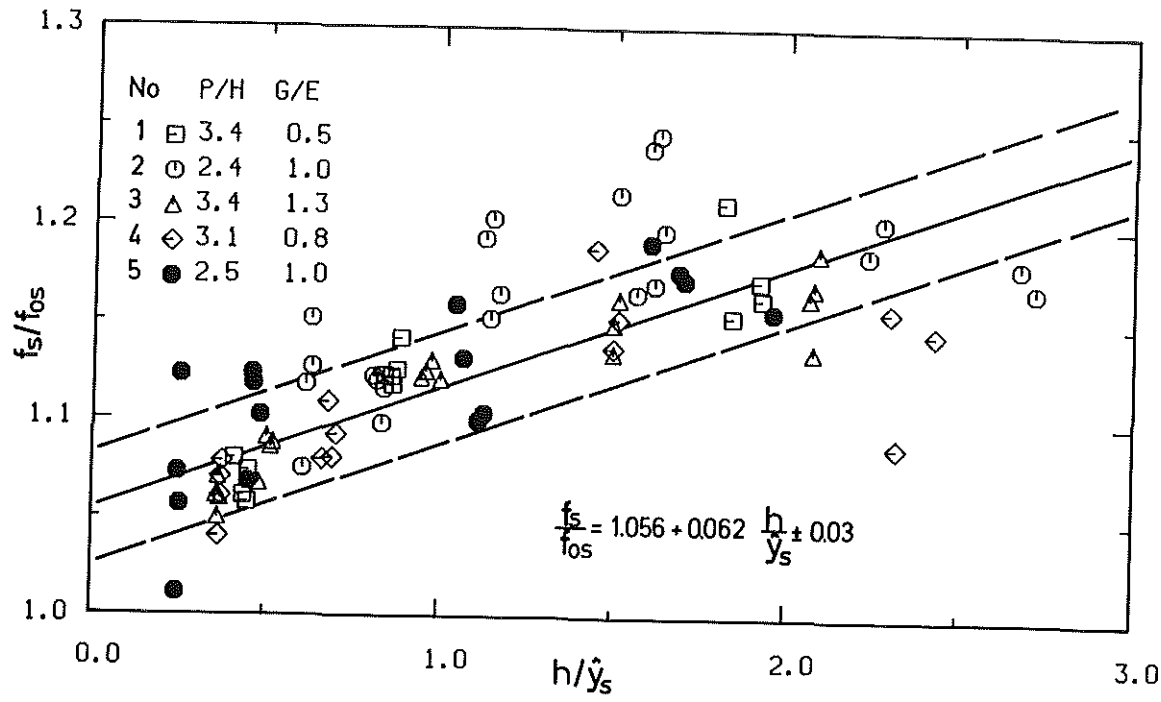

Fig.13: Variation of the friction factor of the smooth zone f_s with the relative length of the smooth zone.

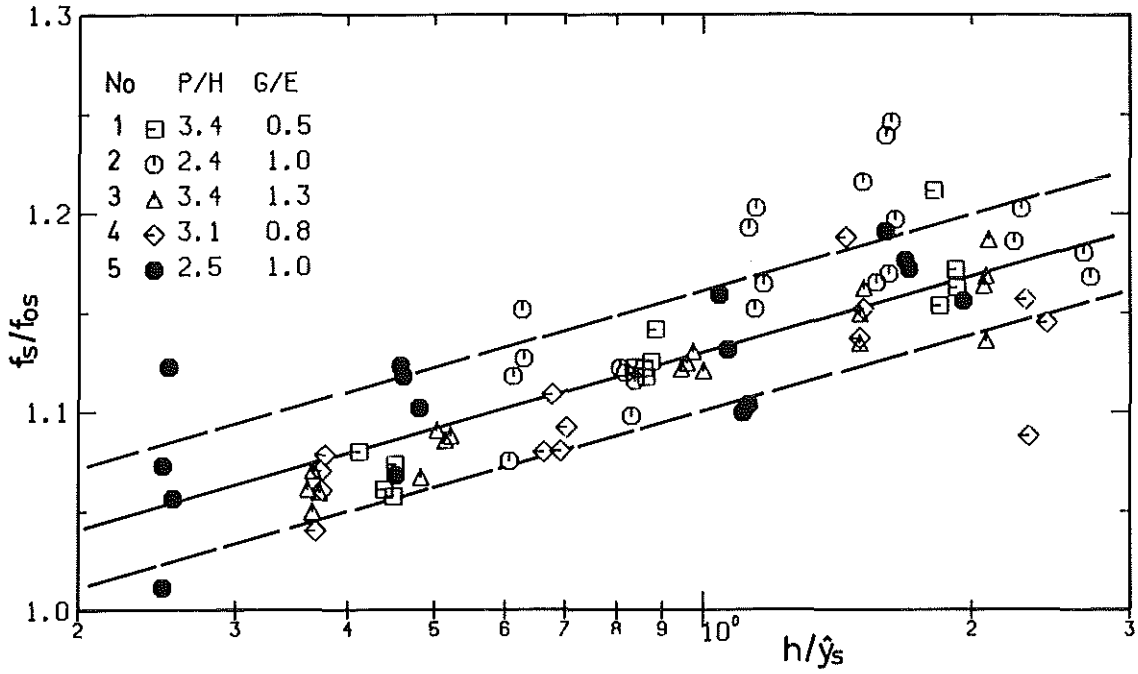

Fig.14: Variation of the friction factor of the smooth zone f_s with the relative length of the smooth zone.

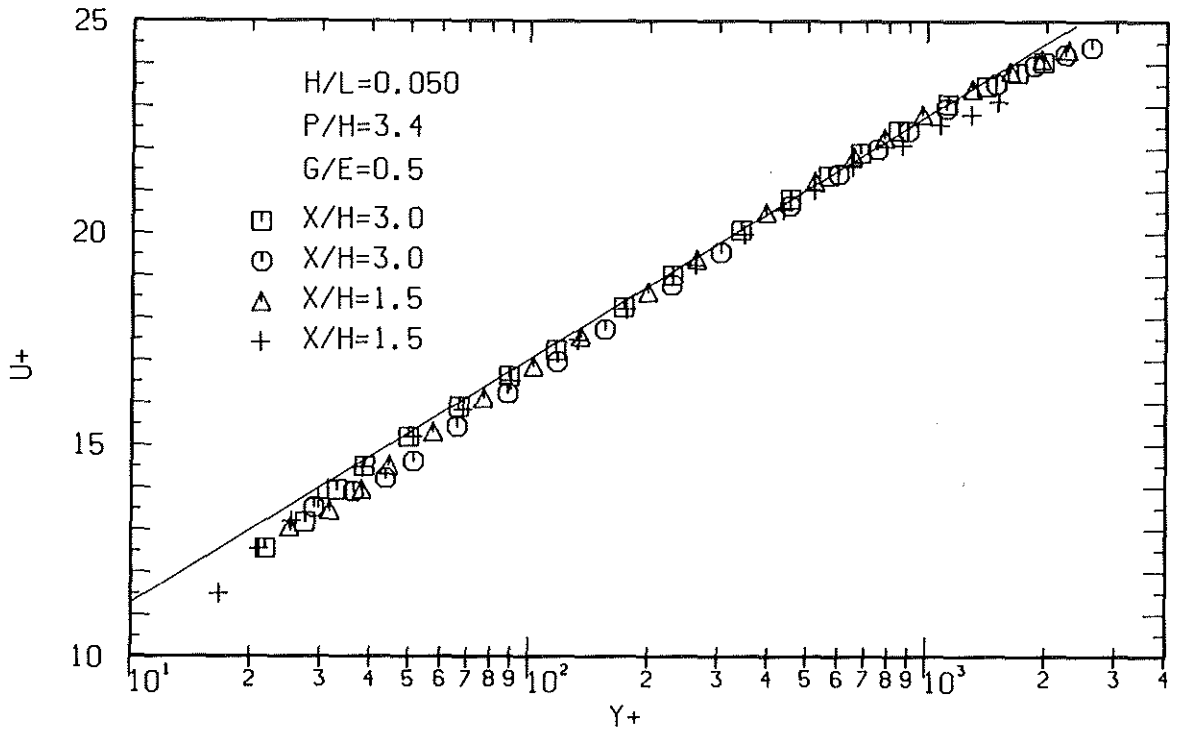

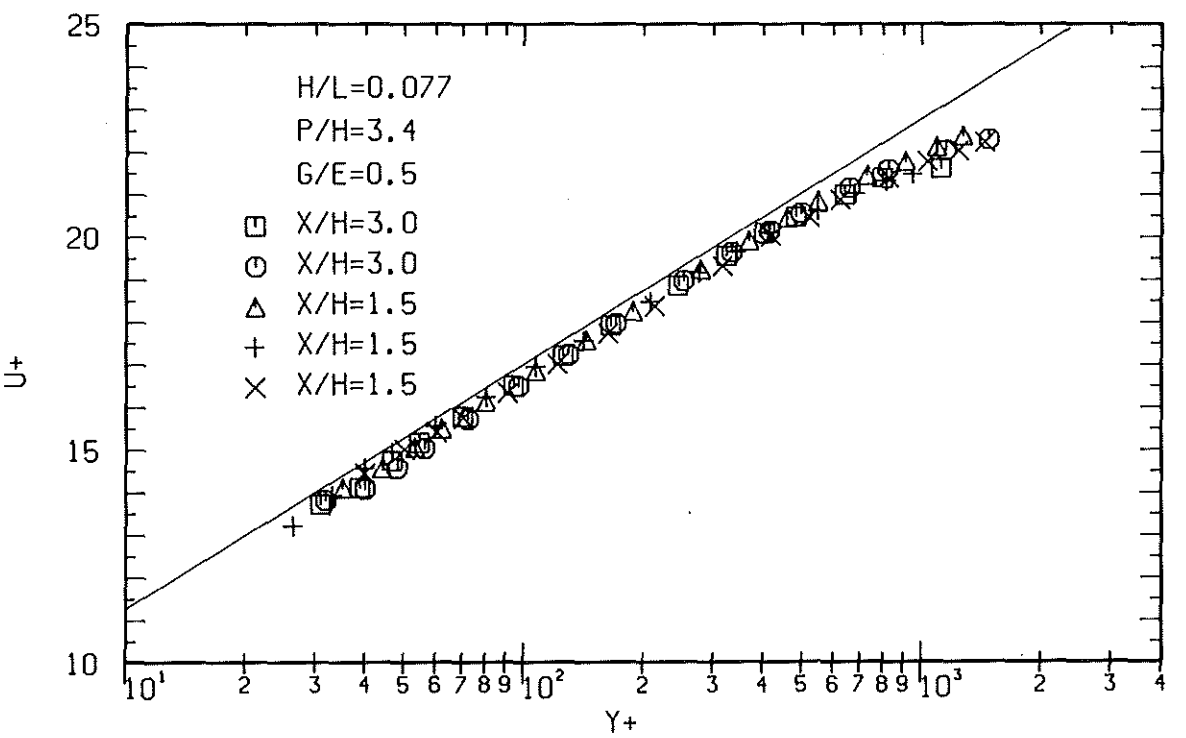

Fig.15.1-15.2: Non-dimensional velocity profiles at the smooth wall with roughness No.1 at opposite wall

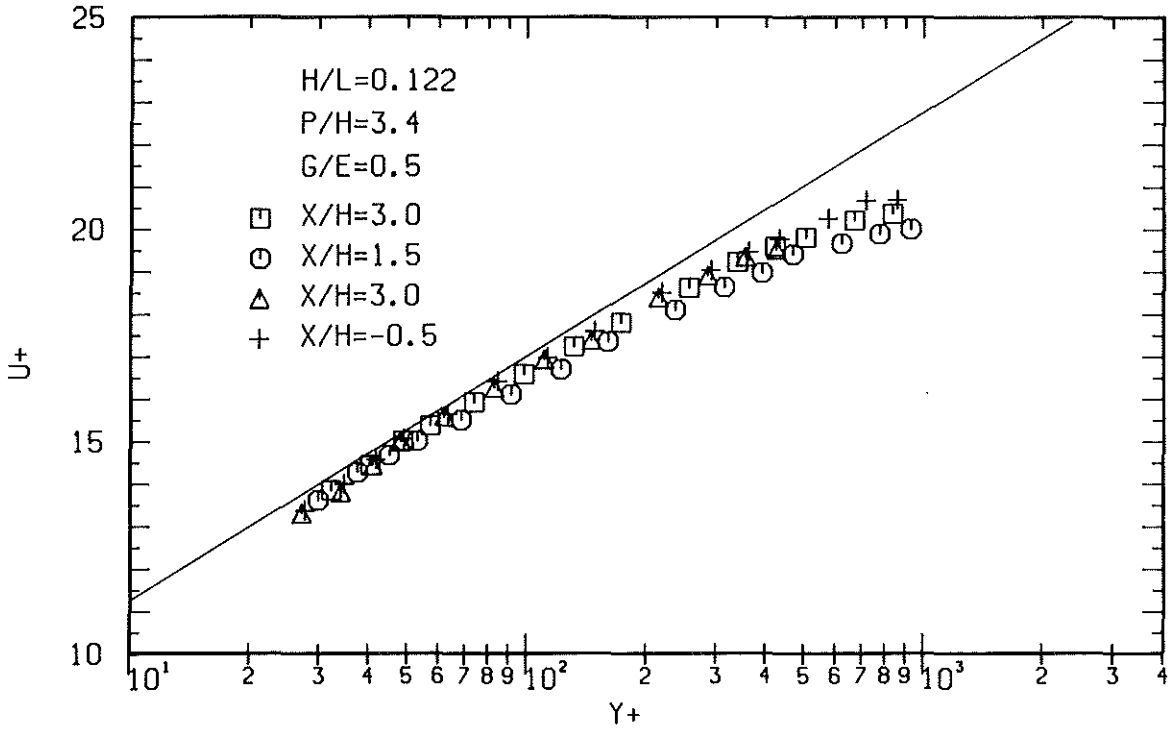

Fig.15.3: Non-dimensional velocity profiles at the smooth wall with roughness No.1 at opposite wall

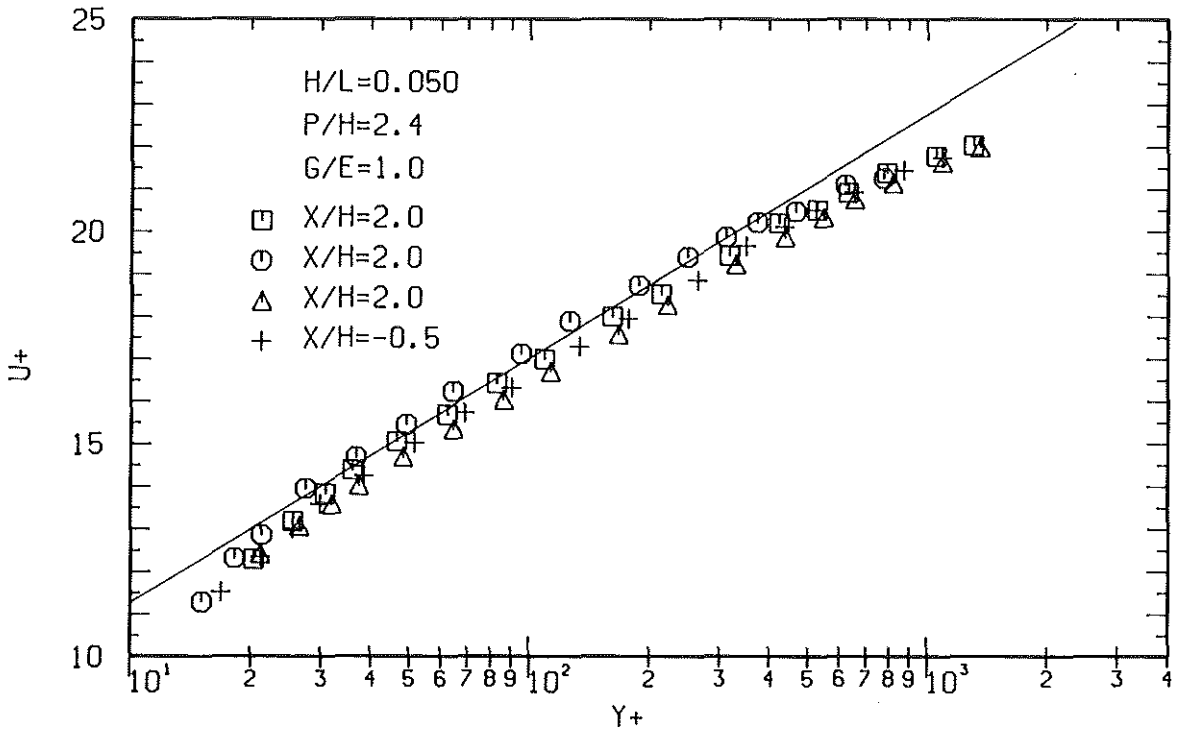

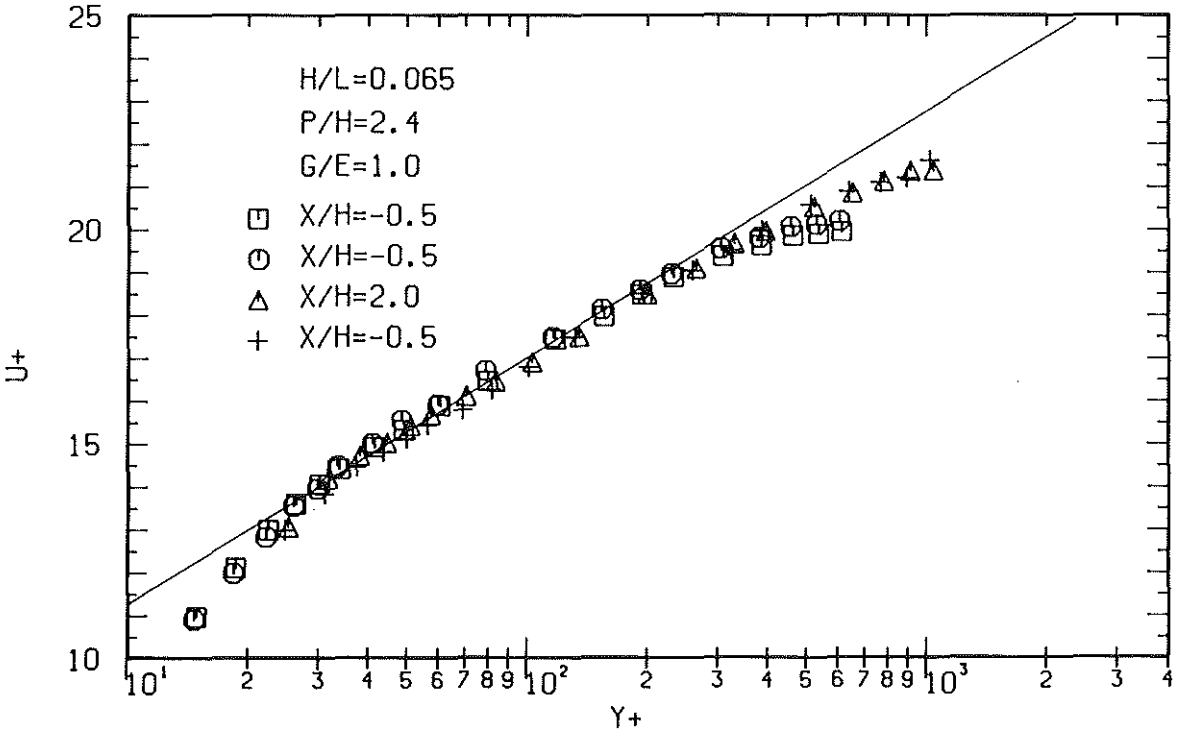

Fig.15.4-15.5: Non-dimensional velocity profiles at the smooth wall with roughness No.2 at opposite wall

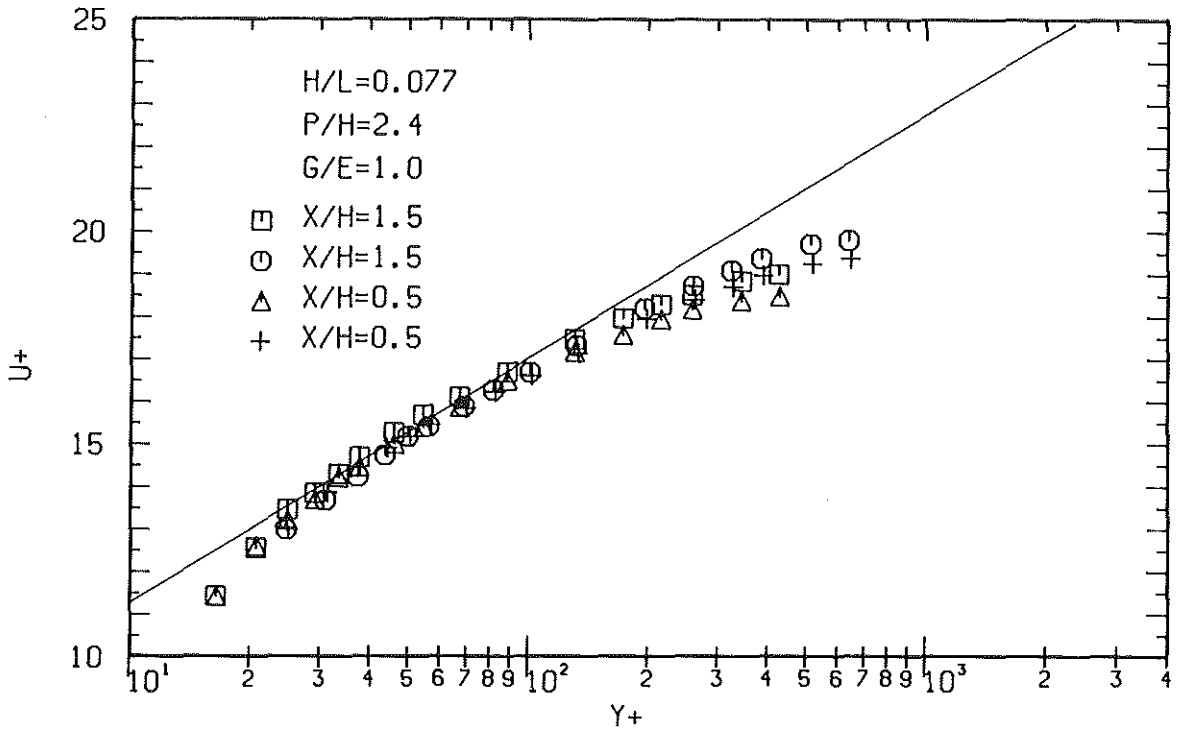

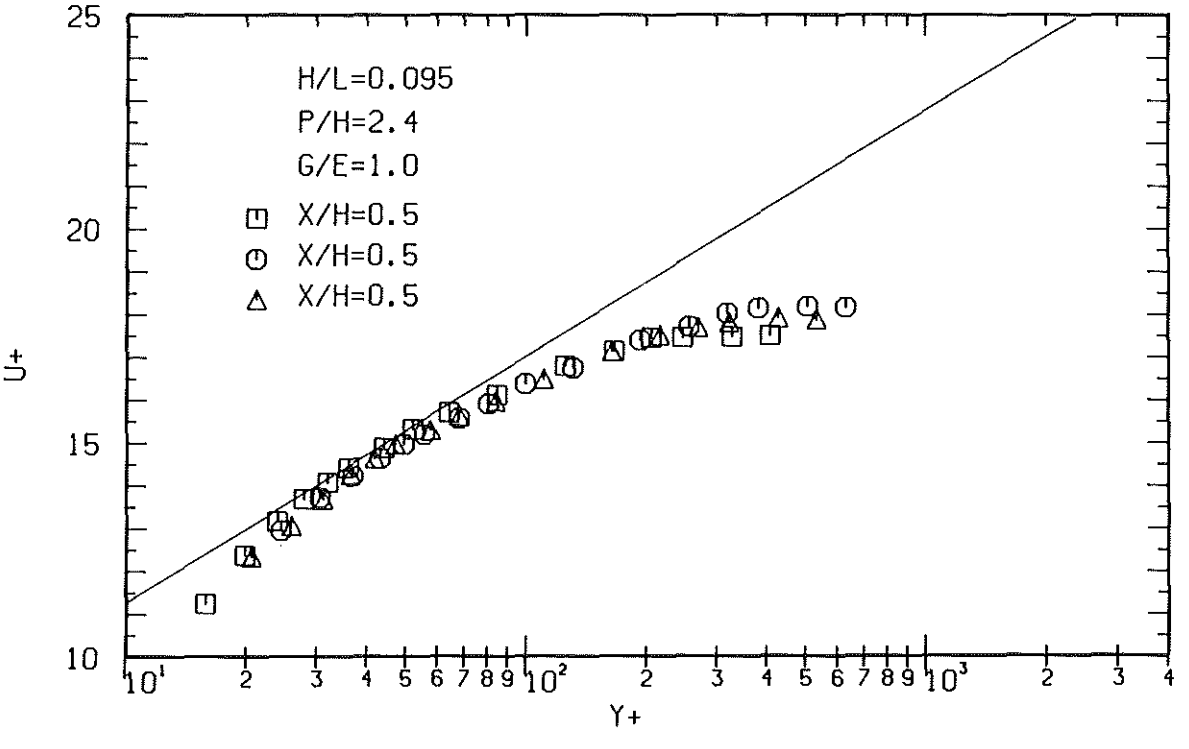

Fig.15.6-15.7: Non-dimensional velocity profiles at the smooth wall with roughness No.2 at opposite wall

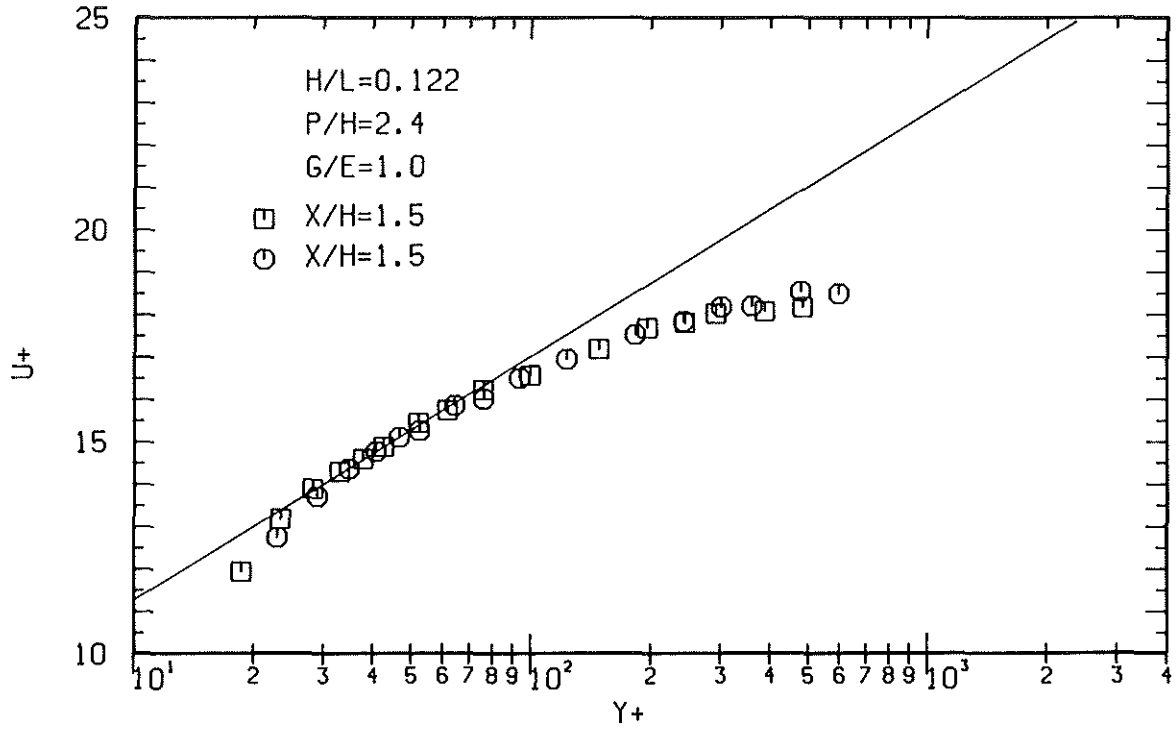

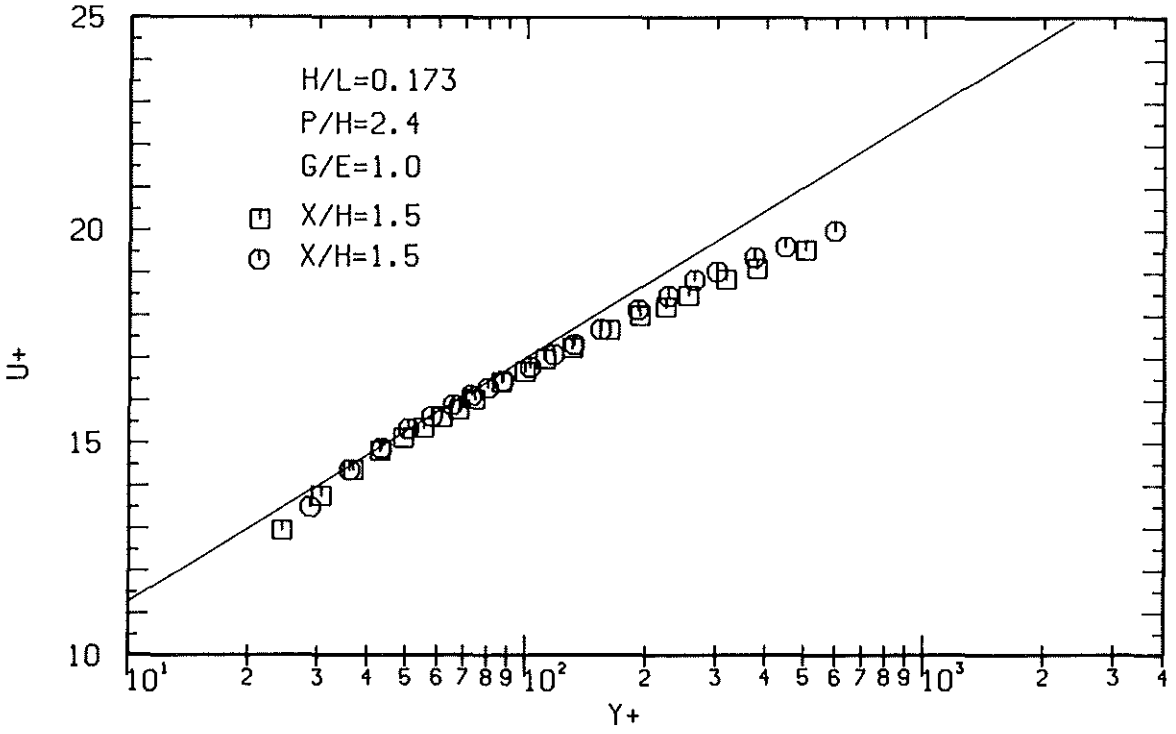

Fig.15.8-15.9: Non-dimensional velocity profiles at the smooth wall with roughness No.2 at opposite wall

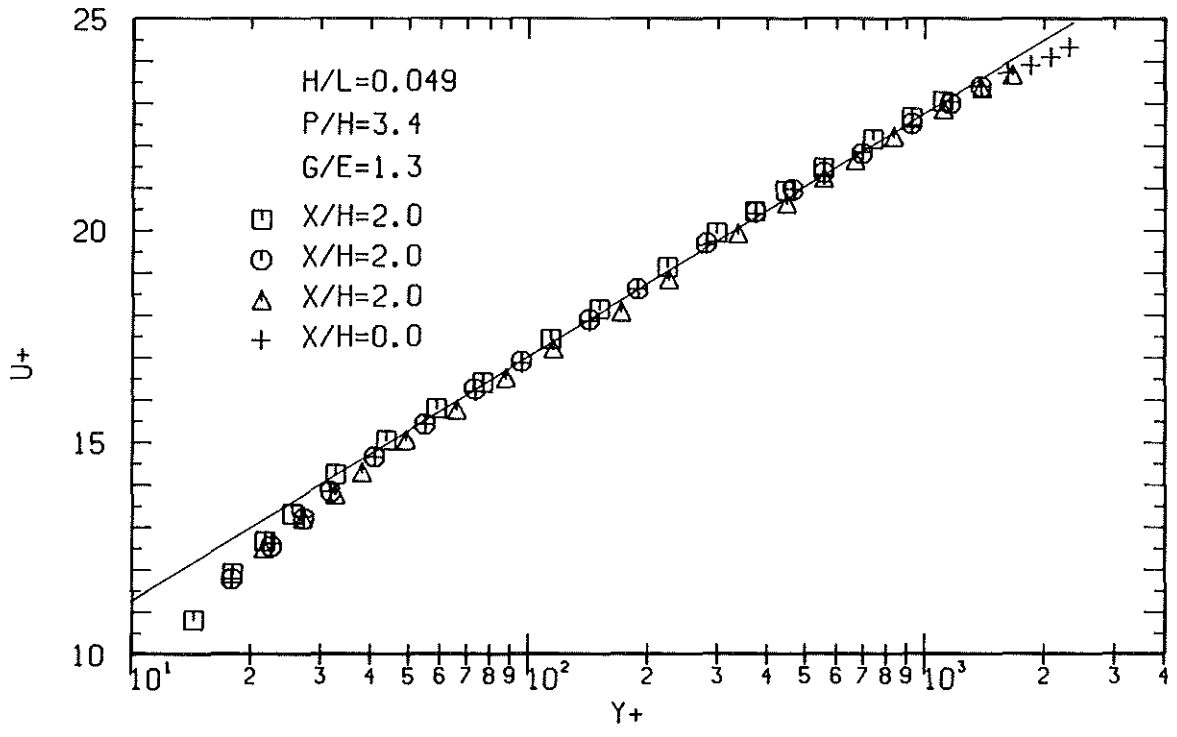

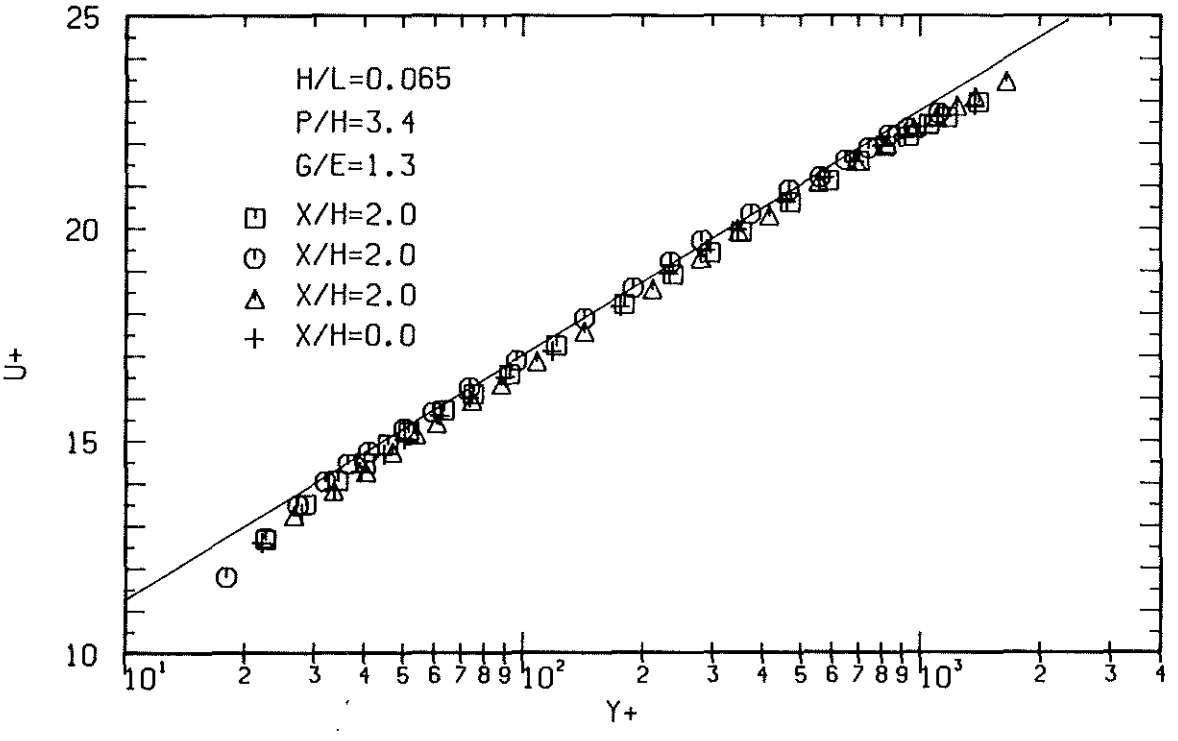

Fig.15.10-15.11: Non-dimensional velocity profiles at the smooth wall with roughness No.3 at opposite wall

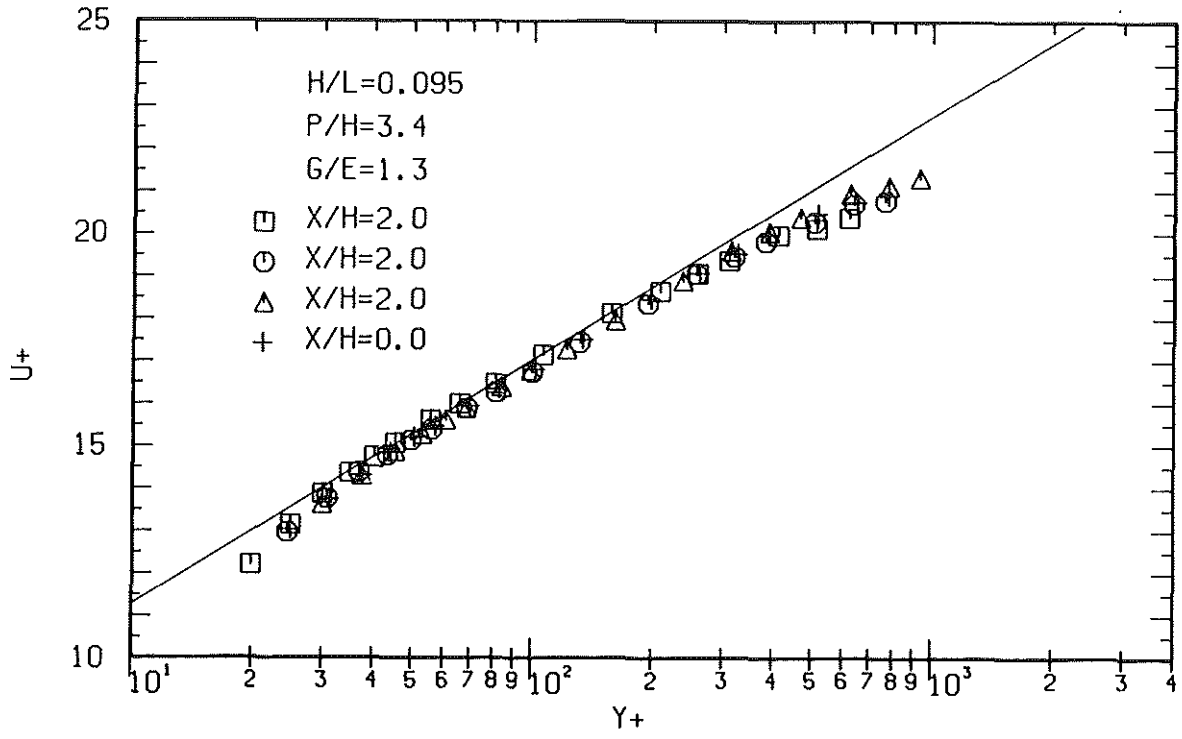

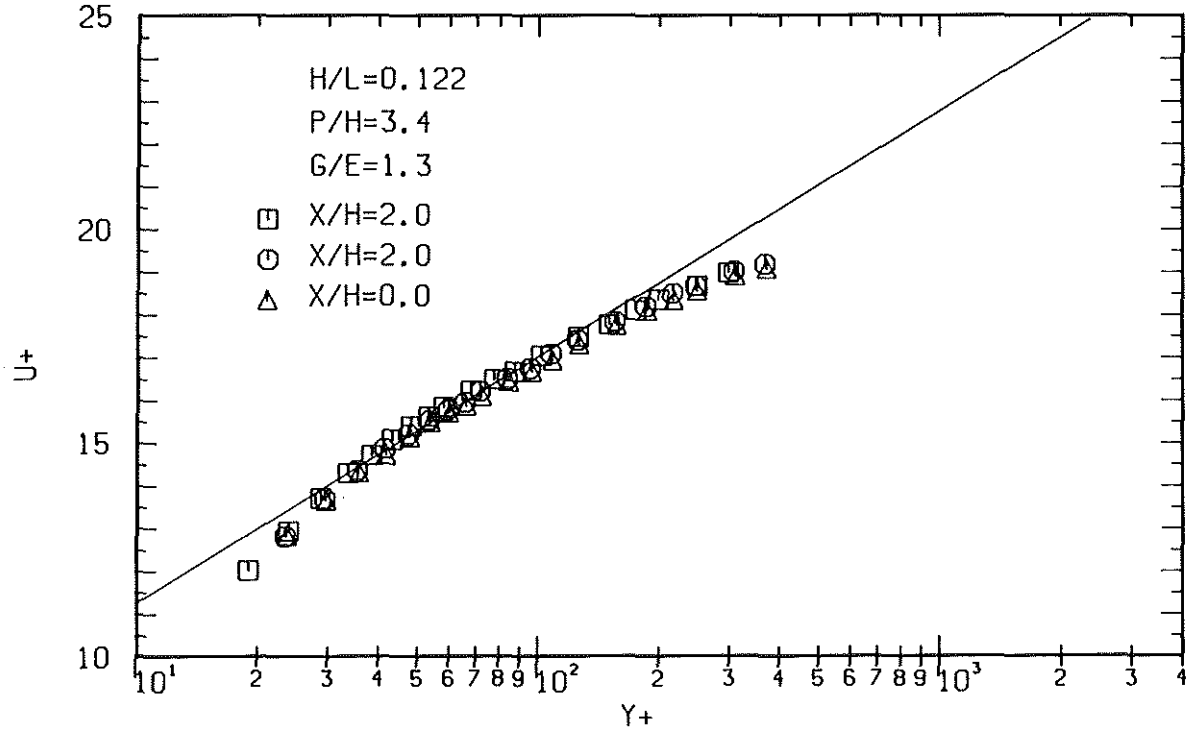

Fig.15.12-15.13: Non-dimensional velocity profiles at the smooth wall with roughness No.3 at opposite wall

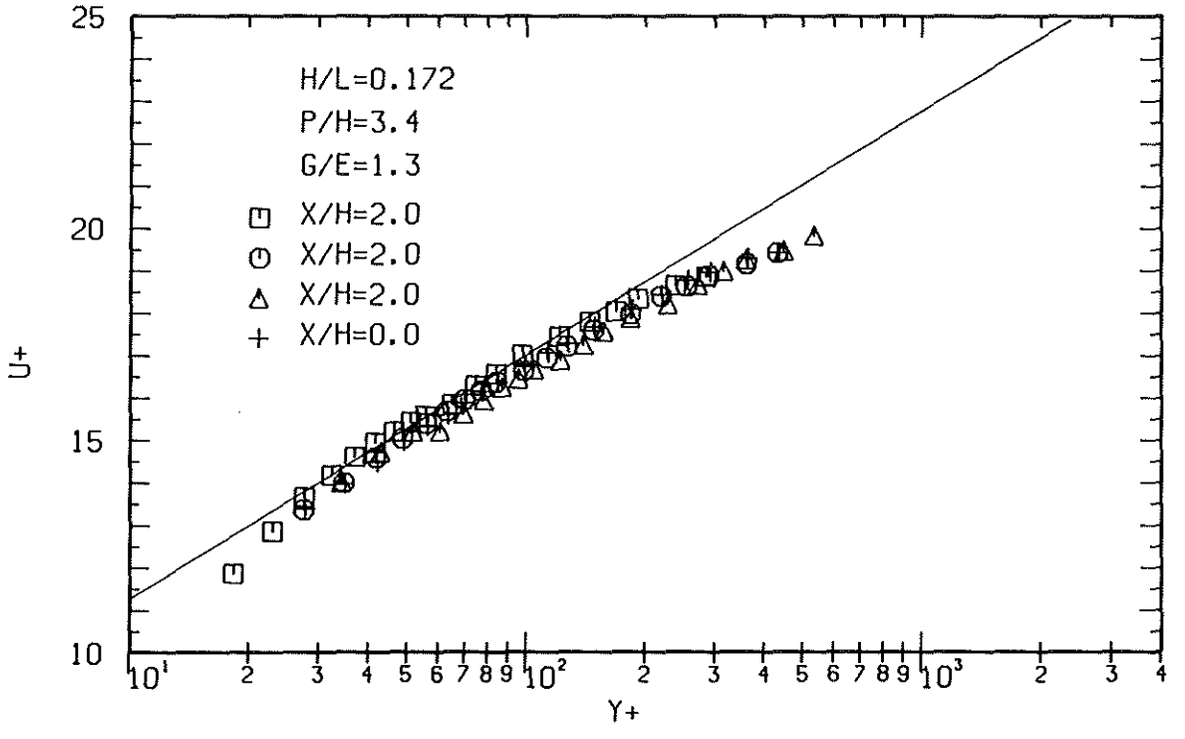

Fig.15.14: Non-dimensional velocity profiles at the smooth wall with roughness No.3 at opposite wall

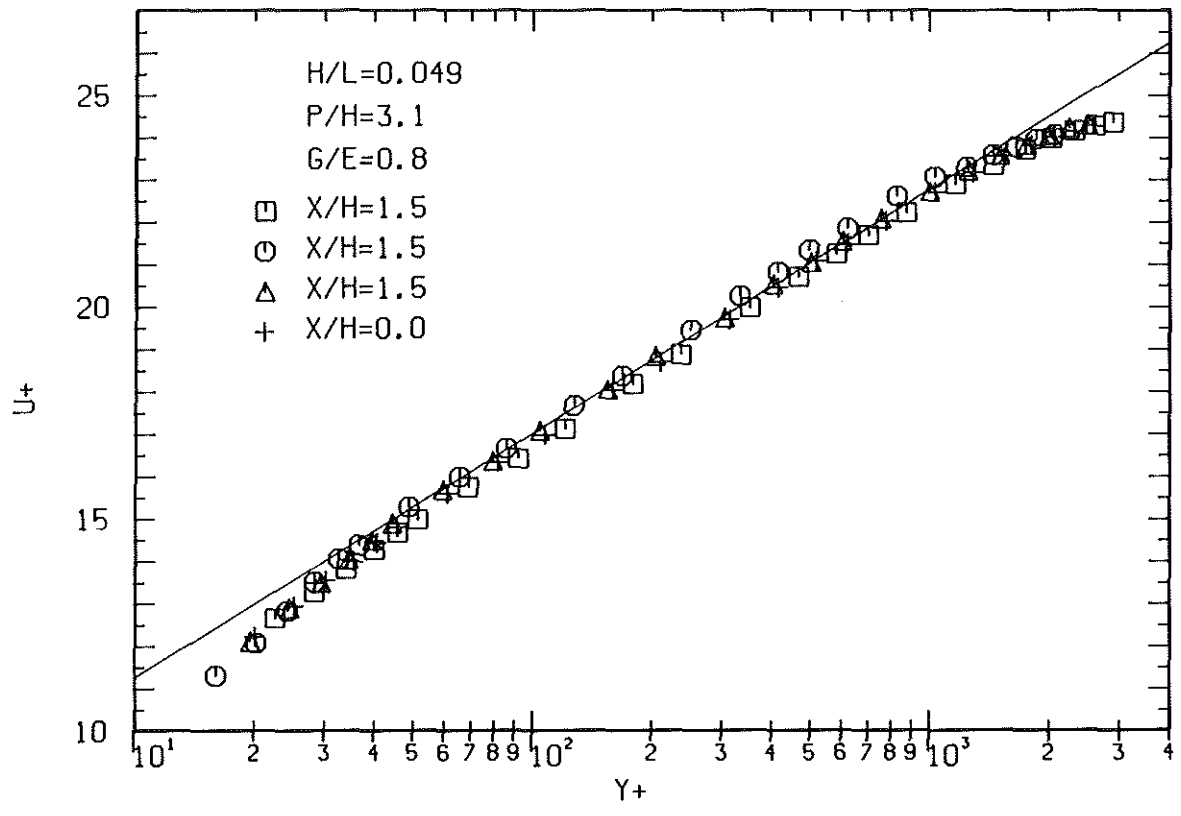

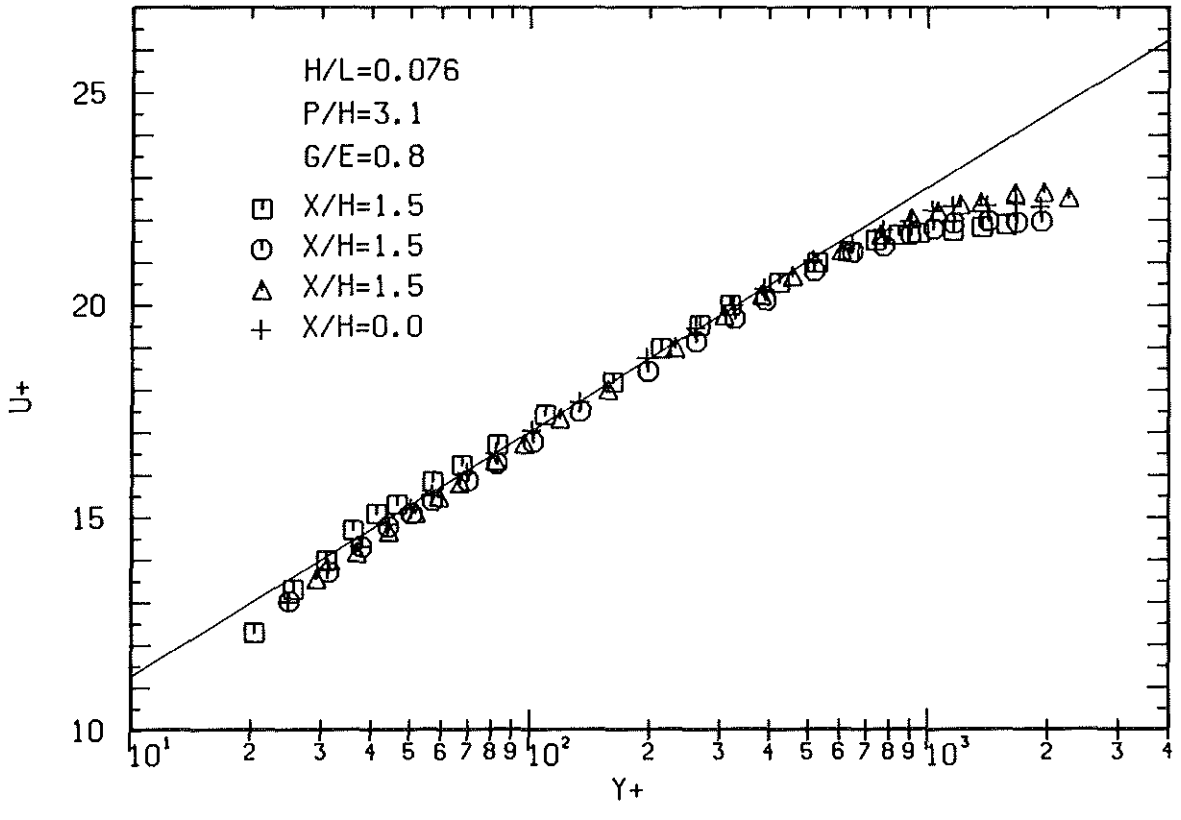

Fig.15.15-15.16: Non-dimensional velocity profiles at the smooth wall with roughness No.4 at opposite wall

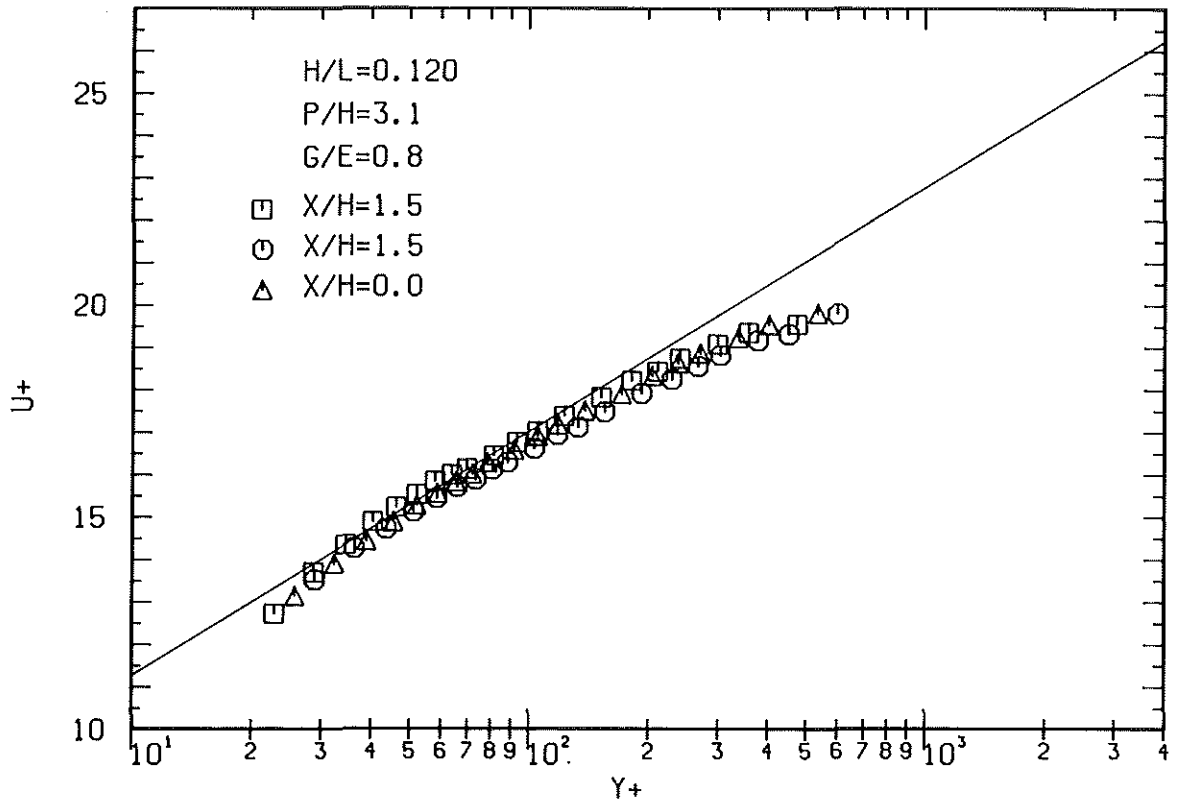

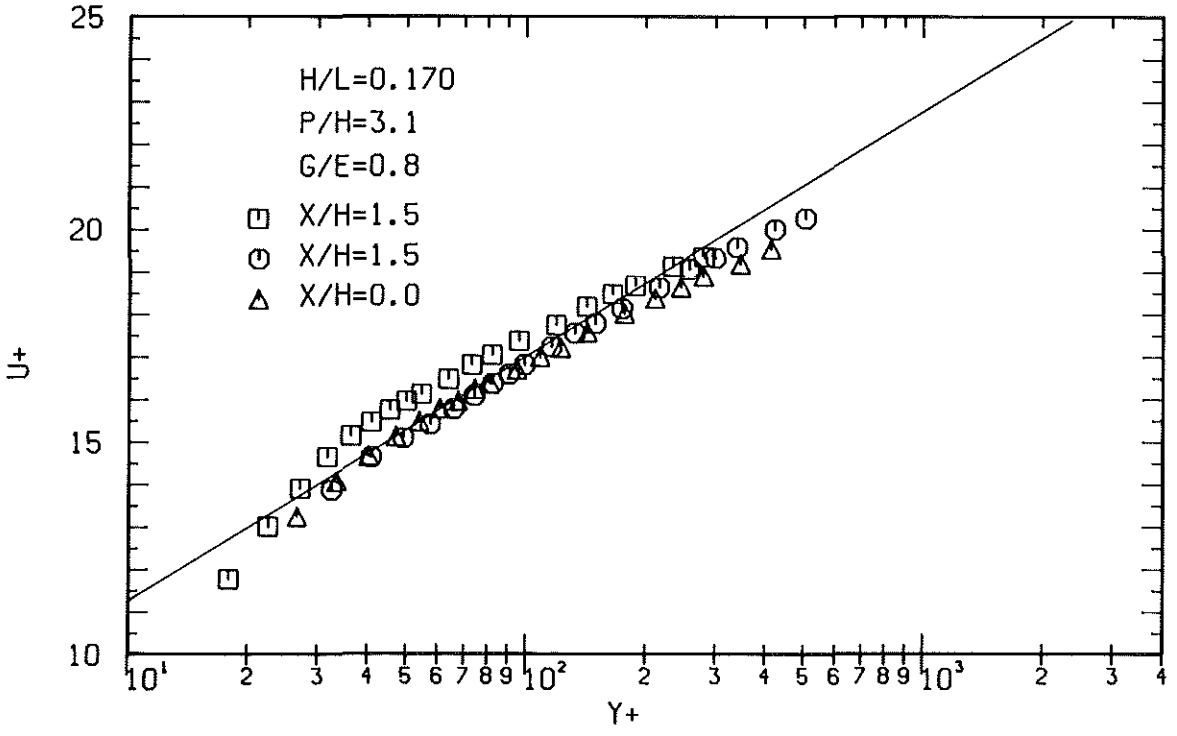

Fig.15.17-15.18: Non-dimensional velocity profiles at the smooth wall with roughness No.4 at opposite wall

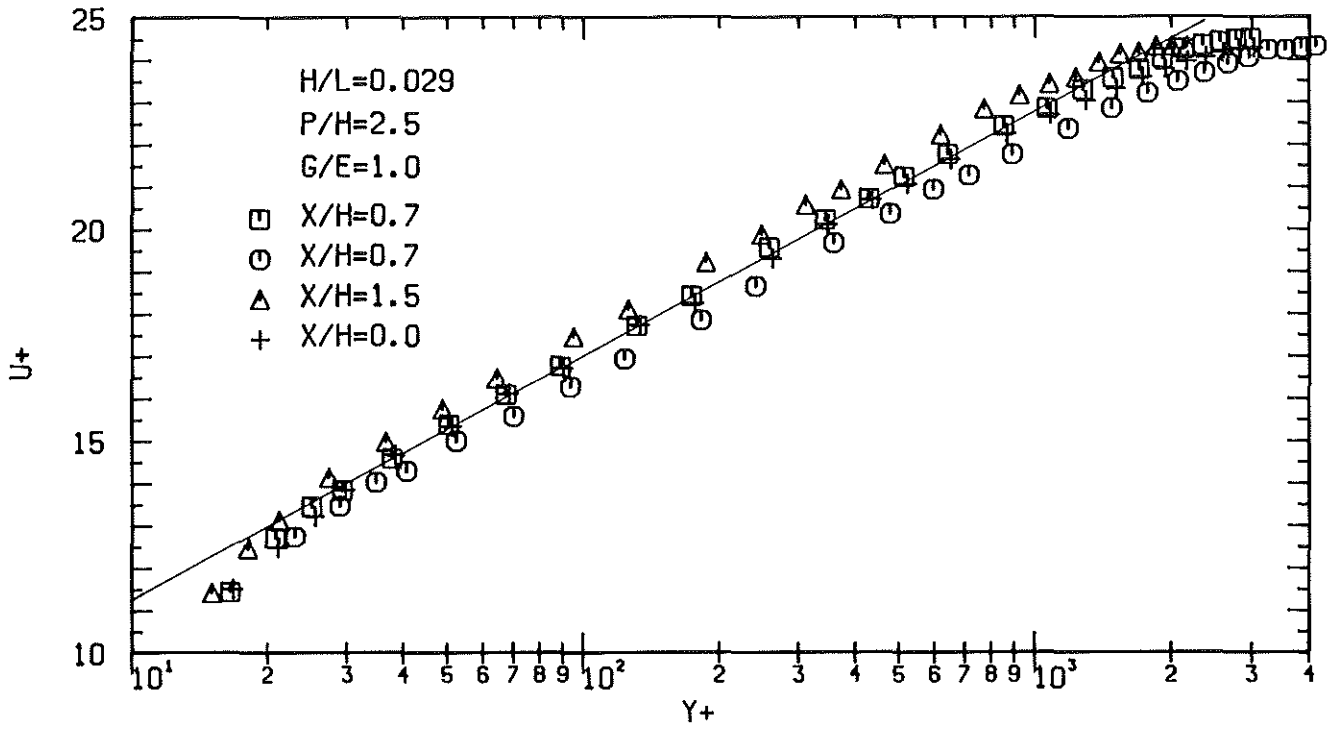

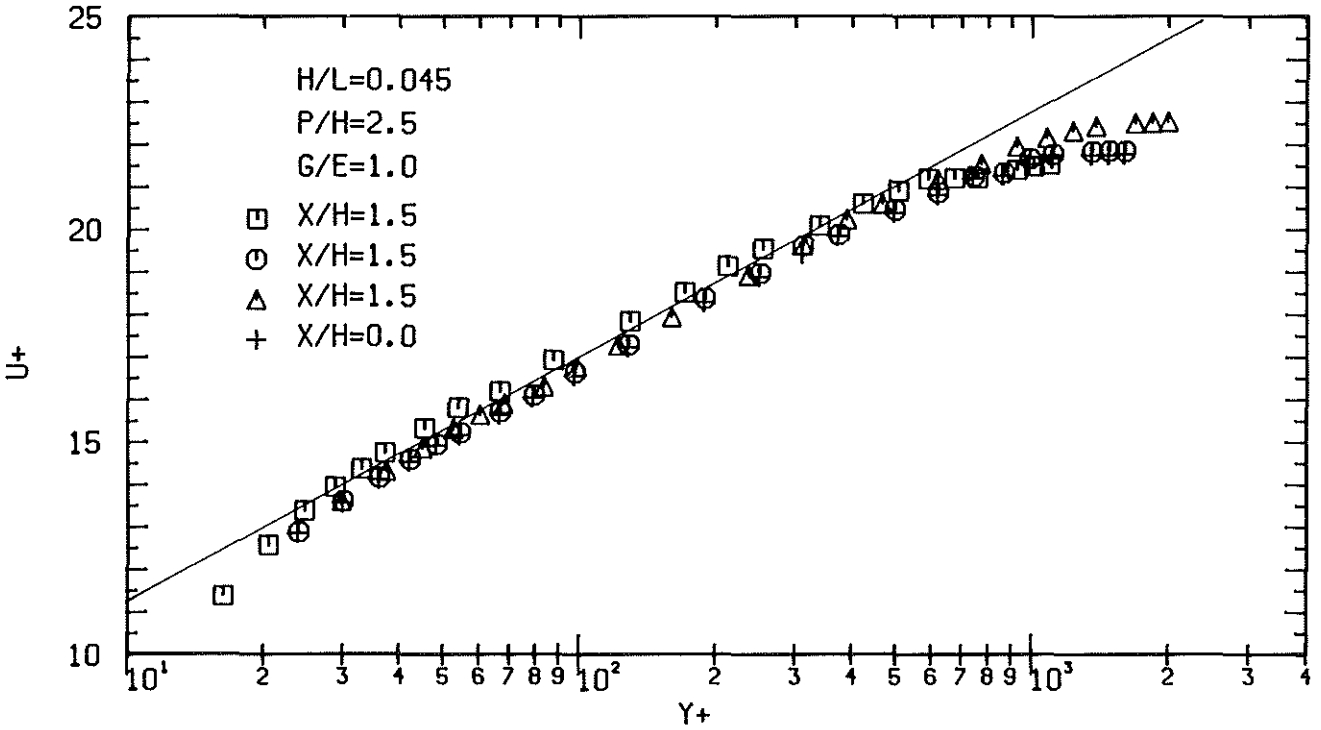

Fig.15.19-15.20: Non-dimensional velocity profiles at the smooth wall with roughness No.5 at opposite wall

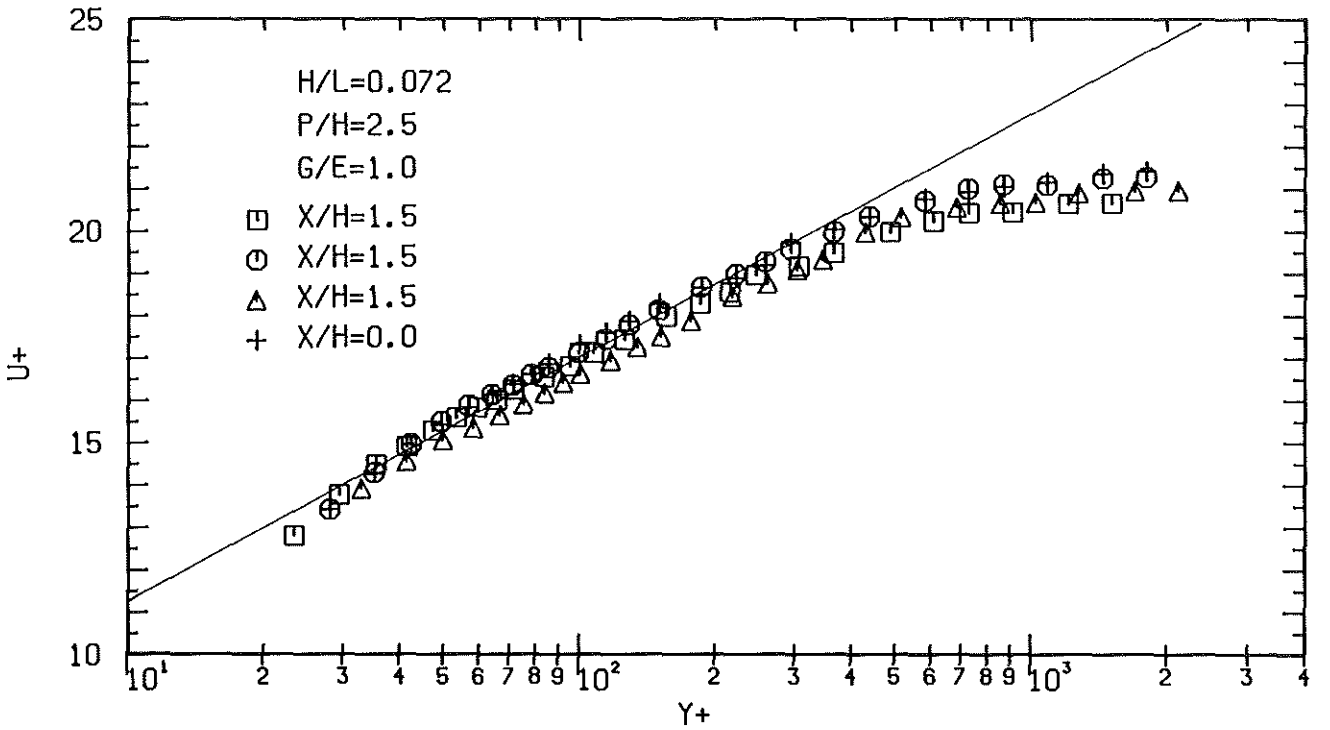

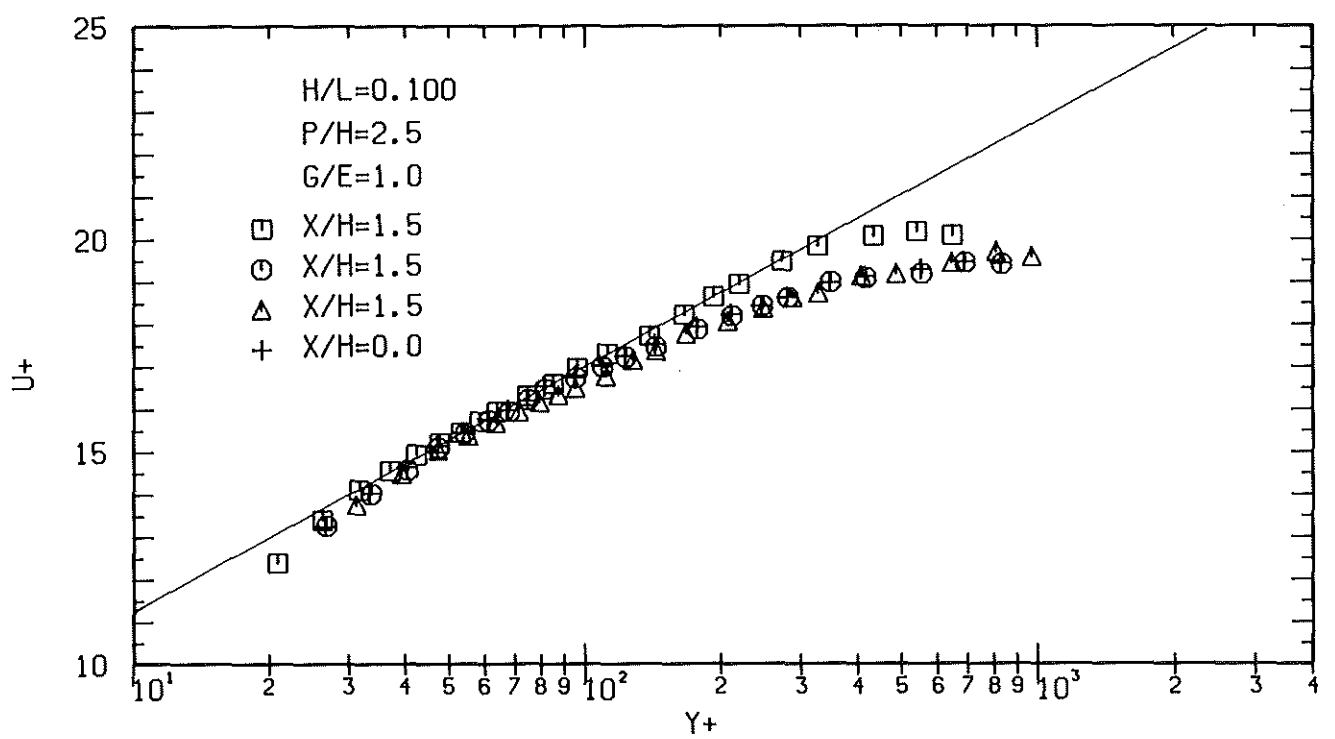

Fig.15.21-15.22: Non-dimensional velocity profiles at the smooth wall with roughness No.5 at opposite wall

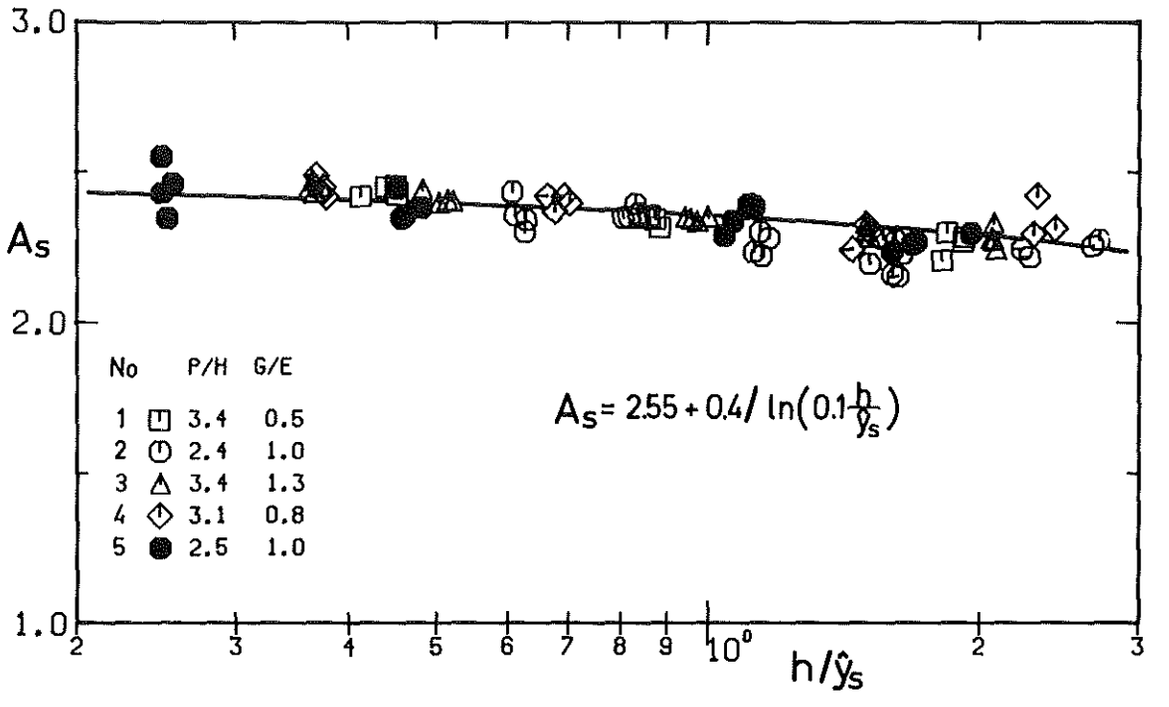

Fig.16: The profile parameter A_s determined by equation (15) with B=5.5

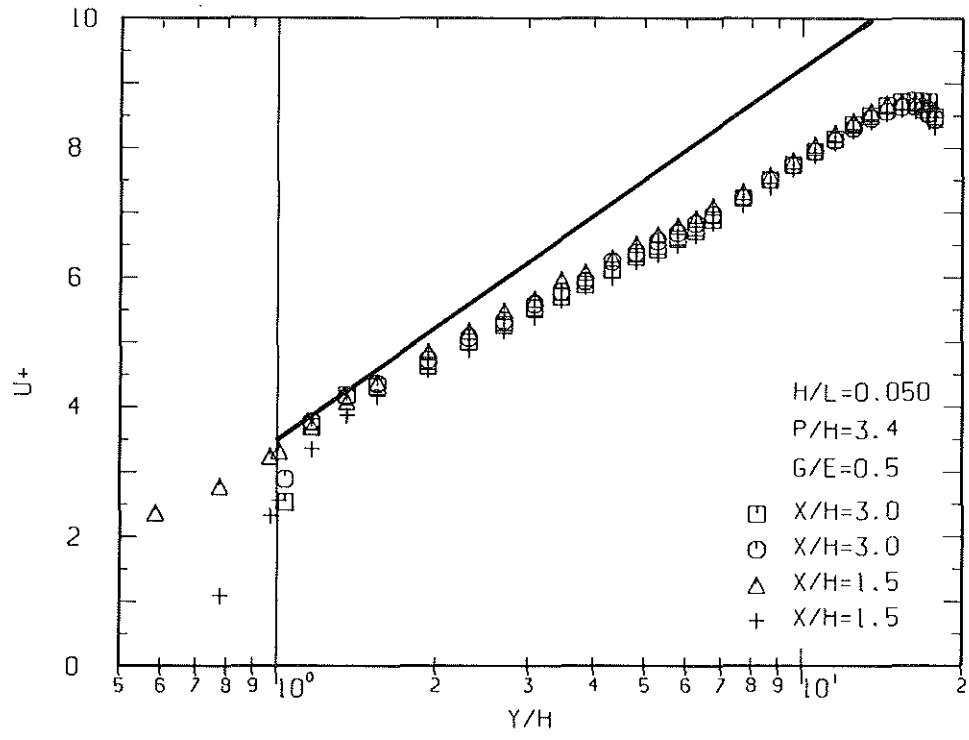

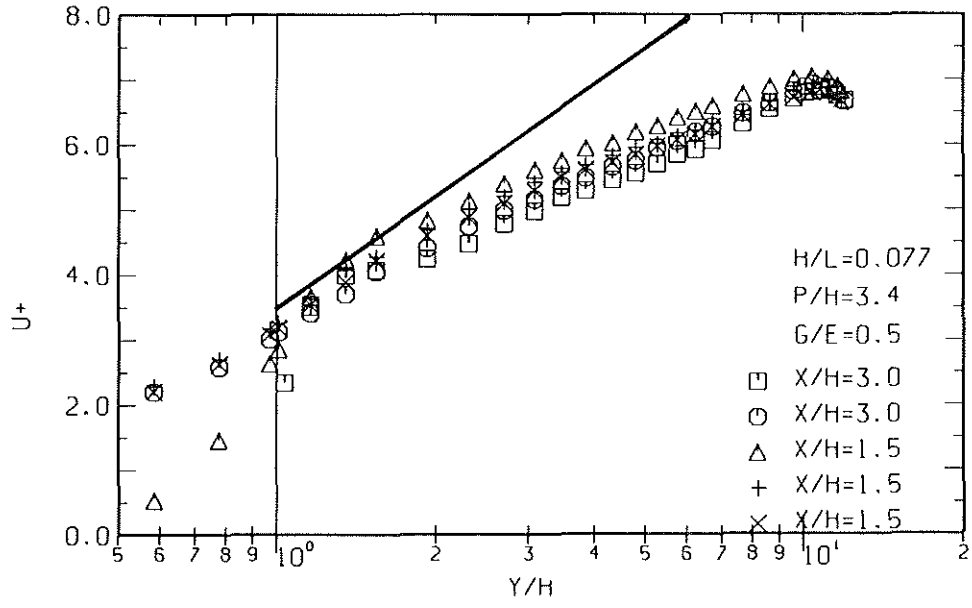

Fig.17.1-17.2: Non-dimensional velocity profiles at the rough wall (No.1)

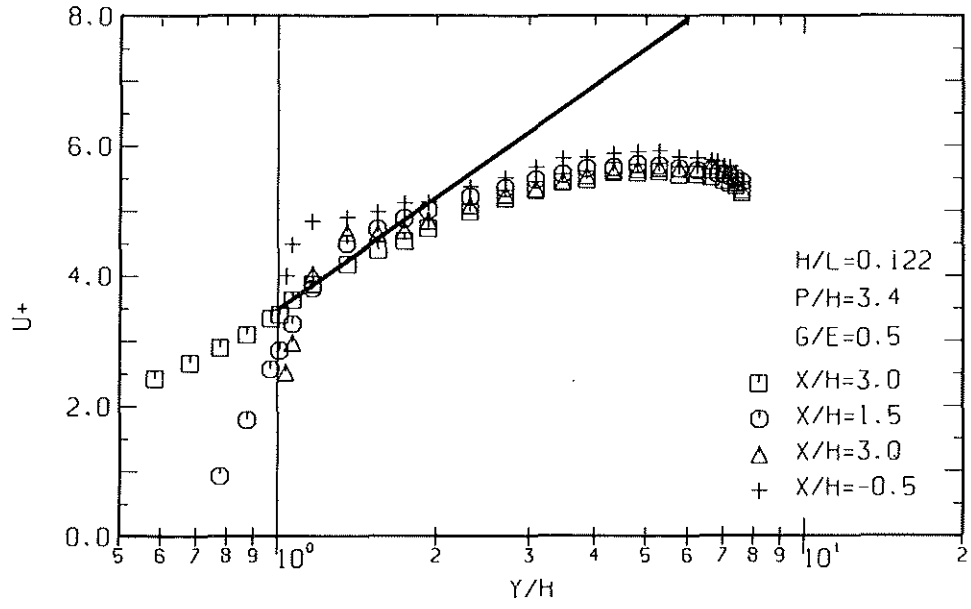

Fig.17.3: Non-dimensional velocity profiles at the rough wall (No.1)

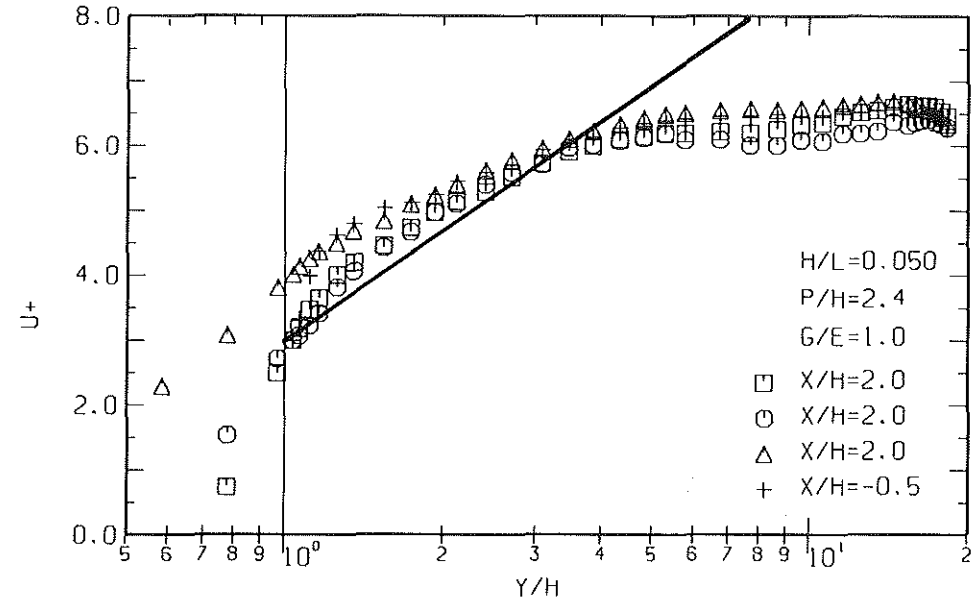

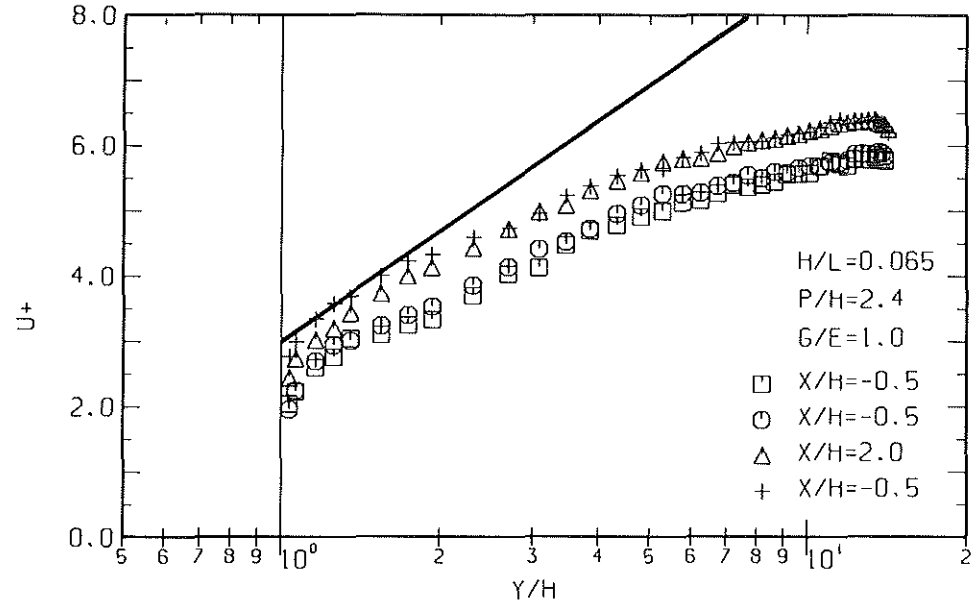

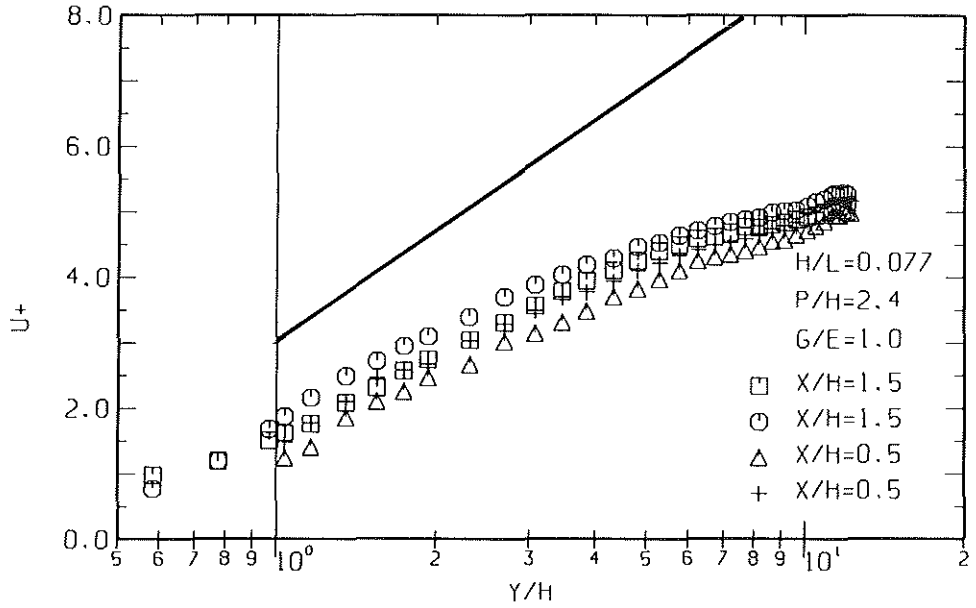

Fig.17.4-17.6: Non-dimensional velocity profiles at the rough wall (No.2)

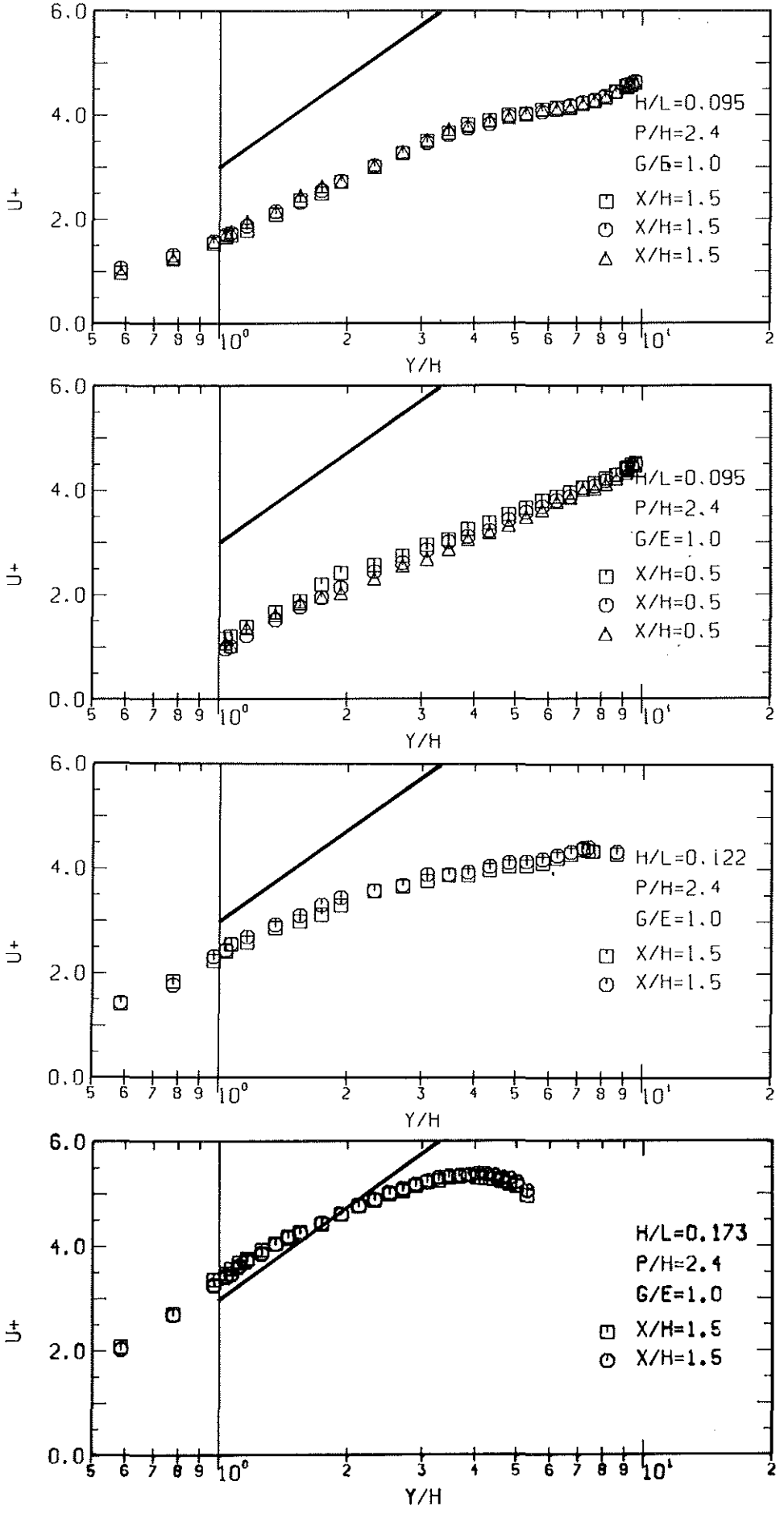

Fig.17.7-17.10: Non-dimensional velocity profiles at the rough wall (No.2)

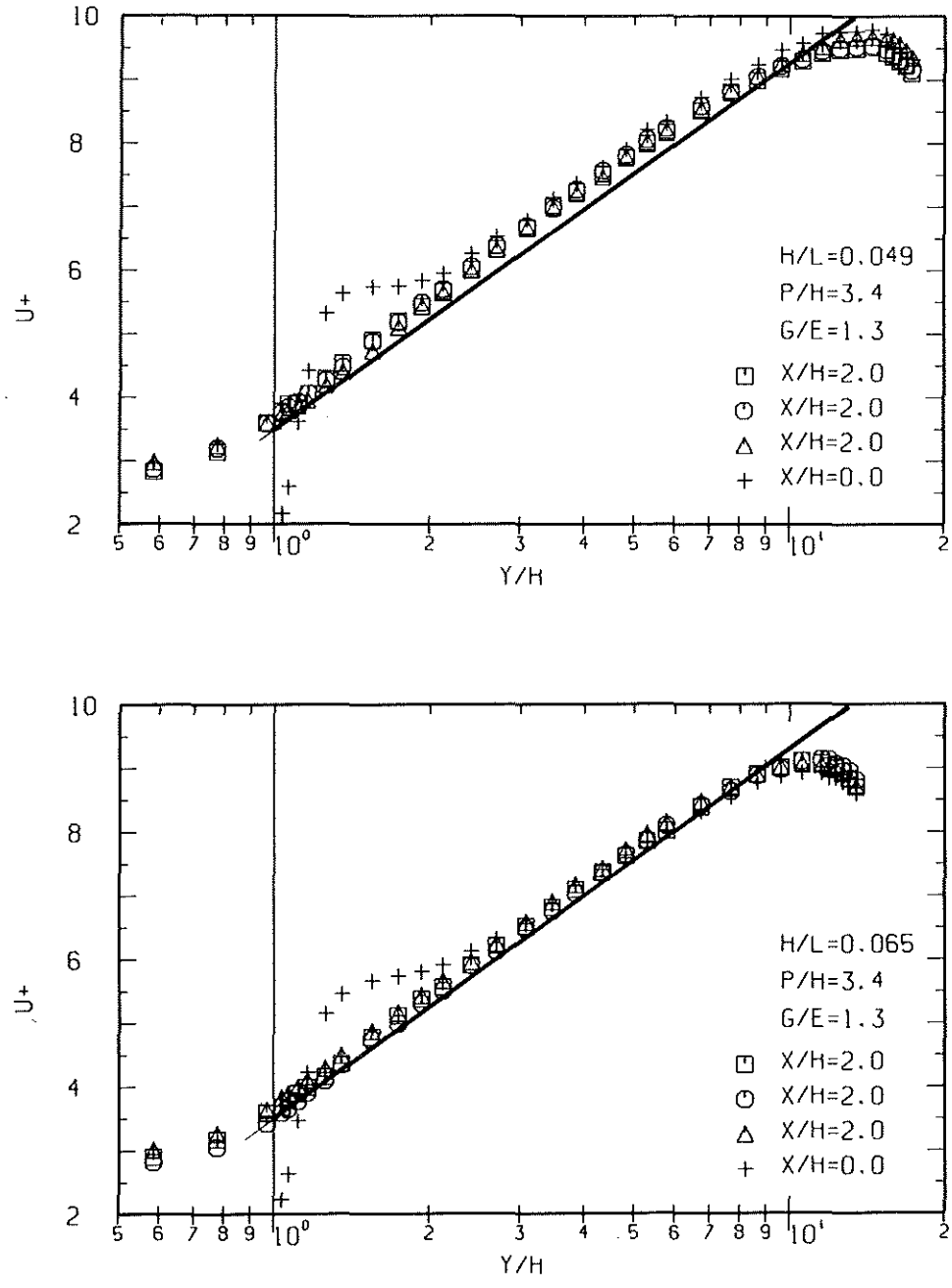

Fig.17.11-17.12: Non-dimensional velocity profiles at the rough wall (No.3)

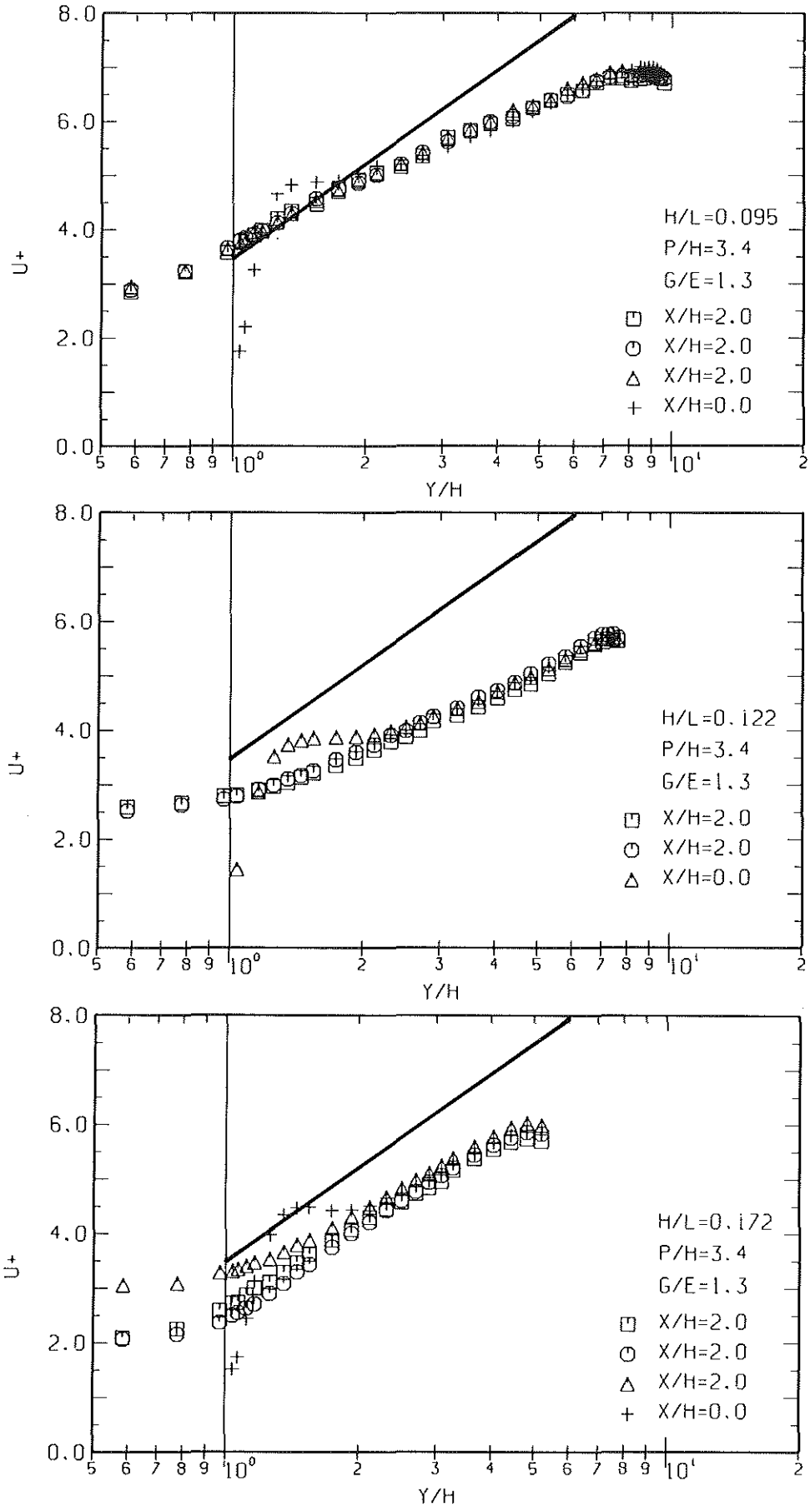

Fig.17.13-17.15: Non-dimensional velocity profiles at the rough wall (No.3)

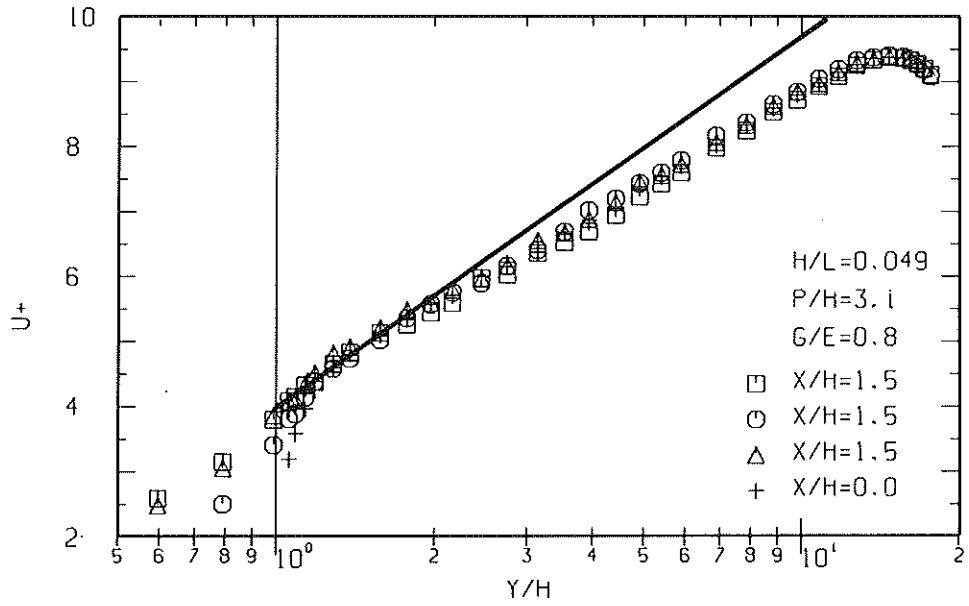

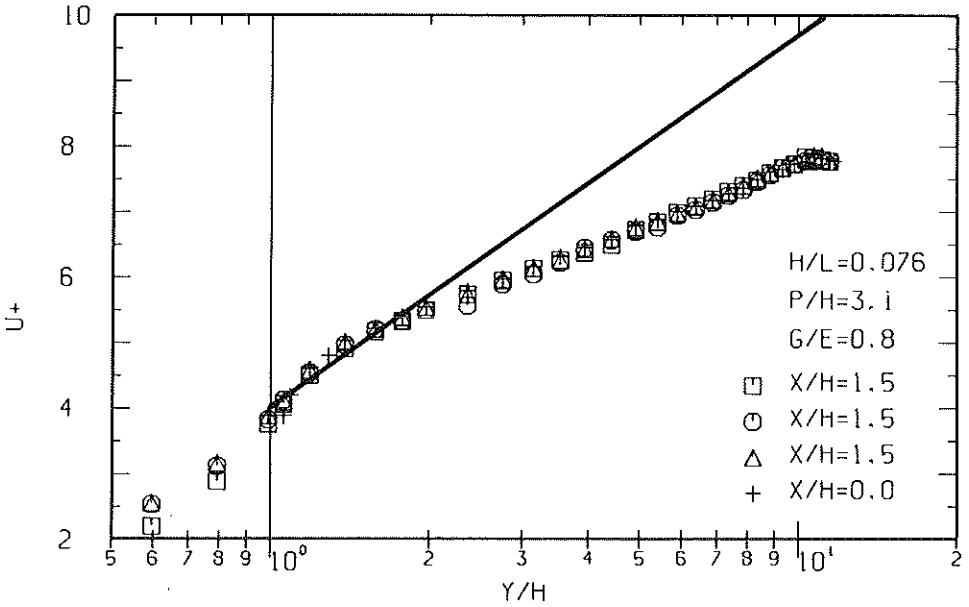

Fig.17.16-17.17: Non-dimensional velocity profiles at the rough wall (No.4)

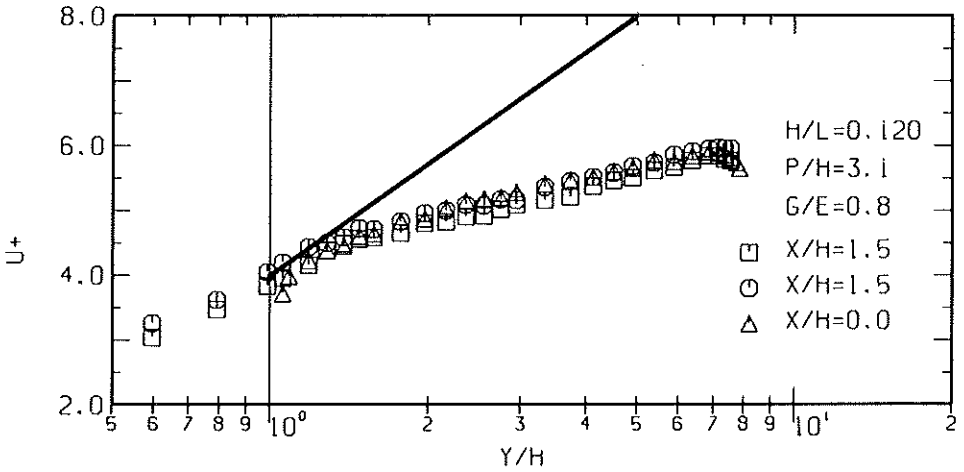

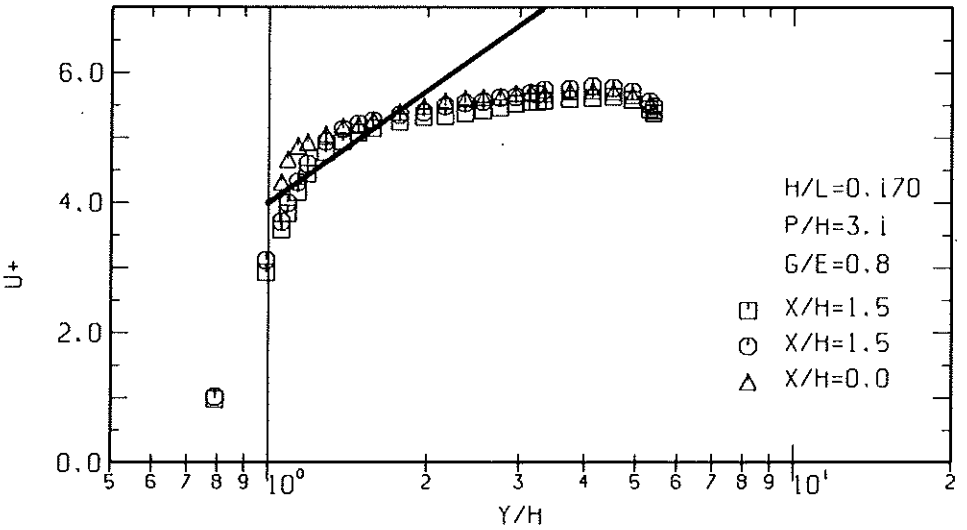

Fig.17.18-17.19: Non-dimensional velocity profiles at the rough wall (No.4)

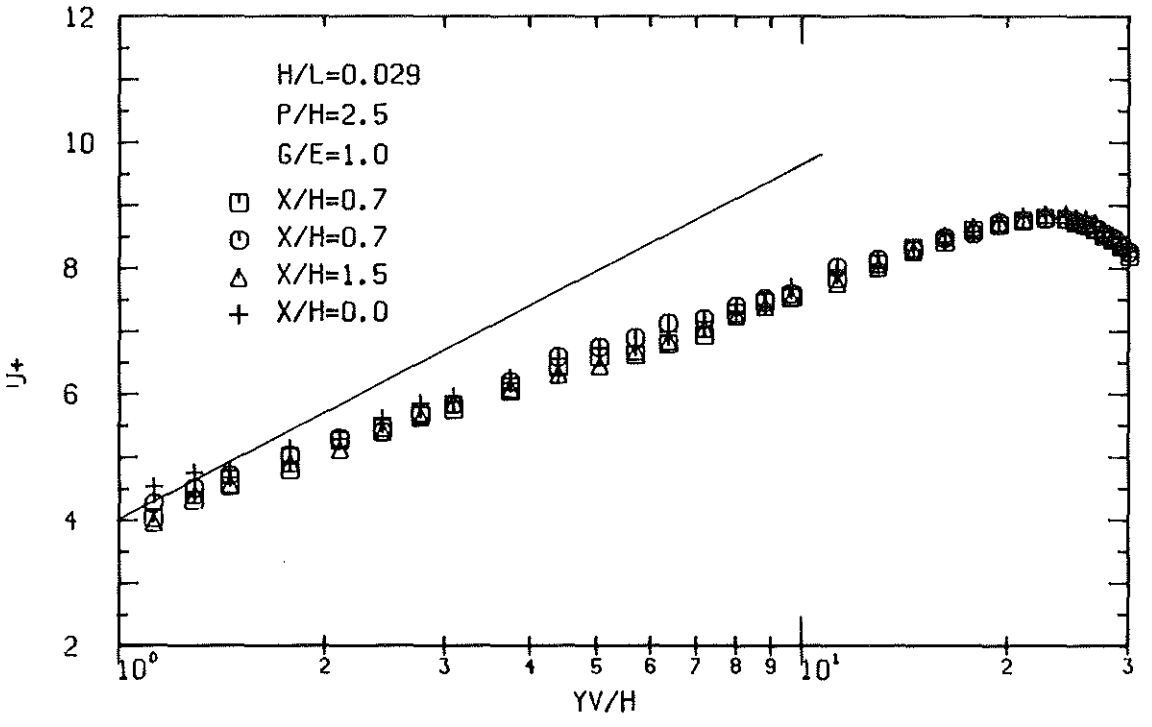

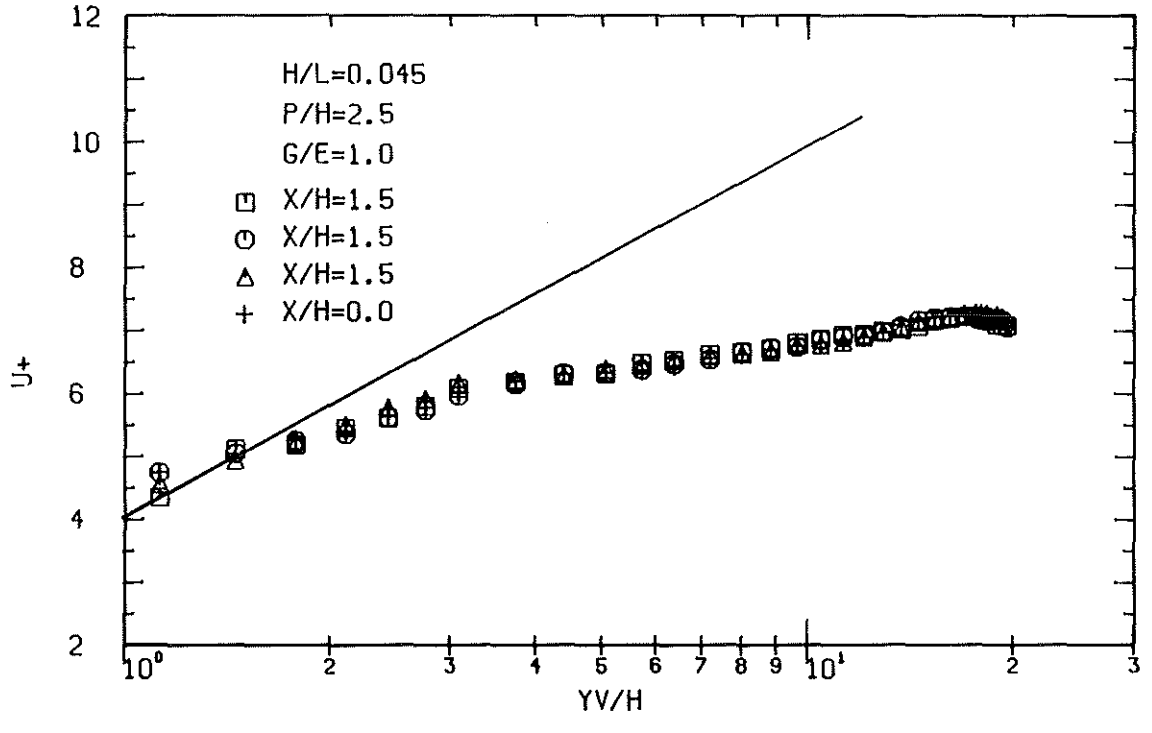

Fig.17.20-17.21: Non-dimensional velocity profiles at the rough wall (No.5)

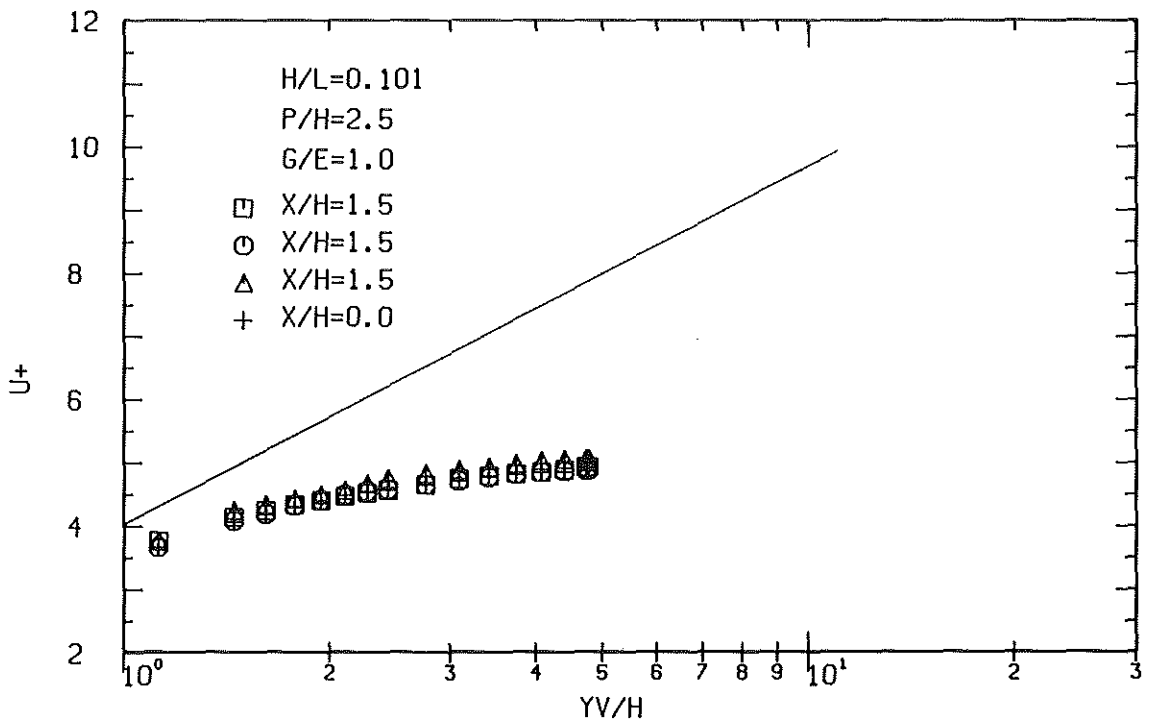

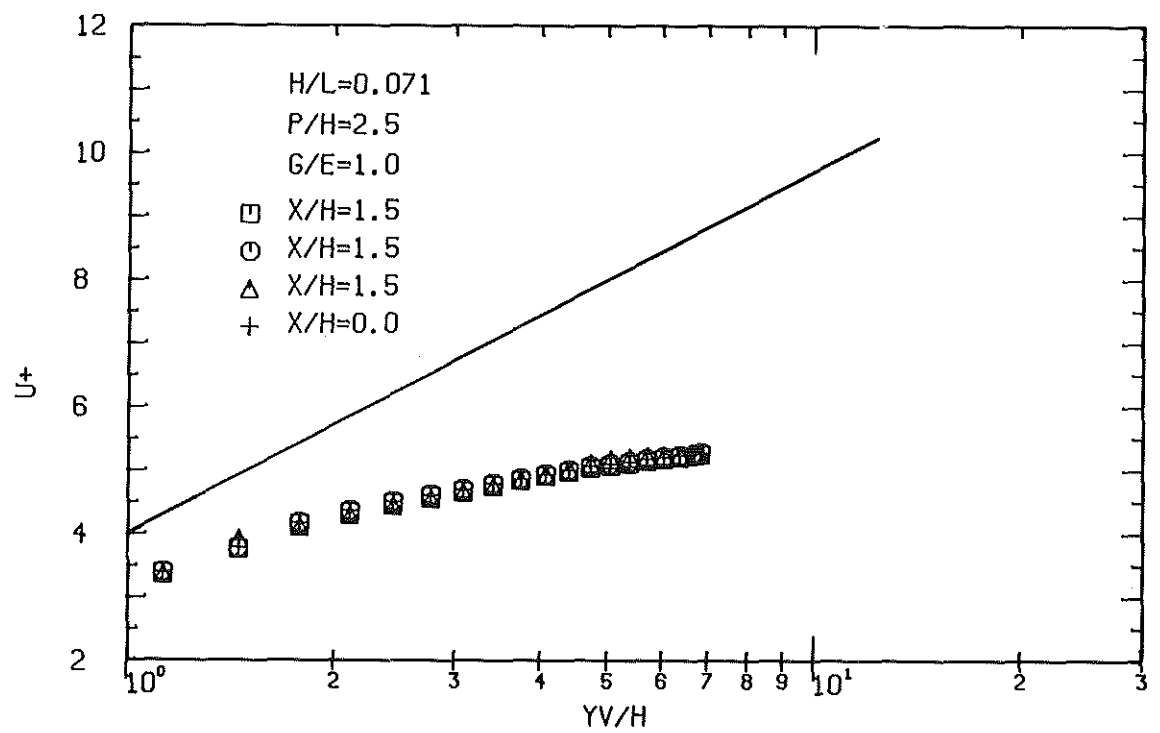

Fig.17.22-17.23: Non-dimensional velocity profiles at the rough wall (No.5)

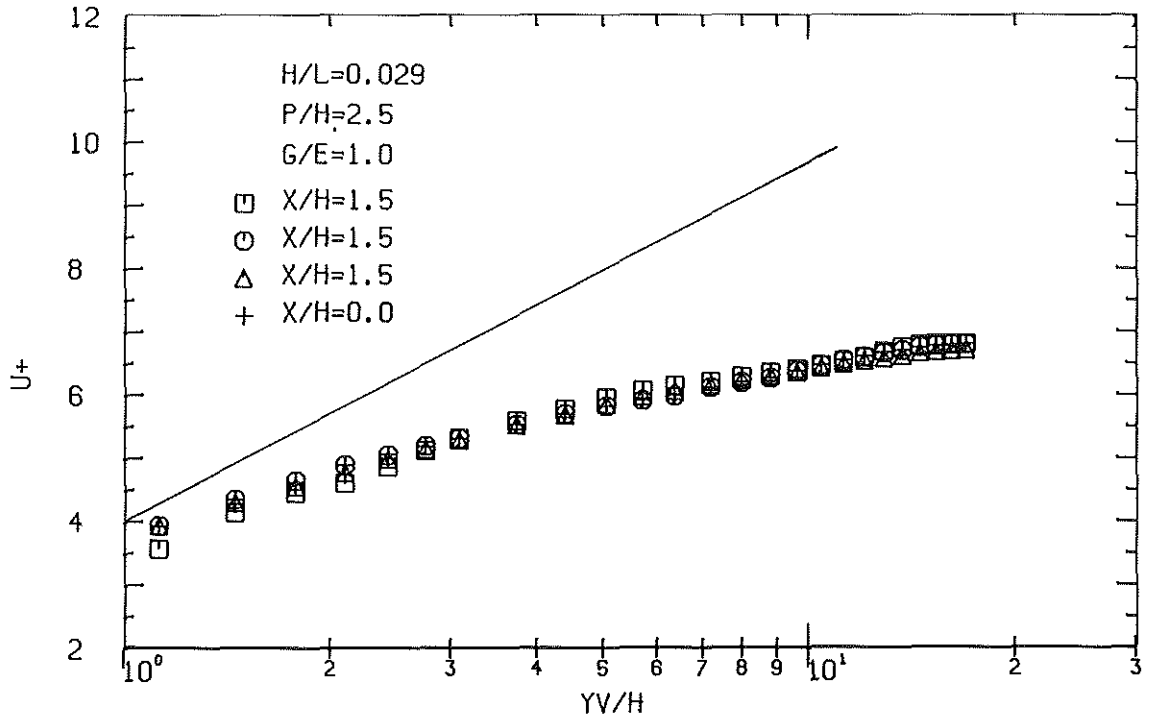

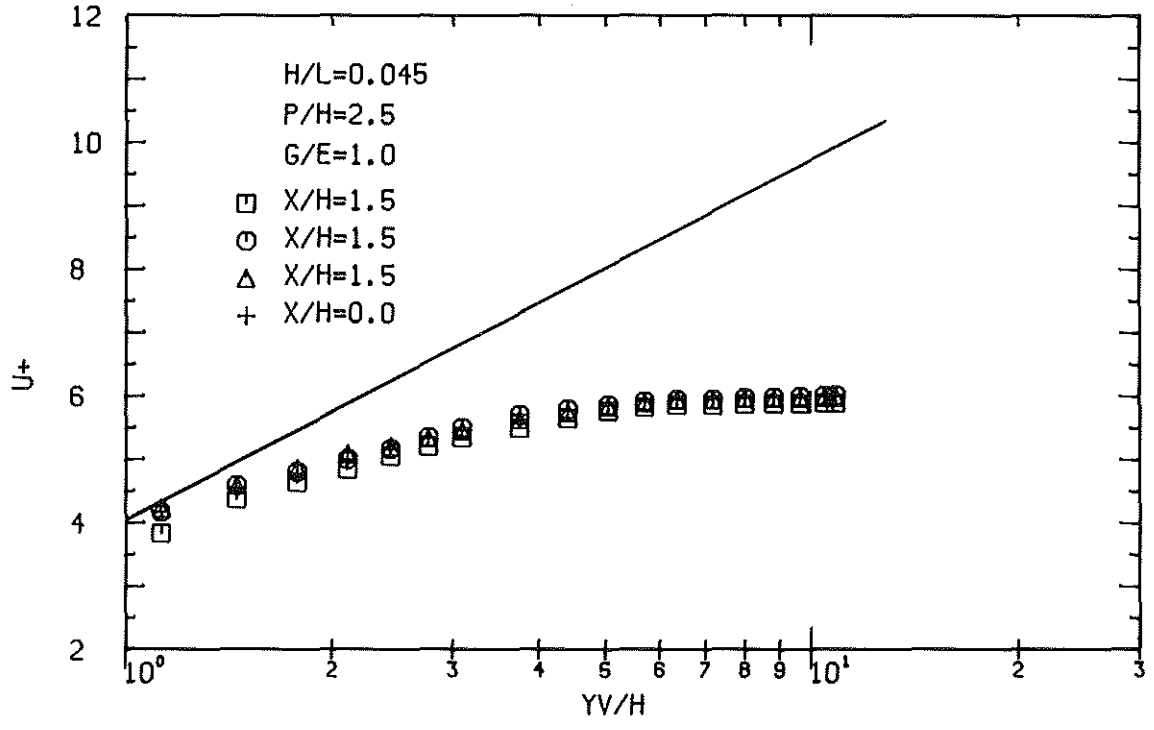

Fig.17.24-17.25: Non-dimensional velocity profiles at the rough wall (No.5, both walls rough)

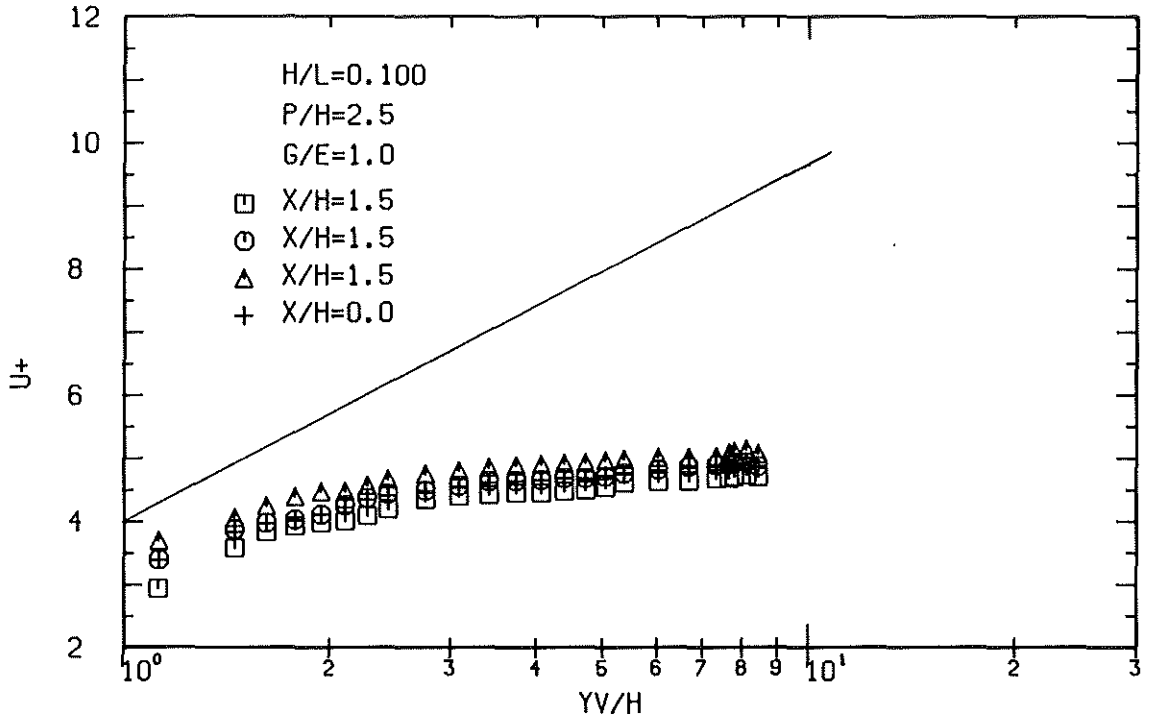

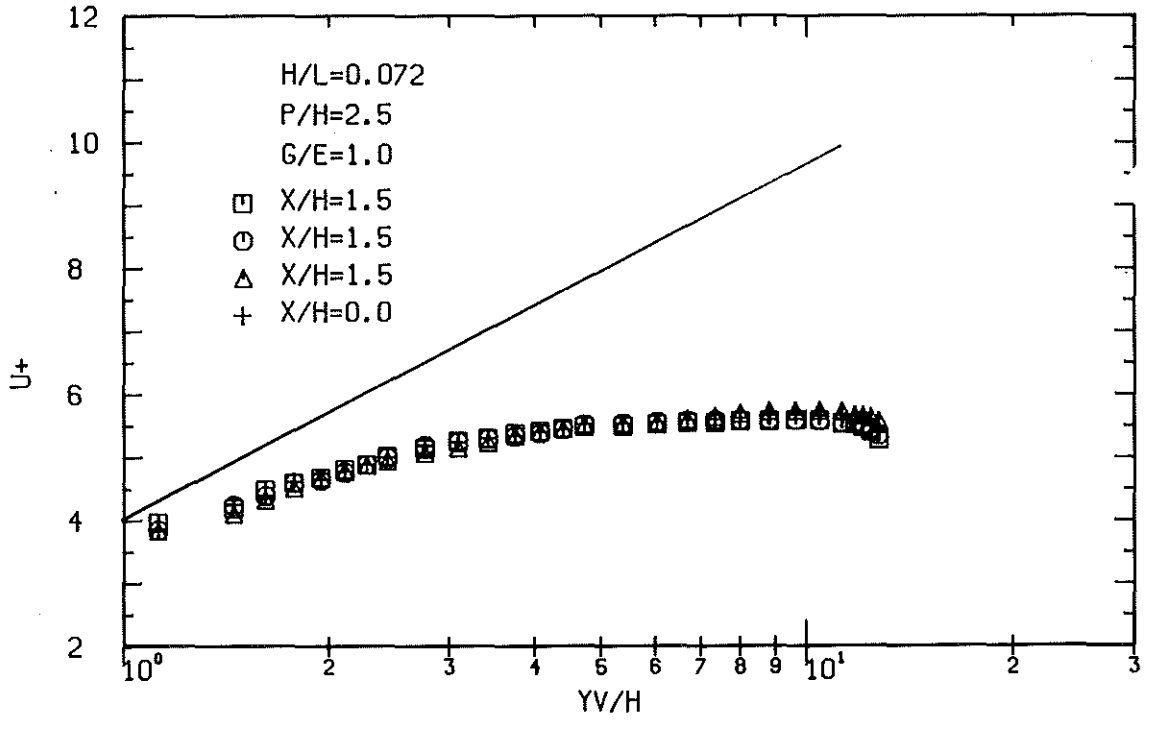

Fig.17.26-17.27: Non-dimensional velocity profiles at the rough wall (No.5, both walls rough)

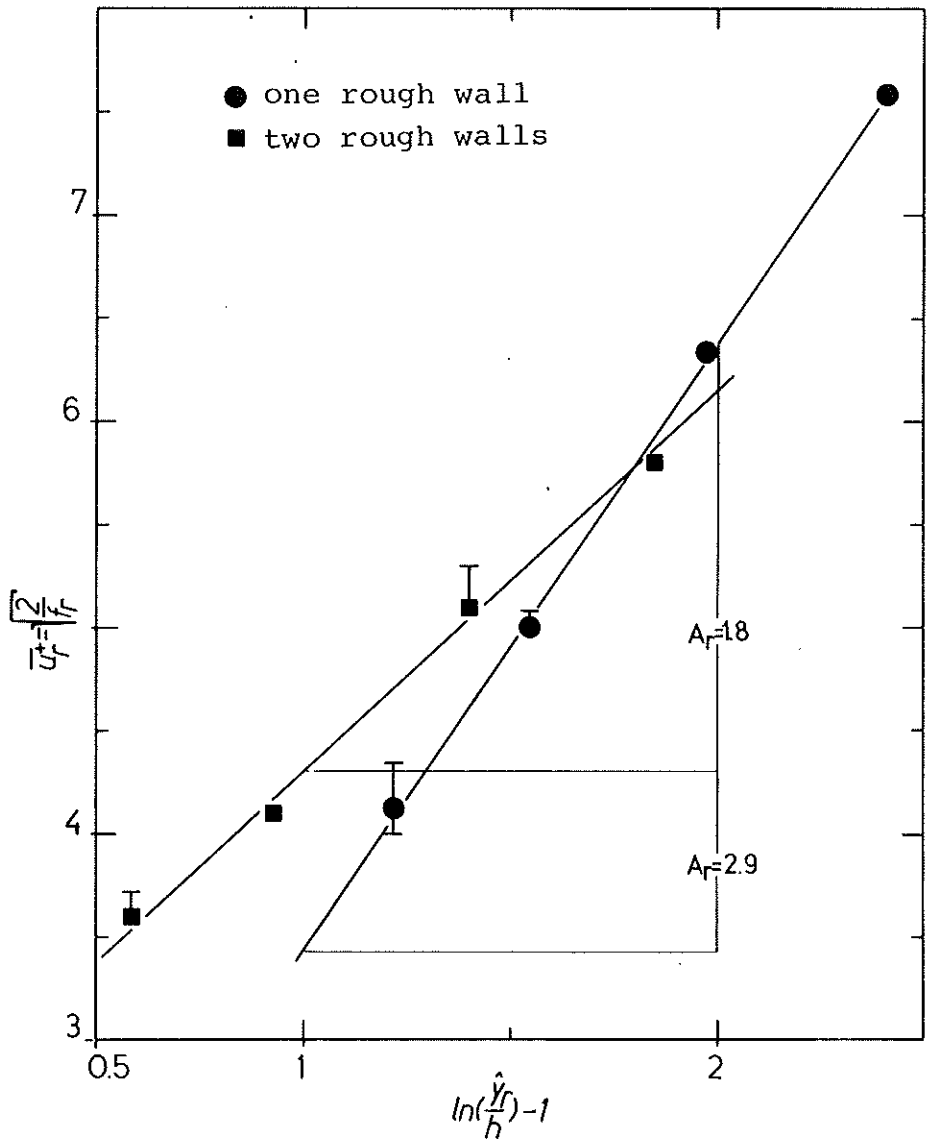

Fig.18: The average dimensionless velocity $\bar{u}_r^+$ of the rough zone versus $\ln(\hat{y}_r/h)-1$ for roughness No.5 in symmetrical and asymmetrical flow ($\varepsilon=\varepsilon_{vol}$)

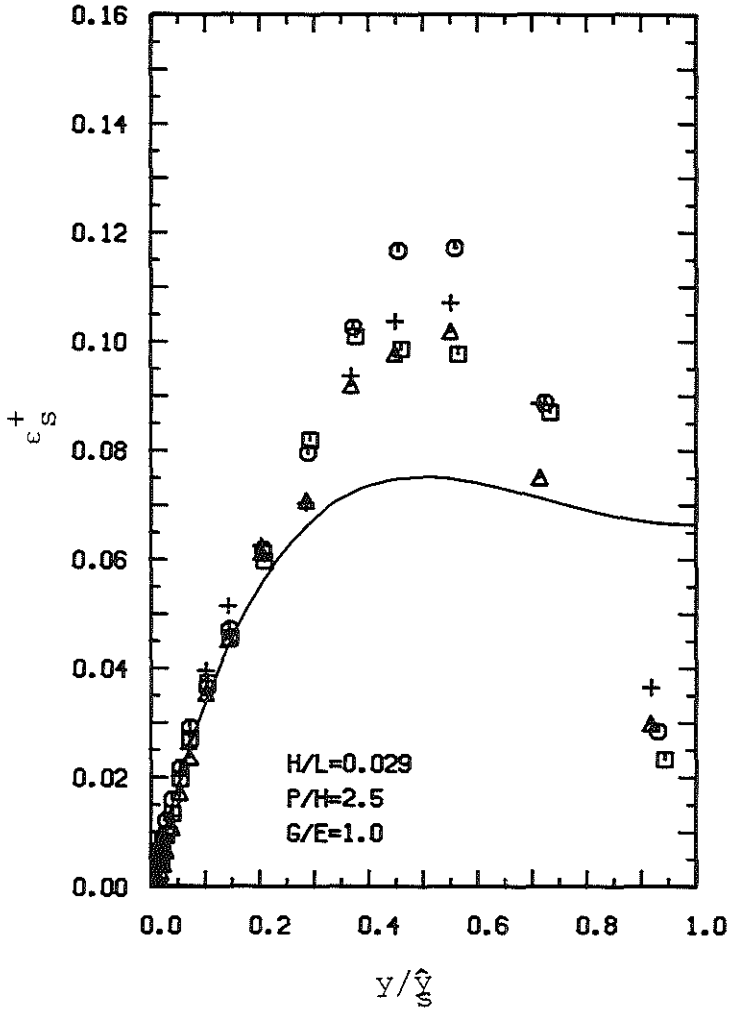

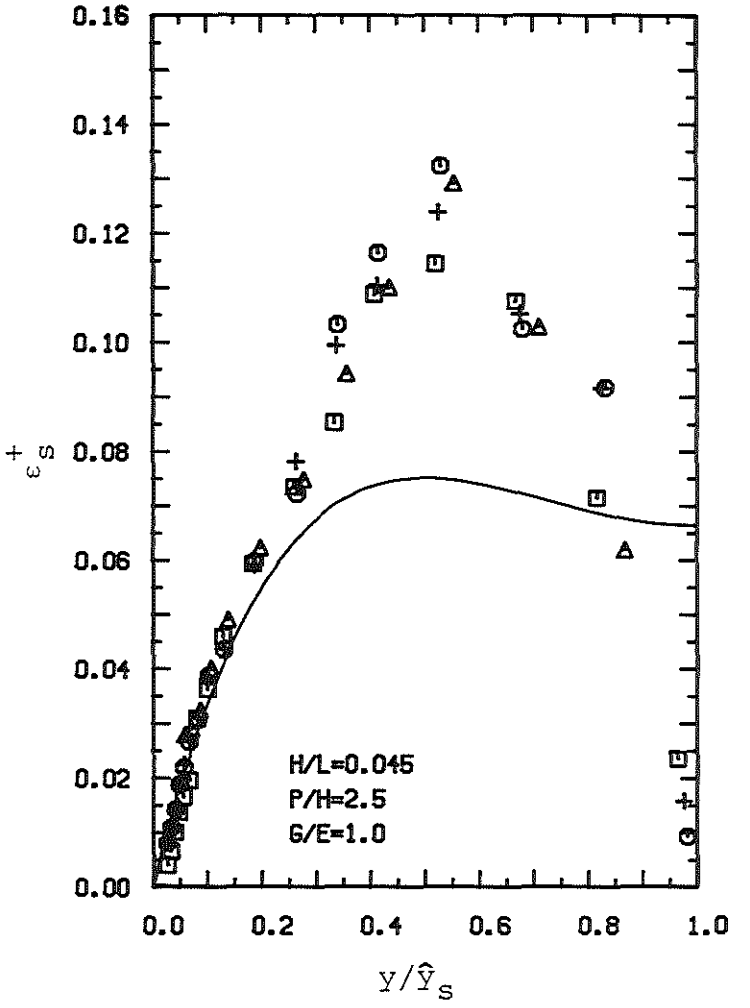

Fig.19.1-19.2: Eddy viscosity ε_s^+ in the smooth zone (No.5)

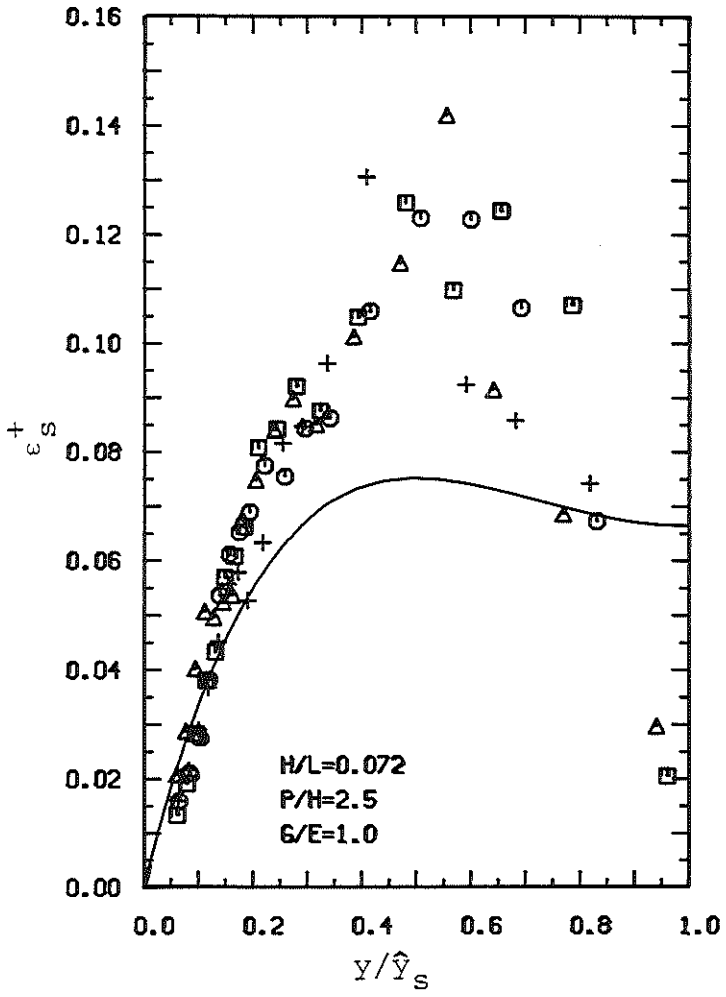

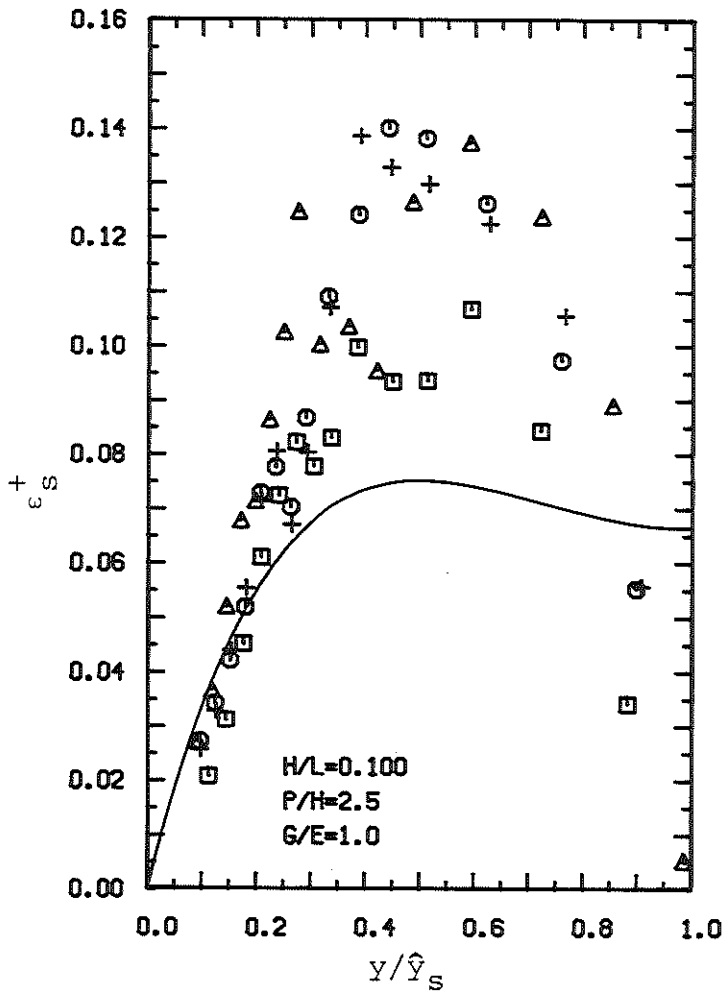

Fig.19.3-19.4: Eddy viscosity ε_s^+ in the smooth zone (No.5)

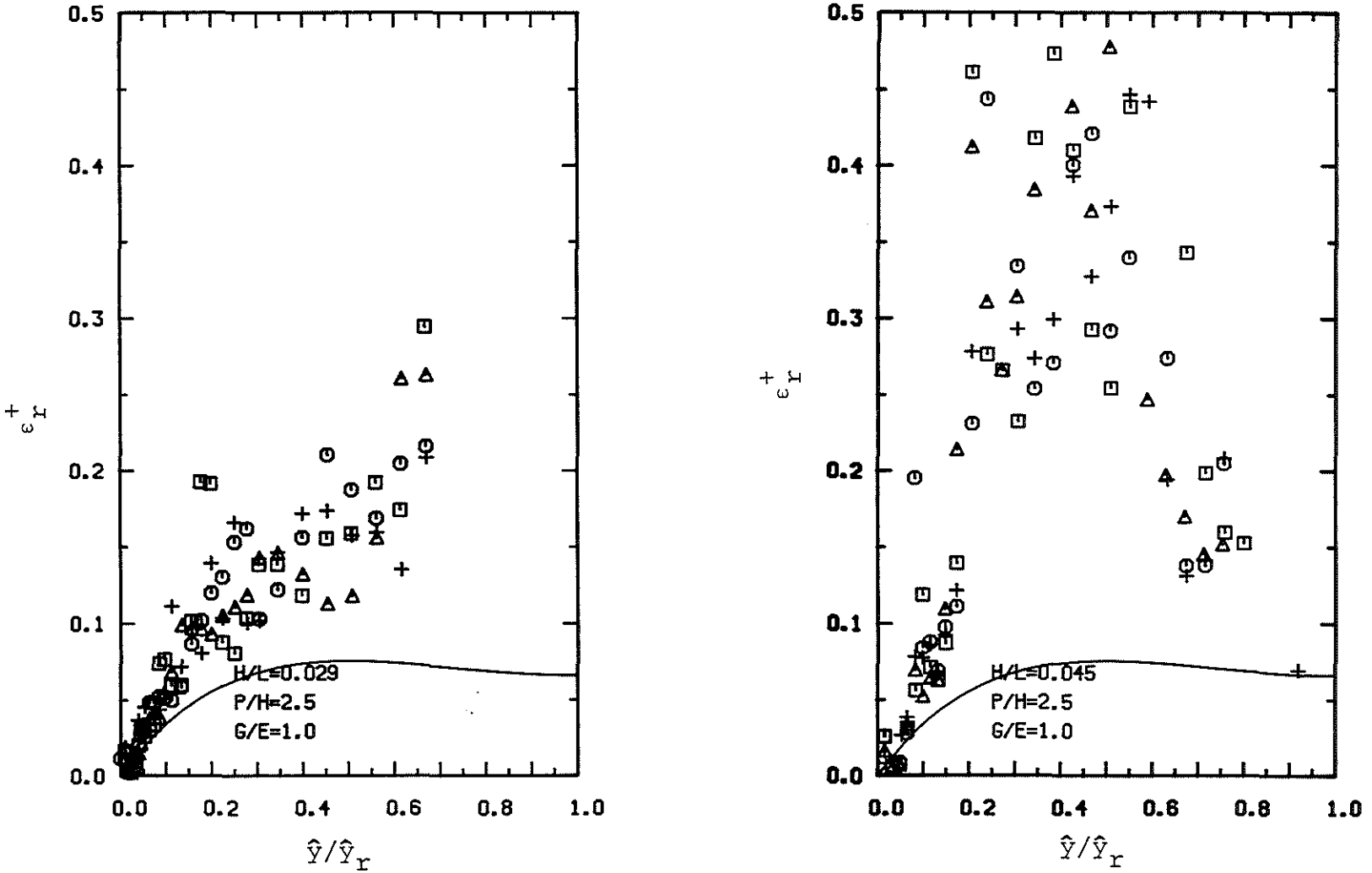

Fig.20.1-20.2: Eddy viscosity ε_r^+ in the rough zone (No.5)

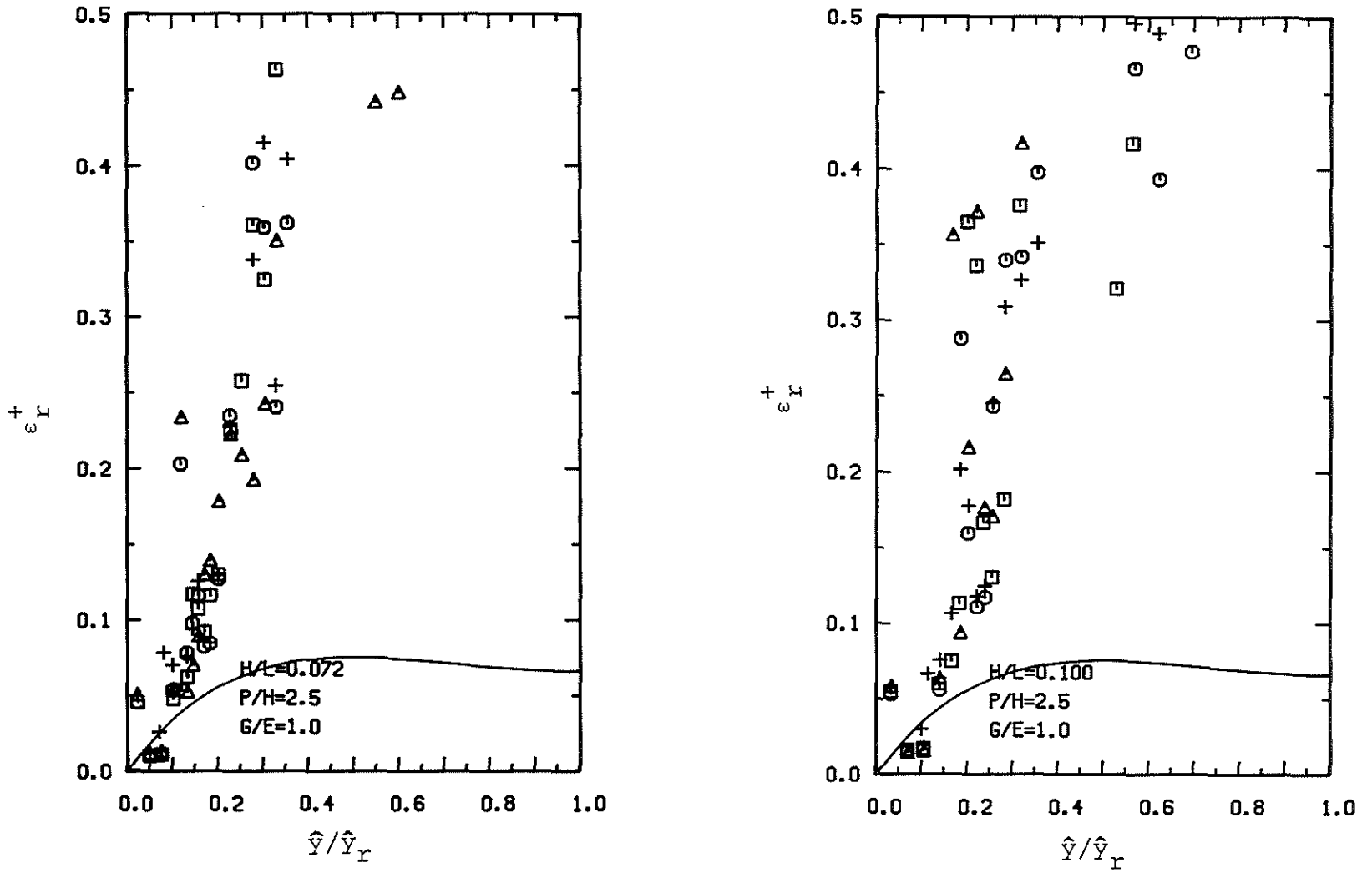

Fig.20.3-20.4: Eddy viscosity ε_r^+ in the rough zone (No.5)